MULTI-COMPONENT TRANSPORT OF GASES AND VAPORS IN POLY(ETHYLENE TEREPHTHALATE)

A Dissertation
Presented to
The Academic Faculty

By

Preeti Chandra

In Partial Fulfillment
Of the Requirements for the Degree of
Doctor of Philosophy in Chemical Engineering

Georgia Institute of Technology

December 2006

MULTI-COMPONENT TRANSPORT OF GASES AND VAPORS IN POLY(ETHYLENE TEREPHTHALATE)

Dr. W. J. Koros
School of Chemical & Biomolecular Engineering
Georgia Institute of Technology

Dr. Haskell Beckham
School of Polymer Textile and Fiber Engineering
Georgia Institute of Technology

Dr. Victor Breedveld
School of Chemical & Biomolecular Engineering
Georgia Institute of Technology

Dr. Robert Kriegel
The Coca-Cola Company

Dr. Sankar Nair
School of Chemical & Biomolecular Engineering
Georgia Institute of Technology

Date Approved: November 8, 2006

Dedicated to
my grandmothers,
my father, mother and sister

ACKNOWLEDGEMENTS

I would like to thank Dr. Koros for his constant guidance in the course of my PhD. His suggestions, and the discussions with him have been very valuable; but more importantly his enthusiasm and his great sense of humor helped make some of the tough times easier to handle. He has been a guide and mentor all through these years, and I cannot thank him enough for all that I have learnt from him, which includes not only transport in polymers, but also a way of working, and an open mindedness to all ideas. I would like to thank Dr Beckham, Dr. Breedveld, Dr. Nair, Dr.Yu Shi Natu and Dr. Rob Kriegel for taking their time out to be a part of my thesis committee, and for their comments. Early interactions with Dr. Yu Shi Natu and later with Dr. Rob Kriegel were very helpful in identifying key issues during the course of this research. I really appreciate their time and input in my work. Funding for this work by Coca Cola Co. is gratefully acknowledged. I would also like to thank Dr. Kumar for the use of his x-ray machine and DMA instrument; and Dr. Beckham for allowing the use of his DSC in the Thermal Analysis Lab. Thanks to Huina Guo for WAXD, Sudhakar Jagannathan for WAXD and DMA measurements, and Chris Hubbell for his help in DSC. Many thanks to Rod Sefton for ensuring that my work is not interrupted due to building maintenance, and to Michelle Martin for all the rush-in orders that she placed for me.

There are not enough words for me to express my gratitude to the Koros Research Group. I received immense help from Ted Moore and Shilpa Damle. They taught me a lot of the basics when I joined this group as a first year, and patiently answered all my questions. They were great people to have around. The friendship of Jason Williams, Bill

Madden, Shabbir Husain, John Perry, Adam Kratochvil and JR Johnson has been invaluable. Their suggestions, ideas, helpfulness around the lab, and a willingness to listen even when they were busy, made work a lot easier. I would like to especially thank Adam Kratochvil for proof reading my thesis. I must also acknowledge all the help of Raymond Chafin, Imona Omole, Madhava Kosuri, Shu Shu, Alexis Hillock and Hensley Sejour. Most of all, I think I will miss my chats with everyone when I did not feel like working. This is an amazing group of people, and I am glad to have been a part of it.

Graduate school and my stay in Atlanta would not have been such a great experience had it not been for the close friendship of Suchitra Konduri, Niket Kaisare, Shabbir Husain, Gracy Wingkono, Manish Gupta, and last but not the least- Ashwini Sinha. Their company was always fun, and I will miss our conversations, dinners and potlucks. Their wonderful attitude, the nerdy and not so nerdy discussions with them, their advice and help made grad school a happy journey. Words alone cannot express my deep gratefulness to Shabbir, Suchitra and Ashwini for their support during the last few months. Ashwini has been my best friend here, and grad school would not have been the same without him.

I would not be the person I am today, but for my parents. Despite being so many miles away, the support of my family never made me feel lonely here. They have been a constant source of inspiration. All that I have achieved in life is owing to them, their faith in me, their encouragement and blessings. My sister, Nitu, wiser than her years, has always provided great encouragement, and imbued me with her enthusiasm. No amount of credit to them will be enough.

Once again, all I can say to everyone is- thank you.

TABLE OF CONTENTS

LIST OF TABLES

LIST OF FIGURES

SUMMARY

Poly(ethylene terephthalate) is a widely used barrier material for food and beverage packaging applications. Expanding markets for PET lie in more challenging applications such as food, flavored (carbonated) beverages and beer packaging. Such products pose advanced challenges where it is important to understand the influence of flavor molecules on the package performance. Multi-component transport of CO_2, O_2, and flavor or aroma components in different morphologies of PET can give an insight into fundamental transport issues. Through such studies, a framework may be established to predict the behavior of not only PET, but also other barrier materials. The use of PET samples with different morphology will enhance the understanding of gas/vapor transport in semi-crystalline, glassy polymers.

Methanol was chosen as the flavor molecule simulant based on its polar, interacting nature, suitable diffusion coefficient, and ability show both dual mode sorption and swelling behavior. Pure methanol vapor equilibrium uptake and sorption kinetics were obtained in different morphologies of PET, namely an amorphous, and an annealed and non-annealed, biaxially oriented semicrystalline film. Crystallinity was found to suppress the extent of swelling, and annealing further reduced the swelling effects.

The gases used in this study- O_2 and CO_2 show dual mode behavior in pure gas form and mixture with each other. In CO_2/O_2 mixtures, depression of O_2 permeability due to competition effects was observed. However, in O_2/MeOH mixtures, complex superposition of dual mode predicted competition and plasticization effects has been shown at intermediate activities of methanol. These effects lead to an enhancement in the

O_2 permeability as compared to the dual mode model prediction. At still higher activities of methanol, the gas permeability rises beyond the pure gas permeability. It has been shown that since annealing leads to better chain packing, the swelling effects are less in this sample as compared to the amorphous and non-annealed films. However, stress relaxation due to sorption of methanol which induces greater chain mobility has been hypothesized to be the cause of permeability enhancements in the non-annealed samples are relatively lower methanol activities. Similar effects have been observed for the CO_2/O_2/MeOH system at high activities of methanol. However, at low activities, presence of CO_2 appears to cause an anti-plasticization effect with the permeabilities of CO_2 being reduced below the dual mode prediction and O_2 being more depressed in the ternary mixture. These observations suggest that different gases might probe the changes induced in the free volume distribution differently.

These results have been examined within the framework of the dual mode model at low to intermediate methanol activities, with modified gas permeabilities, and the free volume model at high methanol activities. It has been proposed that since plasticization affects the chain mobility of the segments which are a part of the equilibrium densified regions of the glass, free volume enhancements should be considered only for these regions. As a simplification, it may be assumed that competition effects for the non-equilibrium sites predicted by the dual mode model still lead to depression of the gas permeability and are superimposed by the plasticization effects. Using this model, free volume parameters have been evaluated for O_2 and CO_2 in PET. This model and the parameters may then be used for future studies with polyester based barrier materials.

CHAPTER 1 : INTRODUCTION

1.1 BARRIER POLYMERS

Polymeric materials, which have very low transmission rates for atmospheric gases such as oxygen, carbon dioxide and water vapor, are used for food and beverage packaging. These materials are called barrier polymers. Their structure is such that gas or vapor transport through them is very slow. Various polyolefins such as polyethylene and polypropylene; fluoropolymers like polyvinylidene fluoride; polyesters such as poly(ethylene terephthalate) and poly(ethylene naphthalate); and poly vinyl alcohol are examples of commonly used polymeric materials for packaging applications. Polymers offer a significant cost advantage over metal foils when used as barrier materials for food and beverage packaging. Their barrier efficacy can be tailored for the application by using blends, composites, and multi-layered structures. Polymer flexibility, heat sealability, transparency and ease of processing by blow molding, injection molding, or melt extrusion are other factors which are encouraging for commercial applications. These properties have led to extensive commercial use for the past few decades.

Packaged foods and beverages place stringent requirements on the barrier material. In the case of carbonated beverages, carbon dioxide loss must be minimized. For dairy products and juices, oxygen invasion, loss of oil and changes in moisture content must be minimal to prevent spoilage or loss of taste. More complex applications involve the need to control the composition of the environment around the product. These include long term storage and ripening of fresh fruits and vegetables; and the storage of biological

samples such as blood, cells, or organs in hospitals. The amount of oxygen for cell respiration, and carbon dioxide from metabolism must be strictly regulated for preservation of these products. Such applications have led to the development of controlled atmosphere packaging and modified atmosphere packaging [1]. Active packages have also been developed which modify the physiological (e.g. respiration) and chemical (e.g. flavor/ lipid oxidation) processes to extend the shelf life [2, 3]. For example, these packages may have oxygen scavengers, which can absorb or react with the incoming oxygen, thus reducing the concentration of oxygen to which the product is exposed. Other packages may contain additives such as carbon dioxide emitters which maintain the desired concentration. Intelligent packages go a step further by providing a system which can be used to monitor the quality of the packaged food during storage and transportation. These could be time-temperature indicators or oxygen and carbon dioxide concentration indicators[2].

Typical requirements for food and beverage packaging to achieve a year long shelf life are [4] :

- 5-15 ppm oxygen ingress in canned foods and juices
- 1-5 ppm oxygen ingress in alcoholic and dairy products
- Less than 20% loss of carbon dioxide in carbonated and alcoholic beverages
- Additional limits on moisture gain/loss and flavor/oil loss are determined by the contents of the packages

Increased understanding of the fundamentals of polymer science has promoted advances in food and beverage packaging technology towards achieving and even exceeding these targets. A better understanding of polymer morphology and the factors

which influence transport properties has led to the development of several new materials and structures to achieve the desired package conditions and extend the shelf life of packaged foods/beverages. Table 1.1 below shows the oxygen, carbon dioxide, and water vapor permeability of various barrier polymers being used.

As can be seen, polymers with polar groups in their backbone tend to transmit more water than those with non-polar groups. On the other hand, this latter group of materials will have a much greater affinity for non-polar organic molecules present in food products. To enhance the overall barrier, multi-layered laminates are often used [4-6]. Thus, poly(ethylene vinyl alcohol) may be sandwiched between two layers of poly(ethylene) to obtain a much better barrier for both oxygen and moisture. Use of blends and composites is also common to improve the barrier properties [7-9]. Impermeable platelet fillers and additives, which may react with the incoming oxygen to reduce oxygen permeability, are also being developed for various applications [10, 11]. However, these compositions add to the cost and the complexity of the package. Such complex structures are also more difficult to recycle.

Table 1.1: Permeability of oxygen, carbon dioxide and water vapor in commonly used barrier materials [12]

Polymer	**Oxygen Permeability**† cc.mm/m^2.day.atm*	**Carbon Dioxide Permeability**† cc.mm/m^2.day.atm*	**Water Vapor Transmission** g.mm/m^2.day
Poly(vinyl alcohol)	0.024 (24°C)	0.040	1247 (40% RH)
Poly(vinyl alcohol)-75%RH	0.090	-	-
Ethylene vinyl alcohol-dry (EVAL F)	0.00008	0.000192	poor barrier
Vectran V100P™ (dry)	0.028		0.008
Vectran V100P™ (wet)	0.024	0.051	
Poly(ethylene)-LDPE	150.00	790.00	2.50
Poly(ethylene)-HDPE	69.568 (30°C)	229.704 (30°C)	
Poly vinylidene chloride-Saran™	0.470 (75%RH)		0.130 γ
Polyamide-Nylon 6	0.61-0.71 (40%RH)	5.90 (30°C)	15-16
Polyamide-Nylon 6		63.00 δ	
Poly acrylonitrile	0.016	1.47	147 (100% RH)
Poly (ethylene terephthalate) oriented	1.2-2.4	5.9-9.8	0.39-0.51
Poly(ethylene naphthalate)- amorphous	0.525	2.43	4.19
Polycarbonate	102.4	307.1	14.9
Polypropylene	39	865	0.79
Polystyrene	118-157	394-590	0.79-3.9

† All permeability values are at 23°C, 0% RH unless otherwise specified
* 1cc.mm/m^2.day.atm = 65.62 Barrer and 1 Barrer = $1x10^{-10}$ ccSTP.cm/cm^2.s.cmHg
γ: At 38°C, 90% RH;
δ: At 30°C, 95-100% RH

A comparison of the different materials in Table 1.1 shows that poly(ethylene terephthalate) (PET) is a good barrier material. Along with low oxygen and carbon dioxide transmission rates, it has a low water vapor transmission rate. Despite the existence of barrier materials with lower transmission rates, such a poly(ethylene naphthalate) (PEN) and Vectra™, PET is more commonly used because it is significantly more economical than the latter two. PET has good mechanical properties, and it can be melt processed to make a resin which is blow- or injection-molded to achieve the shape desired for packages [13]. Crystallinity and bi-axial orientation in the final package further enhance the barrier properties over amorphous PET. It is transparent, even at high levels of crystallinity if oriented at large draw ratios. This makes it suitable for many applications where the visibility of the packaged food is important to enhance consumer appeal. Since PET is light weight, shatter resistant and, transparent, it has many advantages over glass bottles. All these factors combine to promote the continuous expansion of the market for PET. Carbonated beverage packaging, water bottling and food packaging form nearly 60% of the market for this polymer. Textile yarns industry is the second biggest consumer. Other applications of PET exist in the electronics industry and in photographic films.

1.2 MOTIVATION

The market for packaged food and beverage products is continuously expanding. Some new products in the beverage industry include flavored water, single use packages of tea and coffee, energy drinks, oxygen sensitive juices, and beer. These products pose advanced packaging challenges by creating more stringent requirements on the package.

Oxygen invasion, which can lead to degradation of the product, and loss of carbonation limit the shelf life of the product. The flavor and aroma compounds in these products also play a critical role in determination of the shelf life. Flavor scalping by absorption of the aroma molecule into the bottle side wall becomes very important, particularly for complex beverages such as tea or coffee and various food products where parts per million levels of many aroma molecules constitute the final taste. In light of these developments, it becomes important to understand the effect of organic molecules on gas transport and vice-versa. Transport properties in a multi-component environment may be significantly different from that of the pure component. Non-ideal effects such as conditioning or plasticization caused by one species may affect the transport of other species. Conditioning can alter the polymer structure while plasticization leads to increased chain mobility. These effects may lead to increased transmission rates. Pure component transport alone may not sufficient to predict the behavior of mixtures in such cases. In packaged foods, carbon dioxide induced conditioning of the polymer, or swelling and plasticization by organic molecules, can lead increased rate of oxygen ingress or flavor scalping. Multi-component transport studies are needed for a fundamental understanding of these effects.

The packaging industry will also be served in the long term if the package behavior could be predicted for different products. Performing multi-component transport studies for highly complex mixtures will be very time consuming. Therefore, it will be quite useful to have models which can predict barrier polymer performance based on the pure species transport properties of some key components which may be easily measured. To

achieve this, the use of simple models, which incorporate the effects observed with multi-component systems, needs to be investigated.

1.3 RESEARCH OBJECTIVES

The overarching goal of this research is:

- To determine the effect of flavor molecule/simulant on the transport of gases in different morphologies typical of realistic barrier polymers.
- To develop a framework for interpretation and prediction of multi-component transport such that it can be extended to novel barrier materials

One of the challenges in this work has been the identification of a suitable system which can be used to study the effects of organic compounds on transport of gases. Flavor compounds are often large molecules with very low diffusion coefficients which makes their transport time scales experimentally inaccessible. To simulate these molecules, a smaller penetrant- methanol, has been chosen as a *model compound* for the multi-component gas/vapor studies. Poly(ethylene terephthalate) (PET) has been selected as the model barrier polymer. Specific objectives defined for this work are discussed below.

1.1.1 Objective 1

To study the sorption and transport properties of methanol in PET and investigate the differences in transport properties with changes in morphology.

Three representative samples of PET with different morphologies are used. The PET-methanol system has not been previously studied, and the aim is to obtain the pure component sorption and transport data, which can be used for comparison with the multi-

component transport results and for modeling purposes. Moreover, a systematic study across the three samples is needed to illustrate the morphological effects on transport properties and for inclusion of those effects in the modeling.

In the process of choosing a suitable flavor simulant, sorption of other lower alcohols such as ethanol, n-propanol and iso-propanol was performed to determine which molecule is best for the multi-component studies. Thus, sorption isotherms and kinetics of these lower alcohols have been obtained as a by-product of the work undertaken for identification of the model compound. These results have been used to compare the effect of penetrant size and side groups on the transport properties. Such an analysis is valuable for extension of the results from the model system to real multi-component systems which include large flavor molecules. Moreover, the PET-ethanol system is relevant for packaging of beer and ale in plastic bottles.

1.1.2 Objective 2

To study multi-component permeation of CO_2, O_2 and methanol at different activities of methanol in amorphous; annealed, oriented; and non-annealed, oriented PET.

Pure component transport properties of CO_2 and O_2 have been measured by many researchers in different morphologies of PET to evaluate the barrier performance. The effect of relative humidity and temperature on the permeability of the gases has been studied by various researchers[12, 14]. However, to date, very few studies are available which investigate the influence of flavor molecules on gas transport [15, 16]. In many glassy polymers used for gas separation membranes, highly sorbing organic molecules can affect gas transport [17-19]. Highly sorbing, condensable flavor molecules may also affect gas transport in barrier polymers. Non-ideal effects, such as plasticization of the

polymer matrix, will adversely affect the barrier efficacy. Transport of binary and ternary mixtures of O_2, CO_2, and MeOH has been studied to elucidate such effects. The goal of these multi-component studies is to achieve a fundamental understanding of the transport processes which determine the package performance for complex products.

1.1.3 Objective 3

To develop a framework within which the observations of objective 2 can be interpreted and extended for the prediction of transport properties of similar systems.

The results of objective 2 have been interpreted through mathematical models that incorporate various effects such as plasticization and dual mode competition. The latter effect is observed in glassy polymers where multiple penetrants compete for the occupancy of the energetically favorable non-equilibrium sorption sites. The aim is to enable the prediction of gas transport based on pure component sorption and transport data. The analysis has been performed within the framework of the dual mode model for gas sorption and transport. This model was extended for multi-component transport by Koros et al [20, 21]. Moreover, several researchers have suggested modifications in the dual mode model parameters to account for plasticization effects using a single penetrant[22-24]. In this work, these models have been expanded to predict transport of multiple components with one plasticizing penetrant. Apart from the PET-methanol system, the model has been used to predict the behavior of the PET-ethanol-CO_2-O_2 system which is industrially relevant due to growing interest in plastic packaging of alcoholic beverages.

1.4 THESIS OVERVIEW

The dissertation is divided into eight chapters. Chapter 2 provides the fundamentals of transport of gases and organic molecules in glassy polymers along with some models for describing the same. Chapter 3 has a three fold objective: to discuss how methanol was selected as the flavor molecule simulant; to describe the polymer samples used and their properties such as glass transition temperature and crystallinity; and to provide detailed information about the equipment design and procedure for gas transport, mixed gas/vapor permeation, and gas vapor sorption. In chapter 4, sorption kinetics and the equilibrium isotherm measured for methanol are discussed. Chapter 5 extends this sorption work to other lower alcohols such as ethanol, n-propanol, and iso-propanol. Chapter 6, which fulfills objectives 2 and 3, mainly consists of the results obtained for the pure gases, mixed gas transport and mixed-gas/vapor systems. The free volume model and the dual mode model are discussed in detail. The results obtained are analyzed within the framework of these models. Chapter 7 concludes this dissertation by summarizing the contribution of this work along with some future directions.

1.5 REFERENCES

1. Day, B.P.F., *Novel MAP Applications for Fresh Prepared Produce*, in *Novel Food Packaging Techniques*, R. Ahvenainen, Editor. 2003, CRC Press: Cambridge, England.

2. Ahvenainen, R., *Active and Intelligent Packaging*, in *Novel Food Packaging Techniques*, R. Ahvenainen, Editor. 2003, CRC Press: Cambridge, England. p. 590pp.

3. Vermeiren, L., et al., *Oxygen, Ethylene and Other Scavengers*, in *Novel Food Packaging Techniques*, R. Ahvenainen, Editor. 2003, CRC Press: Cambridge, England.

4. Koros, W.J., ed. *Barrier polymers and structures:Overview*. Barrier Polymers and Structures, ed. W.J. Koros. 1990, American Chemical Society: Washington D.C.

5. Rule, M., et al., *Multilayer polymer/inorganic oxide gas/vapor barrier structures for PET beverage containers*. 2002, (The Coca-Cola Company, USA). Application: WO. p. 21 pp.

6. Kanda, T. and K. Maruo, *Gas-barrier multilayer structure and its production process*. 2005, (Mitsubishi Gas Chemical Company, Inc., Japan; Amcol International Corporation). Application: WO. p. 37 pp.

7. Cai, G., T.Y. Ching, and H. Yang, *Oxygen scavenging polymer blends and emulsion-based methods for preparing same*. 2002, (USA). Application: US. p. 29 pp.

8. Flodberg, G., et al., *Barrier properties of blends based on liquid crystalline polymers and poly(ethylene terephthalate).* International Journal of Polymeric Materials, 2001. **49**(2): p. 157-177.

9. Prattipati, V., et al., *Improving the transparency of stretched poly(ethylene terephthalate)/polyamide blends.* Journal of Applied Polymer Science, 2006. **99**(1): p. 225-235.

10. DeRocher, J.P., et al., *Barrier membranes with different sizes of aligned flakes.* Journal of Membrane Science, 2005. **254**(1-2): p. 21-30.

11. Lape, N.K., C. Yang, and E.L. Cussler, *Reactive flake-filled barriers.* Annual Meeting Archive - American Institute of Chemical Engineers, Indianapolis, IN, United States, Nov. 3-8, 2002, 2002: p. 2131-2136.

12. Massey, L., K., ed. *Permeability Properties of Plastics and Elastomers, A Guide to Packaging and Barrier Materials*. 2nd Edn ed. Plastics Design LIbrary. 2002, William Andrew Publishing: Norwich. 601.

13. Kroschwitz, J.I., ed. *Encyclopedia of Polymer Science and Engineering*. Second Edition ed. Vol. Supplement Volume. 1989, John Wiley: New York.

14. Koros, W.J., *Gas Barrier Polymers*, in *Polymeric Materials Encylopedia: Synthesis, properties and applications*. 1996, CRC Press.

15. Van Willige, R.W.G., et al., *Influence of flavor absorption on oxygen permeation through LDPE, PP, PC and PET plastics food packaging.* Food Additives and Contaminants, 2002. **19**(3): p. 303-313.

16. Sadler, G.D. and R.J. Braddock, *Oxygen permeability of low density polyethylene as a function of limonene absorption: an approach to modeling flavor \"scalping\".* Journal of Food Science, 1990. **55**(2): p. 587-8.

17. Moore, T.T., et al., *Effect of humidified feeds on oxygen permeability of mixed matrix membranes.* Journal of Applied Polymer Science, 2003. **90**(6): p. 1574-1580.

18. Al-Juaied, M.A., *Carbon dioxide removal from natural gas by membranes in the presence of heavy hydrocarbons and by aqueous diglycolamine/morpholine*, in *Department of Chemical Engineering*. 2004, University of Texas: Austin.

19. Vu, D.Q., W.J. Koros, and S.J. Miller, *Effect of condensable impurity in CO2/CH4 gas feeds on performance of mixed matrix membranes using carbon molecular sieves.* Journal of Membrane Science, 2003. **221**(1-2): p. 233-239.

20. Koros, W.J., *Model for sorption of mixed gases in glassy polymers.* Journal of Polymer Science, Polymer Physics Edition, 1980. **18**(5): p. 981-92.

21. Koros, W.J., et al., *A model for permeation of mixed gases and vapors in glassy polymers.* Journal of Polymer Science, Polymer Physics Edition, 1981. **19**(10): p. 1513-30.

22. Saxena, V. and S.A. Stern, *Concentration-dependent transport of gases and vapors in glassy polymers. II. Organic vapors in ethyl cellulose.* Journal of Membrane Science, 1982. **12**(1): p. 65-85.

23. Zhou, S. and S.A. Stern, *The effect of plasticization on the transport of gases in and through glassy polymers.* Journal of Polymer Science, Part B: Polymer Physics, 1989. **27**(2): p. 205-22.

24. Kamiya, Y., et al., *Sorption and dilation in poly(ethyl methacrylate)-carbon dioxide system.* Journal of Polymer Science, Part B: Polymer Physics, 1989. **27**(4): p. 879-92.

CHAPTER 2 : BACKGROUND AND THEORY

Transport properties of gases and vapors in polymers have been a subject of immense interest for many decades. Since 1831, when Mitchell first observed that natural rubber balloons filled with different gases deflated at different rates, significant progress has been made in the understanding of the phenomena involved. This chapter introduces the fundamentals of mass transport in polymers that have been used in this research, and will be referred to in subsequent chapters. Basic principles are discussed, and relevant mathematical formulations of the processes involved are presented. The focus is on steady state transport and the sorption kinetics in glassy polymers.

2.1 TRANSPORT PROPERTIES

The ability of a penetrant to move in a polymeric medium is determined by its transport properties, namely diffusivity, solubility and permeability. These, in turn, are determined by a number of factors involving both the penetrant and the polymeric medium. The following sub-sections describe the theory of transport as is applicable to glassy polymers including the effects of semi-crystallinity and orientation. The reader is also referred to [1], and its references, as an excellent source of information on various phenomena observed in both rubbery and glassy polymers.

2.1.1. Diffusion

Diffusion of gases and vapors in polymers is an important phenomenon for barrier materials in food and beverage packaging, as well as for membrane based gas

separations. Mathematically, the diffusion coefficient (D) can be defined as:

$$D = \frac{1}{6} fx^2 \qquad 2.1$$

x is the jump length, and f is the frequency of the jumps. Equation 2.2 states Fick's 1st Law, which can be used to determine the diffusive flux of the penetrant (J_i) at steady state. C_i is the concentration or the driving force in the direction Z, and D is the diffusion coefficient.

$$J_i = -D\frac{\partial C_i}{\partial Z} \qquad 2.2$$

D has the units of length^2/time, and is usually reported in cm^2/s. At unsteady state, the rate of change of penetrant concentration in the material is described by Fick's 2nd Law. This form of the equation is applicable to isotropic, planar systems with constant diffusivity.

$$\frac{\partial C_i}{\partial t} = D\frac{\partial^2 C_i}{\partial Z^2} \qquad 2.3$$

Diffusion in polymers is an activated process [2]. A transient gap is created between the polymer chains, and the penetrant jumps from one gap to another. The jump length and frequency are determined by the availability of large enough transient gaps in the polymer. A bigger penetrant will have a lower probability of finding the right sized gap created by the segmental motion of the polymer chains, and thus, will have a lower diffusion coefficient [2, 3]. Diffusion of gases and vapors is frequently found to be dependent on the concentration of the penetrant in the polymer [4-8]. Such dependence could be due to changes in the chain packing or the mobility of the polymer and/or penetrant. Sufficiently high concentrations of penetrant in the polymer can lead to

swelling effects, resulting in increased polymer chain mobility and penetrant diffusion coefficients [9-12]. Such effects are also observed in rubbery polymers [13]. On the other hand, if the penetrant molecules interact strongly amongst themselves or with the polymer, say through H-bonding, it can lead to a decrease in their diffusion coefficients due to a greater energy penalty involved in making the diffusion jump [8, 14]. Thus, the diffusion coefficient of a molecule in a polymer depends on various factors such as the size of the penetrant, polymer morphology, and interaction between the polymer and penetrant based on their chemical structure [3, 15]. To compare the diffusivities of different species, an infinite dilution diffusion coefficient, evaluated at very low penetrant concentration, is used. This values correlates well with the penetrant diameter, van der Waal's volume or critical volume [1, 3, 16].

When the diffusion coefficient is concentration dependent, only an average diffusivity over a given concentration range can be obtained experimentally. Equation 2.4 gives the mathematical definition of the average diffusivity [17]. C_1 is the initial concentration and C_2 is the final concentration. Experiments are usually performed over small ranges of concentration such that the variation in *D(C)* is small. This equation applies only to two-component systems [15].

$$\bar{D} = \frac{\int_{C_1}^{C_2} D(C)dC}{C_2 - C_1} \qquad 2.4$$

$\bar{D}$ is usually plotted as a function of the average concentration $\bar{C}$ to obtain the functional form of D(C). $\bar{C}$ is the average concentration as shown below.

$$\bar{C} = \frac{C_1 + C_2}{2} \qquad 2.5$$

Crank has proposed that local diffusion coefficients can also be calculated using the diffusivity (D_S) measured when the concentration is incrementally increased from C_1 to C_2 and diffusivity (D_D) measured when the concentration is incrementally decreased from C_2 to C_1 [17, 18]. Thus,

$$\bar{D} = \frac{D_S + D_D}{2} \qquad 2.6$$

Mathematical treatment of diffusion processes has been done extensively. The reader is referred to the works of Crank [19] and Neogi [20]. Some aspects of the unsteady state diffusion process have been discussed in section 2.3.

2.1.1 Sorption

Sorption refers to the dissolution of the penetrant into the polymer. The penetrant can be visualized as going from the gas phase to a condensed phase, as a mixture with the polymer. The concentration of the penetrant in the polymer maintains equilibrium with its concentration outside the polymer. The distribution of pure penetrant between the polymer and the ambient phase is represented as:

$$C = S(p)p \qquad 2.7$$

C is the concentration of the penetrant in the polymer, p is the pressure of the penetrant outside, and S is the solubility constant which may be pressure dependent. Solubility of a gas/vapor molecule depends on various factors such as its condensability, which can be related to its critical temperature, the temperature of the system, the structure of the polymer backbone, the polymer morphology, and polymer interaction with the penetrant

[2]. Experimentally, equilibrium sorption isotherms are used to determine the solubility from the slope of the C vs. p curve. Various models exist which describe such pressure or concentration dependence of solubility and are discussed in section 2.2. At sufficiently low concentrations, the solubility coefficient is often referred to as the infinite dilution solubility constant, and is used to compare the solubility of different penetrants in a given polymer [21].

The time taken to reach sorption equilibrium depends on the diffusion coefficient of the polymer [22]. This makes sorption kinetics a very powerful tool to study the diffusion coefficient of a molecule in a polymer, its concentration dependence, and changes in polymer morphology due to sorption [15, 22, 23]. Dissolution of a species in a polymer can have many effects on the polymer-penetrant system. Many researchers have shown that the glass transition temperature of the polymer-solvent system is less than the pure polymer [24, 25]. At sufficiently high penetrant concentrations, the polymer may even undergo glass transition at the temperature of operation and become rubbery [26]. In crystallizable polymers, further sorption of strongly interacting solvents may lead to crystallization of the chains due to sufficiently high mobility. This phenomenon is called solvent induced crystallization [11, 27, 28]. Even when such extreme effects are not observed, solvents can induce permanent changes in the polymer morphology leading to different sorption and diffusion properties. These are classified as history dependent changes [29, 30]. Often times, either for experimental simplicity or when the new properties are more desirable, the polymer is pre-conditioned with the solvent [31, 32].

2.1.2 Permeability

For barrier materials, the most important figure of merit is the permeability of a molecule which determines its flux across the package. In the case of carbonated, flavored beverages, carbon dioxide loss and oxygen invasion are determined by the permeability of these gases. Permeability of a penetrant is defined as the pressure and thickness normalized flux and is shown below:

$$P = \frac{Flux}{\Delta p / l} \qquad 2.8$$

Δp is the pressure differential across the membrane or package, and l is the thickness of the film. Values are usually reported in units of Barrer where 1 Barrer= $1x10^{-10}$ ccSTP.cm/s.cmHg.cm^2. The permeation process is driven by the concentration or chemical potential difference across the film. Combining equations 2.2, 2.7 and 2.8, an average permeability can be obtained, where the bar represents average values.

$$\bar{P} = \bar{D}\bar{S} \qquad 2.9$$

Equation 2.9 shows that transport of penetrants in polymers follows a sorption-diffusion mechanism. The penetrant first sorbs in the polymer, and then diffuses across its thickness to desorb out on the other side. The quantities of interest are the diffusion coefficient (D), which is the kinetic factor, and the sorption coefficient (S) of the penetrant, which is the thermodynamic factor. These have been discussed in sections 2.1.1 and 2.1.1 respectively. Permeability is a measure of the efficacy of the barrier. However, to design new materials or to understand their properties, knowledge of both sorption and diffusivity is desirable.

As has been discussed in sections 2.1.1 and 2.1.1, diffusivity and sorption coefficient are often concentration dependent. In such cases, permeability must be a function of concentration as well. Then, combining Fick's 1st Law with equation 2.8, the following expression can be obtained

$$\bar{P} = \frac{\int_{C_1}^{C_2} D(C)dC}{p_2 - p_1} \qquad 2.10$$

Thus, if D(C) and equilibrium sorbed concentration, C, can be obtained, $\bar{P}$ can be calculated using equation 2.10. Similarly, combining equations 2.4, 2.9 and 2.10, an expression for calculation of average solubility from known concentrations and pressures can be obtained.

$$\bar{S} = \frac{C_2 - C_1}{p_2 - p_1} \qquad 2.11$$

2.1.3 Effect of Crystallinity and Orientation on Transport Properties

In its simplest form, a semi-crystalline polymer is described as consisting of two phases, crystalline and amorphous domains. Several models have been proposed to describe the morphology of such polymers [33]. PET is a semi-crystalline polymer and most packaging applications use it in the uniaxially or biaxially oriented form. Other polymers such as polyethylene and polypropylene are also frequently used in semi-crystalline, oriented form. Hence, crystallinity and orientation effects on the transport properties are important.

Michaels et al studied the subject in rubbery, unoriented polyethylene [34, 35]. They concluded that the crystallites are randomly distributed with respect to the solution-diffusion process, and are impenetrable. Only the amorphous regions of the polymers are capable of providing passage to the gas or vapor molecules. As a result, the molecule has to diffuse around the crystallites, and has a longer path length that leads to decreased diffusivity. This is characterized by a tortuosity factor, τ. Furthermore, in rubbery polymers, the crystallites can also act as mobility restrictors for the amorphous chains, resulting in a further decrease in the diffusivity. This is characterized by a chain immobilization factor, β. However, glassy polymer chains already have very low mobility and the chain immobilization factor does not play a significant role. Michaels et al observed that τ is inversely proportional to the amorphous fraction in the case of unoriented crystallites [36]. If D^* is the diffusivity of the completely amorphous sample, ϕ_a the amorphous volume fraction of the semi-crystalline sample, then the diffusivity (D) in such a sample can be written as:

$$D = D^* \phi_a \qquad 2.12$$

Studies were also performed for solubility in semi-crystalline poly(ethylene), and it was observed that solubility decreased linearly with the decreasing amorphous fraction. This dependence is shown in equation 2.13 below. S^* is the solubility of the completely amorphous sample, and S is the solubility in the semi-crystalline sample.

$$S = S^* \phi_a \qquad 2.13$$

Based on equation 2.9, permeability of a semi-crystalline polymer can be written as:

$$P = \phi_a^2 P^* \qquad 2.14$$

When similar studies were performed with PET, Michaels et al observed that the linearity of solubility with the amorphous fraction existed only for helium [37]. In many cases the solubility was higher than predicted by equation 2.13. They suggested that the non-equilibrium sites were higher in concentration in a glassy semi-crystalline polymer than in the amorphous material, leading to greater dissolution. Despite the lack of a perfect fit of equation 2.13 for solubility in semi-crystalline, glassy polymers, this two phase model has been used by many researchers [11, 38]. This model is simple to use, and the crystalline fraction can be determined easily by other characterization methods such as density, wide angle x-ray diffraction (WAXD), or differential scanning calorimetry (DSC). Several reports have been published on the existence of at least three phases in semi-crystalline polymers. Researchers have considered a third phase at the interface between the crystals and the amorphous regions with a different morphology from the rest of the amorphous phase of the polymer[39-41]. However, such a detailed morphology of glassy polymers is yet not well understood, and the fraction of the third phase is difficult to estimate accurately. Dependence of the final morphology on various processing parameters prevents generalizations; therefore, these factors preclude the widespread use of the three phase model.

Despite the complications introduced by crystallinity, it must be emphasized that for barrier materials, crystallinity is desirable because it lowers the permeability of the gases and enhances the mechanical properties, such as elastic modulus [42]. On the downside, very high levels of crystallinity lead to opacity of the sample due to scattering of light by the sample. For food packaging, and particularly beverage packaging, transparent

packages are desirable to enhance the consumer appeal of the product. Thus, a balance has to be maintained between the degree of the crystallinity and the clarity of the package.

The presence of orientation adds another level of complication. Materials are oriented during processing steps, such as blow molding or injection molding of packages. In applications involving sheets, the resin is stretched uniaxially or biaxially at a desired draw ratio. Orientation introduces anisotropy in the polymer. The path length for diffusion across the thickness of the sample increases due to an increase in the tortuosity, which leads to a decrease in the diffusivity [43, 44]. The starting morphology, draw temperature, and draw ratio play an important part in the final morphology and transport properties obtained. Annealing after orientation can also be used to tune the properties. Relative to the amorphous, unoriented material, the overall volume available for a penetrant to sorb into is reduced at high enough draw ratios due to better chain packing [45]. This reduction in volume results in decreased solubility of the gases and vapors. Better chain packing also increases the stiffness of the polymer and improves its mechanical properties [46, 47]. High draw ratios can lead to crystallization, and further stretching causes the orientation of these crystallites [48]. It has been observed that the effect of orientation also depends on the initial crystallinity of the sample. For example, if initial crystallinity is low, the relative reduction in permeability after orientation may be larger than if the crystallinity is high to begin with [15]. Moreover, at high elongations, the sorption and transport processes may be concentration dependent, and long term relaxation of the polymer matrix can lead to anomalous kinetics [49]. While a correlation between orientation and refractive index as well as polymer chain conformation is noted

for PET, no clear relation has been developed as of yet that may be used to predict the permeability at different draw ratios [44, 50].

2.2 Modeling of Transport Properties

Several models exist to describe the transport properties in polymeric materials [2]. For glassy polymers, these models can be divided into two categories, 1) phenomenological models and 2) free volume models. These are discussed in the following subsections.

2.2.1 Dual Mode Model

The "dual mode sorption" model is a phenomenological theory which offers a very good description of the sorption, diffusion, and permeation of penetrants in glassy polymers. This model was first described by Barrer et al [51] to explain the concavity of the sorption isotherm to the pressure axis. Considerable work has been done [52-56] to verify the model and extend it to describe the diffusion and permeation coefficients. The key features of this model are:

1. Glassy polymers are a micro-heterogeneous medium. As the polymer is cooled below glass transition temperature, segmental motion is reduced, leading to molecular scale micro-voids being frozen into the structure in the form of excess free volume. These molecular sized non-equilibrium domains are often referred to as 'holes' and form one of the modes of dissolution. At a given temperature, there is a fixed distribution of the number and size of such holes in the polymer that can be likened to the adsorption sites of a zeolite. Thus, sorption in these sites is described by a Langmuir type of isotherm shown in the equation below. C_H is the concentration of the

penetrant in the holes, C_H' is the saturation capacity of these holes, b is the affinity constant, and p is the pressure of the penetrant outside the polymer.

$$C_H = \frac{C_H' bp}{(1+bp)} \qquad 2.15$$

2. The other mode of solubilization is in the polymer chains that have an equilibrium packing density. This mode often referred to as the 'dissolved' mode. The equilibrium chain packing is envisioned to be the same as that in liquid-like rubbery polymers, and penetrant solubilization follows Henry's Law. C_D is the penetrant concentration in the dissolved region and k_D is the Henry's Law solubility constant.

$$C_D = k_D p \qquad 2.16$$

3. Total penetrant concentration in the polymer can be described as shown below.

$$C = C_H + C_D$$

$$C = \frac{C_H' bp}{(1+bp)} + k_D p \qquad 2.17(a, b)$$

4. Local equilibrium is maintained between the holes and the dissolved regions. The equilibrium constant K is defined as:

$$K = \frac{C_H' b}{k_D} \qquad 2.18$$

5. Sorption of a penetrant is an exothermic process in the holes and endothermic in the dissolved regions. Sorption in the dissolved regions requires that the polymer chains be pried apart, which is an energy consuming process. On the other hand, sorption in holes requires filling up of existing void spaces. Thus, the holes are energetically favored and are the first to fill up. Equilibrium is maintained with the dissolved

regions as per 4 above. The dual mode model thus, satisfactorily explains the high negative heats of sorption observed for glassy polymers. In the low pressure regime where bp<<1, equation 2.17 reduces to

$$C = (k_D + C_H^{'} b) p \qquad 2.19$$

As the pressure increases, the holes will become saturated with the penetrant and further dissolution will take place only in the Henry's Law domains. Thus, in the high pressure regime, when bp>>1, penetrant concentration is

$$C = k_D p + C_H^{'} \qquad 2.20$$

Equations 2.19 and 2.20 indicate that in both, low pressure, and high pressure limits, the sorption isotherm is linear, but with different slopes.

6. Vieth [57] and Barrer [51] postulated that the penetrant was completely immobilized in the holes. Thus, molecules present in the equilibrium liquid alone contribute to the diffusion and permeation process. On the other hand, Koros [52] proposed that the penetrant molecules have partial mobility. Thus, penetrant molecules diffuse in and out of these holes and contribute to the permeability. Penetrant jumps from the hole to dissolved region can effectively be represented by a diffusion coefficient D_H. Penetrant jumps from one dissolved mode site to another can be effectively described by diffusion coefficient D_D. The ratio of these diffusivities is F

$$F = \frac{D_H}{D_D} \qquad 2.21$$

Thus, the flux N can be written as

$$N = -D_D \frac{\partial C_D}{\partial z} - D_H \frac{\partial C_H}{\partial z} \qquad 2.22$$

Using equations 2.17 and 2.18, an effective local diffusion coefficient can be found and the flux written as shown below:

$$N = -D_{eff}\frac{\partial C}{\partial z} \qquad 2.23$$

$$\bar{D}_{eff} = D_D\left[\frac{\left(1+FK/(1+\alpha C_D)^2\right)}{\left(1+K/(1+\alpha C_D)^2\right)}\right] \qquad 2.24$$

F, K, and D_D are as defined above, and $\alpha = b/k_D$. According to equation 2.24, the diffusion coefficient increases with increasing pressure and eventually reaches a constant value.

Koros [52] also suggested an alternate physical meaning to F. Instead of the ratio of diffusion coefficients, F can be assumed to be the fraction of the species in the holes that are mobile and have a constant diffusivity D. Such an interpretation results in the same flux and effective diffusivity equations as described above. Combining equations 2.24 and 2.4 and using $C_1=0$, the expression for the effective, average diffusion coefficient can be written as shown below.

$$\bar{D}_{eff} = D_D\left[\frac{\left(1+FK/(1+\alpha C_D)\right)}{\left(1+K/(1+\alpha C_D)\right)}\right] \qquad 2.25$$

7. Based on the definition of permeability, an expression for the average permeability for the case of zero downstream pressure can be derived as

$$P = k_D D_D\left[1+\frac{FK}{1+bp}\right] \qquad 2.26$$

where p is the upstream pressure. According to equation 2.26, the permeability decreases with increasing pressure and, in the absence of Plasticization, eventually

becomes independent of pressure. In the low pressure region, solubility is higher due to hole filling (equation 2.19), leading to higher permeability.

8. Initially proposed for pure components, the dual mode model has been successfully extended to mixtures by Koros and coworkers [53, 58]. In the presence of a binary mixture of A and B, where neither species is a plasticizing agent, sorbed concentration of A can be written in terms of partial pressures, p_A and p_B, for components A and B respectively

$$C_A = k_{DA} p_A + \frac{C'_{HA} b_A p_A}{1 + b_A p_A + b_B p_B} \qquad 2.27$$

The physical basis of the second term in the expression is that the penetrant molecules compete for occupancy of a fixed number of Langmuir type sites. During pure penetrant transport, all of these sites were available to species A; however, in mixture, sorption of species B in these microvoids is also energetically favorable. Hence, some of the molecules of A are excluded, leading to a reduction in the concentration of A in the polymer. This results in a decrease in the permeability of A in mixture as compared with pure A. The expression for permeability in mixture is shown below.

$$P = k_{DA} D_{DA} \left[1 + \frac{F_A K_A}{1 + b_A p_A + b_B p_B} \right] \qquad 2.28$$

All the parameters in equations 2.27 and 2.28 are pure component parameters. Thus, this model can be effectively used to predict the transport properties of a mixture using the pure component transport properties. It must be noted here that this model does not account for changes in polymer chain mobility, and hence, changes in solubility and diffusivity due to effects such as plasticization or antiplasticization.

Plasticization effects have been discussed in section 2.4. Anti-plasticization effects have not been seen in this work and therefore, not further discussed [1, 59, 60]. The reader is referred to [1, 61, 62] for reviews of the dual mode model.

2.2.2 Flory Huggins Equation

As was mentioned above, the dual mode model describes the concavity of the sorption isotherm to the pressure axis. However, in several instances, it has been observed, especially for strongly sorbing organic vapors and gases, that at high enough penetrant activity, the sorption isotherm becomes convex to the x-axis [63]. This behavior is well explained by the Flory-Huggins sorption theory [64]. The isotherm described by equation 2.29 is also applicable to rubbery polymers which show linearity of concentration with pressure at low uptakes.

$$\ln\left(\frac{p}{p_o}\right) = \ln\phi + (1-\phi) + \chi(1-\phi)^2 \qquad 2.29$$

p is the pressure of the gas/vapor, p_o is the saturation vapor pressure at the temperature of operation, χ is the Flory-Huggins interaction parameter and ϕ is the volume fraction of the penetrant in the polymer. While the interaction parameter is a constant in most cases; if needed, its concentration dependence can be written as shown below [16].

$$\chi = \chi_o + \chi_1\phi \qquad 2.30$$

An advantage of equation 2.29 is that with only one sorption point, the value of χ can be calculated, and the whole isotherm may be predicted.

2.2.3 Free Volume Models

As has been mentioned before, the movement of a penetrant in a polymer requires some unoccupied volume in the polymer that can be occupied by the penetrating species. The unoccupied volume is defined by the free volume of the system, and the mobility of a penetrant is dependent on the fractional free volume of the polymer. Fractional free volume is defined as

$$V_f = \frac{\hat{V}_g - \hat{V}_o}{\hat{V}_o} \qquad 2.31$$

where $\hat{V}_g$ is the specific volume of the glassy polymer at a given temperature, and $\hat{V}_o$ is the specific occupied volume of the glass. Based on this concept of the fractional free volume, Fujita [65] proposed that the diffusivity of a gas can be written as

$$D = A_d \exp\left(\frac{-B_d}{FFV_o}\right) \qquad 2.32$$

where A_d and B_d are empirical parameters with A_d depending on the size and the kinetic velocity of the penetrant in the polymer, and B_d being determined by the volume needed to diffuse in the polymer. To account for crystallinity, equation 2.32 was modified by assuming that the free volume reduction is proportional to the amorphous fraction. ϕ_a is the amorphous volume fraction.

$$D = A_d \exp\left(\frac{-B_d}{\phi_a FFV_o}\right) \qquad 2.33$$

An increase in temperature leads to dilation of the volume of the polymer resulting in an increase in its free volume. Additionally, free volume also depends on the pressure and

the concentration of a penetrant in the polymer. Therefore, incorporating these effects, the fractional free volume can be written as.

$$FFV_{mix} = FFV_o(T_s, P_s, 0) + \alpha(T - T_s) + \beta(p - p_s) + \gamma\phi_p \qquad 2.34$$

Here, V_{fs} is the fractional free volume of the penetrant free polymer at the reference temperature, T_s, and pressure, p_s. α, β and γ are constants that are usually evaluated empirically. The reference state is usually taken to be the glass transition temperature, T_g, at zero pressure. Stern showed that permeability of both, small gases and large organic molecules depends on the free volume of the polymer-penetrant system [66, 67].

2.3 SORPTION KINETICS

Until now, models for steady state transport properties have been considered; that is solubility and permeability are measured at equilibrium. This section is devoted to the time dependent uptake/removal of a species in the polymer. Experimentally, the mass of penetrant absorbed/desorbed is measured as a function of time. This measurement becomes a very powerful tool since the diffusion coefficient and solubility can be found from the same experiment. Moreover, comparisons of different samples can provide useful information about the morphology of the materials.

2.3.1 Fickian Kinetics

The most common time dependence of sorption and desorption is governed by Fick's 2nd Law, as shown in equation 2.3 for an isotropic, flat sheet with a constant diffusivity. In flat sheets, the thickness dimension is much less than the length or width. Therefore, diffusion is uni-dimensional. Crank [19] has provided a comprehensive collection of

solutions to Fick's 2nd Law for other geometries, as well as concentration dependent diffusion coefficients. The specific case of a sheet of thickness 2*l* is considered here. The boundary conditions for equation 2.3 are

$$\begin{aligned} &C = C_o \text{ at } t = 0 \ \ \forall -l < z < l \\ &C = C_1 \text{ at } t > 0 \text{ for } z = l \\ &\frac{\partial C}{\partial z} = 0 \text{ at } z = 0, \forall t \end{aligned} \qquad 2.35$$

With these boundary conditions, equation 2.3 can be solved for concentration in the polymer at a given z and t, which is used to obtain the total mass of the penetrant in the polymer at any time t. This is shown in the expression below.

$$\frac{M_t}{M\infty} = 1 - \frac{8}{\pi^2}\sum_{n=0}^{\infty}\frac{1}{(2n+1)^2}\exp\left[-\frac{(2n+1)^2\pi^2 Dt}{4l^2}\right] \qquad 2.36$$

M_t is the mass uptake/removal at time t, M_∞ is the amount absorbed/desorbed at equilibrium, D is the diffusivity, and *l* is the film half thickness. Equation 2.36 can be simplified for the calculation of D, where $t_{1/2}$ is the time when $M_t/ M_\infty = 0.5$.

$$D = 0.1968\frac{l^2}{t_{1/2}} \qquad 2.37$$

Key features of the Fickian kinetics are-

a) M_t/ M_∞ is linear with $\sqrt{t}$ at short times (where $M_t/ M_\infty < 0.5$)

b) $\ln(1-M_t/ M_\infty)$ is linear with t at long times (where $M_t/ M_\infty > 0.5$)

c) Sorption kinetics measured with films of different thicknesses collapse onto the same curve when plotted against $\sqrt{t}/l$. This master curve confirms that the kinetics is, indeed, Fickian.

As long as the kinetics follows Fick's 2nd Law, concentration dependent diffusion coefficients and/or average diffusivities can be evaluated using equations 2.36 and 2.37. M_∞ is used to evaluate solubility at the given penetrant partial pressure. The diffusion and solubility coefficients can then be used to calculate permeability as described in section 2.1.2.

2.3.2 Non-Fickian Kinetics

Sorption and transport in polymers often exhibit features which do not follow Fick's 2nd Law with constant boundary conditions and concentration dependent diffusion coefficients. Mathematically, the generalized time dependence of M_t can be written as

$$M_t = kt^n \qquad 2.38$$

Fickian kinetics is the case of n = ½. As shown in Table 2.1, below, non-Fickian or anomalous kinetics occurs when n lies between ½ and 1. Glassy polymers and semi crystalline polymers (above and below T_g) are known to show such characteristics for highly sorbing penetrants. In the non-Fickian case, the diffusion coefficient is a function of time, concentration, position and even history of the sample [15, 19]. Such effects are usually attributed to slow relaxations in glassy polymers. At low penetrant concentrations, the segmental motion is much more rapid than diffusion and Fickian kinetics is observed. As the penetrant concentration increases, the polymer structure may be unable to respond fast enough to accommodate the equilibrium uptake of the solvent molecule. In that case, the rate of penetrant uptake is influenced by the rate at which the polymer segments can rearrange or relax. Unlike the Fickian case, where the rate of diffusion depends on the square of the characteristic length, the rate of relaxation is

independent of the characteristic dimension of the sample. Non-Fickian kinetics is observed when diffusion and relaxation have comparable rates. Anomalous effects may also be related to changes induced by the sorbent in the polymer structure. Case II, a special case of non-Fickian kinetics, is a completely relaxation controlled regime.

Table 2.1: Types of sorption kinetics observed in polymer-penetrant systems

Exponential Factor-*n*	**Type of Sorption**
½	Fickian or Case I
1	Case II
0<n< ½	Pseudo-Fickian
½<n<1	Anomalous or Non-Fickian
n>1	Super Case II

Depending on the rates of diffusion and relaxation, swollen and unswollen regions have been observed in the polymer [68, 69]. The swollen regions exert stresses on the unswollen material, which are gradually relieved by the relaxation process. Apart from this, stresses that may be inbuilt in the polymer due to crystallization or mechanical deformation may also relax gradually in the presence of the sorbing species leading to non-Fickian kinetics. Sorption curves for anomalous kinetics are either sigmoid or two stage. In the latter case, a quick initial uptake (diffusion controlled) is followed by a long period of slow penetrant absorption leading to equilibrium (relaxation controlled).

Petropoulos, Berens, Hopefenberg, and Durning have performed some detailed studies of non-Fickian effects in polymer-penetrant systems [10, 12, 62, 70, 71]. Several models have also been proposed which describe the phenomena. Yet, no single model can successfully predict all the observations. Crank [19] has an excellent overview of some of these models. Berens and Hopfenberg proposed a model to describe the two stage behavior [72]. This model has been discussed in detail in Chapter 4.

2.4 PLASTICIZATION

Plasticization of a polymer is said to occur when the presence of a penetrant at high concentration leads to increased segmental mobility. In terms of transport properties, this is characterized by an increase in the diffusion coefficient of the species in the polymer and a corresponding increase in its permeability [1]. In glassy polymers, with increasing pressures, the diffusion coefficient first increases and then asymptotically achieves a constant value. Plasticization leads to an increase in the diffusion coefficient beyond this asymptote. Similarly, based on the arguments related to the dual mode model, the permeability first drops with increasing pressure and then stays independent of pressure. With increasing concentrations of highly soluble gases such as CO_2, C_3H_8 or organic vapors at high pressure, the permeability starts increasing once more. The minimum in the permeability vs. pressure plot is called the plasticization pressure [73]. Figure 2.1 shows the nature of the permeability curve obtained.

In polymer membrane based gas/vapor separations, the separation efficiency of a material or its selectivity is very important. Ideal selectivity is defined as

$$\alpha^{*}_{ideal} = \frac{P_A}{P_B} = \frac{D_A S_A}{D_B S_B} \qquad 2.39$$

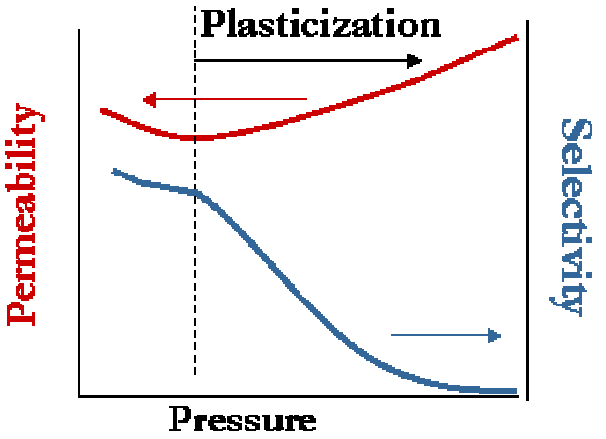

Figure 2.1: Nature of the permeability and selectivity vs. pressure plot when plasticization occurs

For mixed gas feeds, accounting for the ratio of the components in the feed, a separation factor is defined as

$$\alpha^{*} = \frac{(y_A^P / y_B^P)}{(x_A^F / x_B^F)} \qquad 2.40$$

where y_i is the component mole fraction in the permeate and x_i is the mole fraction in the feed. When feeds consist of a mixture, an increase in the polymer chain mobility is concomitant with an increase in the diffusion coefficient and permeability of both, the plasticizing and the non-plasticizing penetrants. Plasticization affects the slower gas more than the faster gas. Thus, it leads to a decrease in the diffusivity selectivity of the membrane. If the faster diffusing gas is also the faster permeating gas, the permselectivity also drops. This characteristic of gas transport becomes a very powerful tool in detecting plasticization. Even though selectivity is not very important for barrier materials, its

measurement can be used to confirm plasticization effects and gas mixtures can be used to provide valuable information about the polymer morphology.

2.5 REFERENCES

1. Kroschwitz, J.I., ed. *Encyclopedia of Polymer Science and Engineering*. Second Edition ed. Vol. Supplement Volume. 1989, John Wiley: New York.

2. Stern, S.A., *Gas diffusion in rubbery and glassy polymers,*, in *Barrier Polymers and Structures*, W.J. Koros, Editor. 1990, American Chemical Society: Washington DC.

3. Berens, A.R. and H.B. Hopfenberg, *Diffusion of organic vapors at low concentrations in glassy PVC, polystyrene, and PMMA.* Journal of Membrane Science, 1982. **10**(2-3): p. 283-303.

4. Stannett, V., et al., *Sorption and transport of water vapor in glassy polyacrylonitrile.* Polymer Engineering and Science, 1980. **20**(4): p. 300-4.

5. Koros, W.J., et al., *Effect of pressure on carbon dioxide transport in poly(ethylene terephthalate).* Journal of Applied Polymer Science, 1977. **21**(11): p. 2899-904.

6. Koros, W.J., A.H. Chan, and D.R. Paul, *Sorption and transport of various gases in polycarbonate.* Journal of Membrane Science, 1977. **2**(2): p. 165-90.

7. McDowell, C.C., B.D. Freeman, and G.W. McNeely, *Acetone sorption and uptake kinetics in poly(ethylene terephthalate).* Polymer, 1999. **40**(12): p. 3487-3499.

8. Stannett, V., et al., *Sorption and transport of water vapor in glassy polyacrylonitrile*. 1978, Dep. Chem. Eng.,North Carolina State Univ.,Raleigh,NC,USA. p. 21 pp.

9. Billovits, G.F. and C.J. Durning, *Penetrant transport in semicrystalline poly(ethylene terephthalate).* Polymer, 1988. **29**(8): p. 1468-84.

10. Durning, C.J., L. Rebenfeld, and W.B. Russel, *Integral sorption with induced crystallization.* Polymer Engineering and Science, 1986. **26**(15): p. 1066-78.

11. Serad, G.E., et al., *Gas and vapor sorption and diffusion in poly(ethylene terephthalate).* Polymer, 2001. **42**(16): p. 6929-6943.

12. Berens, A.R., *Transport of plasticizing penetrants in glassy polymers.* Polymer Preprints (American Chemical Society, Division of Polymer Chemistry), 1989. **30**(1): p. 5-6.

13. Paul, D.R., M. Garcin, and W.E. Garmon, *Solute diffusion through swollen polymer membranes.* Journal of Applied Polymer Science, 1976. **20**(3): p. 609-25.

14. Skirrow, G. and K.R. Young, *Sorption, diffusion, and conduction in polyamide-penetrant systems. 1. Sorption phenomena.* Polymer, 1974. **15**(12): p. 771-6.

15. Rogers, C.E., *Permeation of gases and vapors in polymers*, in *Polym. Permeability*. 1985. p. 11-73.

16. Dhoot, S.N., B.D. Freeman, and M.E. Stewart, *Sorption and Transport of Linear Esters and Branched Alkanes in Biaxially Oriented Poly(ethylene terephthalate).* Industrial & Engineering Chemistry Research, 2004. **43**(12): p. 2966-2976.

17. Crank, J., *Methods of deducing the diffusion coefficient and its concentration dependence from sorption experiments.* Transactions of the Faraday Society, 1955. **51**: p. 1632-41.

18. Crank, J., *Diffusion coefficients in solids, their measurement and significance.* Discussions of the Faraday Society, 1957. **No. 23**: p. 99-104.

19. Crank, J., *The Mathematics of Diffusion. 2d Ed*. 1975. 414 pp.

20. Neogi, P., ed. *Diffusion in Polymers*. Plastics Engineering, ed. H.D. E. 1996, Marcel Dekker Inc: New York. 309

21. Dhoot, S.N., B.D. Freeman, and M.E. Stewart, *Sorption and transport of linear and branched ketones in biaxially oriented polyethylene terephthalate.* Polymer, 2004. **45**(16): p. 5619-5628.

22. Hines, A.L. and R.N. Maddox, *Mass Transfer-Fundamentals and Applications*. 1985, New Jersey: Prentice-Hall, Inc.

23. Crank, J., *The Mathematics of Diffusion*. 1956. 347 pp.

24. Chow, T.S., *Glass transition temperature of polymer-diluent systems.* Ferroelectrics, 1980. **30**(1-4): p. 139-45.

25. Couchman, P.R. and F.E. Karasz, *A classical thermodynamic discussion of the effect of composition on glass-transition temperatures.* Macromolecules, 1978. **11**(1): p. 117-19.

26. Chiou, J.S., Y. Maeda, and D.R. Paul, *Gas and vapor sorption in polymers just below Tg.* Journal of Applied Polymer Science, 1985. **30**(10): p. 4019-29.

27. Durning, C.J., et al., *Solvent-induced crystallization. I. Crystallization kinetics.* Journal of Polymer Science, Part B: Polymer Physics, 1986. **24**(6): p. 1321-40.

28. Mizoguchi, K., et al., *Crystallization of poly(ethylene terephthalate) under high-pressure gases.* Polymer Communications, 1990. **31**(4): p. 146-8.

29. Osborne, J.L., H.B. Hopfenberg, and W.J. Koros, *The effect of sorbed penetrants on the aging of previously dilated glassy polymer powders. IV.* Journal of Applied Polymer Science, 1991. **43**(12): p. 2317-28.

30. Al-Juaied, M. and W.J. Koros, *Performance of natural gas membranes in the presence of heavy hydrocarbons.* Journal of Membrane Science, 2006. **274**(1-2): p. 227-243.

31. Koros, W.J., S.M. Jordan, and G.K. Fleming, *Processes to condition gas permeable membranes*. 1988, (University of Texas System, USA). Application: US
US. p. 21 pp.

32. Damle, S. and W.J. Koros, *\"Sorp-vection\": An unusual membrane-based separation.* AIChE Journal, 2005. **51**(5): p. 1396-1405.

33. Billmeyer, J.W., *Textbook of Polymer Science*. 3rd ed. 1984, New York: John Wiley & Sons Inc. 578 pp.

34. Michaels, A.S. and H.J. Bixler, *Solubility of gases in polyethylene [and rubbery polymers].* Journal of Polymer Science, 1961. **50**: p. 393-412.

35. Michaels, A.S. and R.B. Parker, Jr., *The determination of solubility constants for gases in polymers.* Journal of Physical Chemistry, 1958. **62**: p. 1604.

36. Michaels, A.S., *Diffusion of gases in polyethylene terephthalate.* Journal of Applied Polymer Science, 1963. **34**(1): p. 13.

37. Michaels, A.S., *Solution of gases in Polyethylene Terephthalate.* Journal of Applied Polymer Science, 1963. **34**(1): p. 1-12.

38. Lin, J., et al., *The effect of crystallinity on oxygen and carbon dioxide gas barrier properties of PET.* Annual Technical Conference - Society of Plastics Engineers, 2001. **59th**(Vol. 3): p. 3488-3492.

39. Olson, B.G., et al., *Positron Annihilation Lifetime Spectroscopy of Poly(ethylene terephthalate): Contributions from Rigid and Mobile Amorphous Fractions.* Macromolecules, 2003. **36**(20): p. 7618-7623.

40. Lin, J., S. Shenogin, and S. Nazarenko, *Oxygen solubility and specific volume of rigid amorphous fraction in semicrystalline poly(ethylene terephthalate).* Polymer, 2002. **43**(17): p. 4733-4743.

41. Dlubek, G., et al., *Glass transition and free volume in the mobile (MAF) and rigid (RAF) amorphous fractions of semicrystalline PTFE: a positron lifetime and PVT study.* Polymer, 2005. **46**(16): p. 6075-6089.

42. Thistlethwaite, T., R. Jakeways, and I.M. Ward, *The crystal modulus and structure of oriented poly(ethylene terephthalate).* Polymer, 1988. **29**(1): p. 61-9.

43. Ward, I.M., *Development of molecular orientation and mechanical properties in polyethylene terephthalate.* Polymer Preprints (American Chemical Society, Division of Polymer Chemistry), 1999. **40**(1): p. 575-576.

44. Slee, J.A., et al., *The transport of oxygen through oriented poly(ethylene terephthalate).* Journal of Polymer Science, Part B: Polymer Physics, 1989. **27**(1): p. 71-83.

45. Foot, J.S. and I.M. Ward, *Cold drawing of amorphous poly(ethylene terephthalate).* Journal of Materials Science, 1975. **10**(6): p. 955-60.

46. Bower, D.I., et al., *Molecular orientation in biaxially oriented sheets of poly(ethylene terephthalate). II. Correlation of orientation averages with measured mechanical compliances.* Journal of Polymer Science, Part B: Polymer Physics, 1986. **24**(7): p. 1481-92.

47. Kotani, T., J. Sweeney, and I.M. Ward, *The measurement of transverse mechanical properties of polymer fibers.* Journal of Materials Science, 1994. **29**(21): p. 5551-8.

48. Lapersonne, P., D.I. Bower, and I.M. Ward, *Molecular orientation and conformational changes due to uniaxial-planar deformation of poly(ethylene terephthalate) films.* Polymer, 1992. **33**(6): p. 1277-83.

49. Peterlin, A., *Dependence of diffusive transport on the morphology of crystalline polymers.* Journal of Macromolecular Science, Physics, 1975. **B11**(1): p. 57-87.

50. Lapersonne, P., D.I. Bower, and I.M. Ward, *Benzene ring orientation in uniaxial-planar poly(ethylene terephthalate) films.* Polymer, 1992. **33**(6): p. 1266-76.

51. Barrer, R.M., J.A. Barrie, and J. Slater, *Sorption and diffusion in ethyl cellulose. III. Comparison between ethyl cellulose and rubber.* Journal of Polymer Science, 1958. **27**: p. 177-97.

52. Koros, W.J., *Sorption and transport of gases in glassy polymers*, in *Chemical Engineering*. 1977, University of Texas: Austin. p. 274 pp.

53. Koros, W.J., et al., *A model for permeation of mixed gases and vapors in glassy polymers.* Journal of Polymer Science, Polymer Physics Edition, 1981. **19**(10): p. 1513-30.

54. Barrer, R.M., *Diffusivities in glassy polymers for the dual mode sorption model.* Journal of Membrane Science, 1984. **18**: p. 25-35.

55. Petropoulos, J.H., *On the dual mode gas transport model for glassy polymers.* Journal of Polymer Science, Part B: Polymer Physics, 1988. **26**(5): p. 1009-20.

56. Petropoulos, J.H., *A generalized, topologically consistent, dual-mode transport model for glassy polymer-gas systems.* Journal of Polymer Science, Part B: Polymer Physics, 1989. **27**(3): p. 603-20.

57. Vieth, W.R. and K.J. Sladek, *Model for diffusion in a glassy polymer.* Journal of Colloid Science, 1965. **20**(9): p. 1014-33.

58. Koros, W.J., *Model for sorption of mixed gases in glassy polymers.* Journal of Polymer Science, Polymer Physics Edition, 1980. **18**(5): p. 981-92.

59. Maeda, Y. and D.R. Paul, *Effect of antiplasticization on gas sorption and transport. III. Free volume interpretation.* Journal of Polymer Science, Part B: Polymer Physics, 1987. **25**(5): p. 1005-16.

60. Vrentas, J.S., J.L. Duda, and H.C. Ling, *Antiplasticization and volumetric behavior in glassy polymers.* Macromolecules, 1988. **21**(5): p. 1470-5.

61. Vieth, W.R., J.M. Howell, and J.H. Hsieh, *Dual sorption theory.* Journal of Membrane Science, 1976. **1**(2): p. 177-220.

62. Petropoulos, J.H., *Mechanisms and theories for sorption and diffusion of gases in polymers.* Polym. Gas Sep. Membr., 1994: p. 17-81.

63. Berens, A.R., *Sorption of organic liquids and vapors by rigid PVC.* Journal of Applied Polymer Science, 1989. **37**(4): p. 901-13.

64. Flory, P.J., *Statistical Mechanics of Swelling of Networks Structures.* J. Chem. Phy., 1949. **18**(1): p. 108-113.

65. Fujita, H., *Diffusion in Polymer-Diluent Systems.* Fortschr. Hochpolym.-Forsch.,, 1961. **3**: p. 1-47.

66. Stern, S.A., S.M. Fang, and H.L. Frisch, *Effect of pressure on gas permeability coefficients. New application of \"free volume\" theory.* Journal of Polymer Science, Polymer Physics Edition, 1972. **10**(2): p. 201-19.

67. Stern, S.A., S.S. Kulkarni, and H.L. Frisch, *Tests of a \"free-volume\" model of gas permeation through polymer membranes. I. Pure carbon dioxide, methane, ethene, and propane in polyethylene.* Journal of Polymer Science, Polymer Physics Edition, 1983. **21**(3): p. 467-81.

68. Thomas, N.L. and A.H. Windle, *A theory of case II diffusion.* Polymer, 1982. **23**(4): p. 529-42.

69. Hopfenberg, H.B., L. Nicolais, and E. Drioli, *Relaxation controlled (case II) transport of lower alcohols in poly(methyl methacrylate).* Polymer, 1976. **17**(3): p. 195-8.

70. Peterlin, A., *Type II diffusion.* Organic Coatings and Plastics Chemistry, 1978. **39**: p. 121-2.

71. Durning, C.J. and W.B. Russel, *A mathematical model for diffusion with induced crystallization. 1.* Polymer, 1985. **26**(1): p. 119-30.

72. Berens, A.R. and H.B. Hopfenberg, *Diffusion and relaxation in glassy polymer powders. 2. Separation of diffusion and relaxation parameters.* Polymer, 1978. **19**(5): p. 489-96.

73. Bos, A., *High pressure CO2/CH4 separation with glassy polymer membranes - Aspects of CO2-induced plasticization*, in *Membrane Technology Group*. 1996, University of Twente: Twente.

CHAPTER 3 : MATERIALS AND EXPERIMENTAL METHODS

The aim of this chapter is to describe the polymer samples and the characterization methods used in this work. The polymer-penetrant system is introduced in section 3.1. Apart from polymer sample selection, identification of methanol as a flavor molecule simulant is discussed in detail. Transport properties of the barrier material have been characterized using pure and mixed gas/vapor permeation. The equipment and procedure adopted for these measurements are described in section 3.2. Pure gas and vapor sorption has also been used extensively in this research, and is described in section 3.3. Finally, polymer properties such as glass transition and crystallinity are discussed in section 3.4.

3.1 MATERIALS

Poly(ethylene terephthalate) (PET) has been chosen as the model barrier material for this research. It is the current state-of-the-art beverage packaging material being used in the beverage industry. This polymer has been studied by many researchers for gas permeation and vapor sorption properties of pure penetrants but there are no studies on multi-component permeation. Samples have been chosen to suitably model the package morphology. While the choice of gases was fairly straight forward, choosing a flavor molecule or a simulant required considerable effort. Several compounds were tested, and finally methanol was chosen as the model flavor compound.

3.1.1 Polymer Samples

For beverage packaging, the PET resin is blow molded to obtain the desired bottle shape. This process leads to bi-axial orientation and crystallization in the bottle side wall. The orientation and crystallinity add more complexity to the sample morphology as compared to the completely amorphous sample. To understand differences induced by these effects, comparison with an amorphous, unoriented sample is essential. Therefore, three samples have been chosen to span the range of morphologies observed. These samples have been supplied by The Coca Cola Co. and are believed to have been prepared by melt extrusion [1]. These samples have been used for methanol sorption and multi-component transport studies. A fourth sample, a thin film, has been chosen primarily for pure vapor sorption studies.

- *Unoriented Amorphous PET*- This sample represents the base case as mentioned above. The film is 29.2 ± 1.25 microns in thickness
- *Oriented, Semicrystalline, Annealed PET*- This sample has an added level of complexity due to crystallinity and orientation. However, annealing of the sample at temperatures above glass transition relieves stresses that are built in during the crystallization and orientation process. This film is 18.6 ± 1.0 microns thick. Upon heating at 120^{o}C, this film shrank by 3% in either direction, indicating its shrinkage stabilized morphology.
- *Oriented, Semicrystalline, Non-annealed PET*- This film closely mimics the actual bottle sample as it is not annealed and residual stresses are expected to be present in the sample. These residual stresses can affect the transport properties. The thickness of the film is 15.2 ± 1.0 microns. Annealing at 120^{o}C of this film caused shrinkage of

20% in the x- and y-dimensions. This suggests that the film is biaxially oriented with equal draw ratio in the machine and transverse direction.

- *Biaxially Oriented, Semicrystalline PET*- This is a 1.5 ± 0.15 microns thick film, which has been procured from GoodFellow Co. (Devon, PA). Being very thin, this sample was used for sorption studies to obtain an initial estimate of the diffusion coefficients of various organics. Equilibrium sorption and kinetics of lower alcohols were later measured for this sample.

3.1.3 Gases

The important gases for carbonated beverage packaging are carbon dioxide and oxygen. 99.999%, Research Grade, carbon dioxide and oxygen, supplied by Air Gas (Radnor, PA), have been used for the present studies. A maximum testing pressure of 100 psia has been chosen for carbon dioxide because it is close to the bottle filling pressure in the industry [2]. Higher pressures have been avoided because CO_2 can condition or plasticize the polymer [3, 4]. Oxygen is used up to a maximum pressure of 150 psia. Higher than atmospheric pressure is employed because oxygen flux at low pressure is small. Being a "non-interacting gas", high pressure oxygen does not change the polymer matrix and can be used to get a higher permeation rate with the measurements easily extrapolated to lower pressures.

3.1.3 Vapor Selection

Identification of methanol as a suitable organic for multi-component permeation was an essential part of this work. The most important issue which impacted the identification of a suitable flavor compound was its diffusion coefficient. Flavor molecules are organic

compounds, often large molecules with branching and cyclization [5]. As a result, their diffusion coefficients are quite low, and typically of the order of $10^{-14}cm^2/s$ or less. In a film of thickness 29.2μm, the time lag (refer to Figure 3.4) is determined to be 4.5 years using Equation 3.1. This necessitates the need to look at smaller molecules which act as flavor simulants. Moreover, from a fundamental standpoint, use of larger molecules holds no advantages over smaller organics. Smaller molecules with polar groups that can interact with the polymer work well for the purposes of this study. With this in mind, lower alcohols were studied to estimate their diffusion coefficients. The McBain quartz spring sorption method, described in section 3.3.2 has been used for the measurements.

Isopropanol (IPA) was the first *model* compound that was considered. Thin, bi-axially oriented films of thickness 1.5μ, procured from GoodFellow Co. were used so that equilibrium is attained in a much shorter time. While the kinetics shows some polymer relaxation effects at 13.1mm Hg, the diffusion coefficient is determined to be 4.8±0.2 $x10^{-14}$ cm^2/s using the data at small times and equation 2.37. Figure 3.1 shows the plot of the kinetics obtained.

While permeation studies with PET films of thickness 1.5μm can be performed in a reasonable time frame with IPA, available unsupported films of this thickness were defective. This film is manufactured by bi-axial stretching from the melt which leads to small pin-hole type defects [6]. Such defects are too numerous to caulk while obtaining a large enough testable area. Moreover, the caulking layer may add artifacts in the permeation results. Consequently, this film is unsuitable for permeation experiments. This necessitated the consideration of compounds with higher diffusion coefficients which could be studied with the 29.2μ thick films. n-propanol, ethanol and methanol

were studied in the order of decreasing size to estimate their diffusion coefficients. As can be seen in figure 3.1, n-propanol at 5.7mm Hg, has a diffusion coefficient of 2.7×10^{-13} cm^2/s, and ethanol was found to have a diffusion coefficient of 3.4×10^{-12} cm^2/s at 10.5 mmHg. Even though these diffusivities are higher than i-propanol, they are still too low for convenient permeation studies. The diffusivity of methanol was found to be 2.4×10^{-10} cm^2/s at 40mmHg, 35°C in the amorphous PET film (thickness 29.2µm) and is ideal for permeation studies. The kinetics, shown in Figure 3.2, is also Fickian at these low activities. Given the polar nature of methanol, it is a reasonable simulant of flavor molecules that interact with the polymer matrix. *Therefore, methanol was selected for the detailed work to probe the effects of organic penetrants on both CO_2 and O_2.*

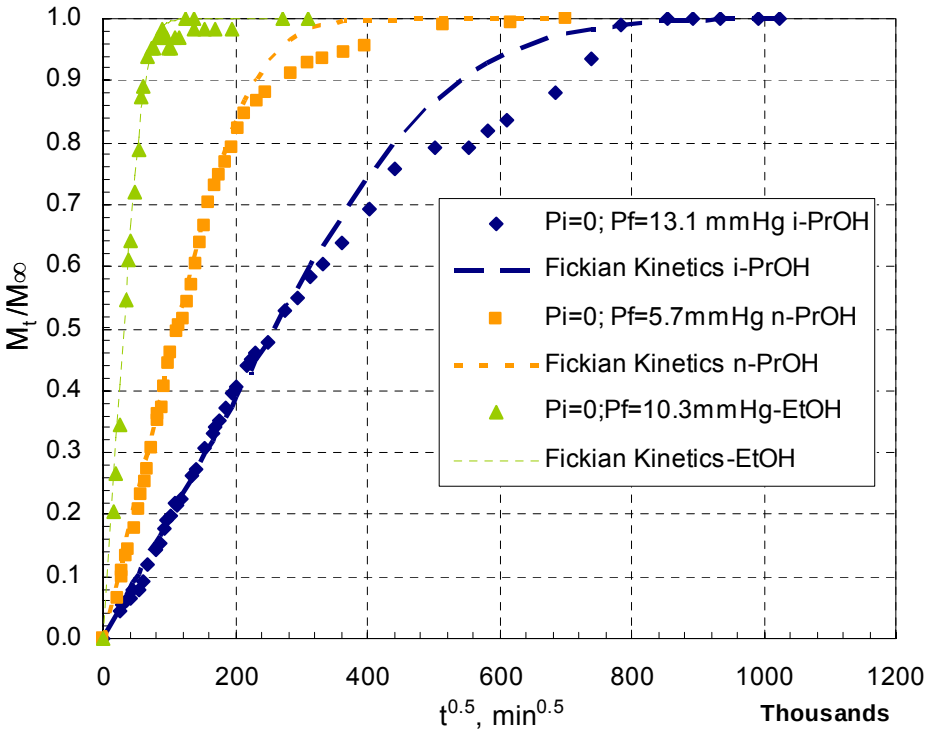

Figure 3.1: Sorption kinetics of ethanol, n-propanol and isopropanol at 35°C, in 1.5µm thick PET film

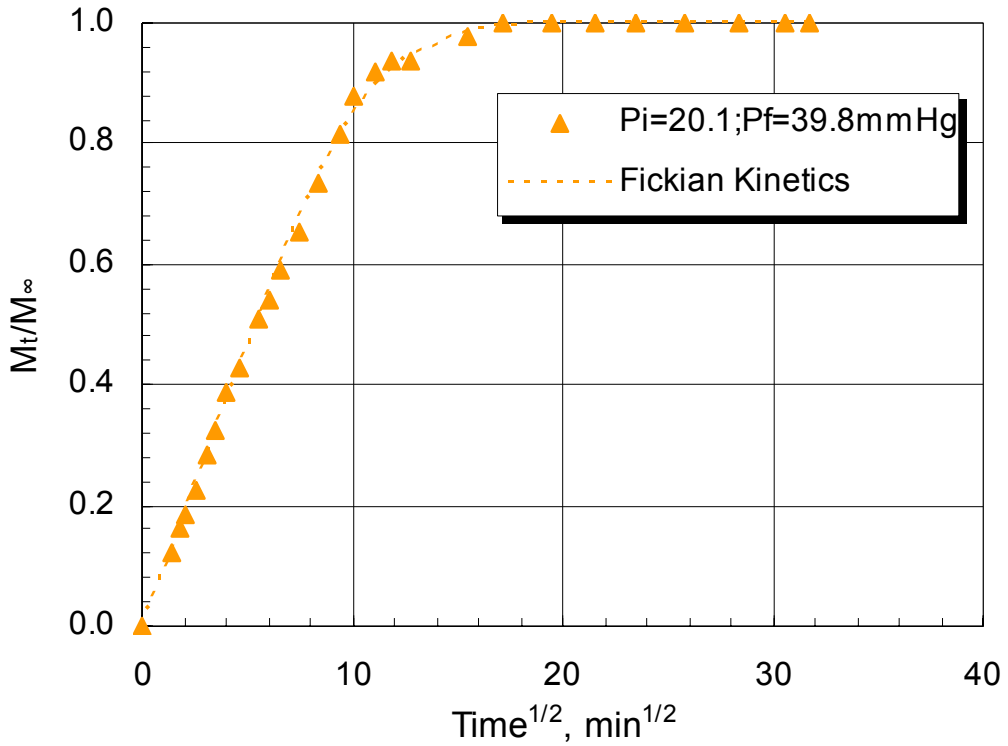

Figure 3.2: Methanol sorption kinetics at 39.8 mmHg, 35°C in the amorphous PET film

3.2 Gas Permeation Methods

Pure and mixed gas/vapor permeation experiments are the primary methods of material characterization used in this research. This section describes the procedure and the equipment used for pure gas, mixed gas, and multi-component gas/vapor permeation. The constant volume, variable pressure method has been used for all permeation experiments [7]. The equipment design, along with the sample mounting methods, has been discussed below.

3.2.1 Gas Permeation Equipment

A schematic of the permeation set-up used for pure O_2, CO_2, and mixtures of O_2/CO_2 is shown in Figure 3.3 below. The system is enclosed in an insulated box and the

temperature is regulated at 35°C by a temperature controller from Thermoworks (Alpine, UT) and an RTD probe thermocouple from Cole-Parmer (Vernon-Hills, IL). All fittings and valves are 316 SS, Swagelok® VCR® fittings. Valves B, C, D, and G in Figure 3.3 are long handle, bellows sealed metal valves (SS-4UW-V13) with handles outside the box to allow opening and closing without disturbing the temperature. Valves A, E, F, I and J are bellows sealed valves (SS-4H-V13); while H is a metering valve (SS-MGVR4-MH). Upstream pressures are measured with an absolute pressure transducer (maximum pressure 1000 psia) and accompanying readout (Sensotec, Columbus, OH). Downstream pressures are measured using a Baratron® 121AA capacitance manometer with a maximum pressure output of 10Torr (MKS, Wilmington, MA). The signal conditioner for the transducer is placed outside the box to eliminate any influence of temperature. The pressure is read using an MKS readout and power supply, model PDR 5-B. The system is evacuated using a 3-stage mechanical pump, model RV-3 (BOC Edwards, Wilmington, MA), fitted with an alumina filled trap (ForeLine®, model FL20K) to prevent back diffusion of pump oil. The permeation cell (labeled 5 in Figure 3.3) and masking methods have been described in section 3.2.1.1.

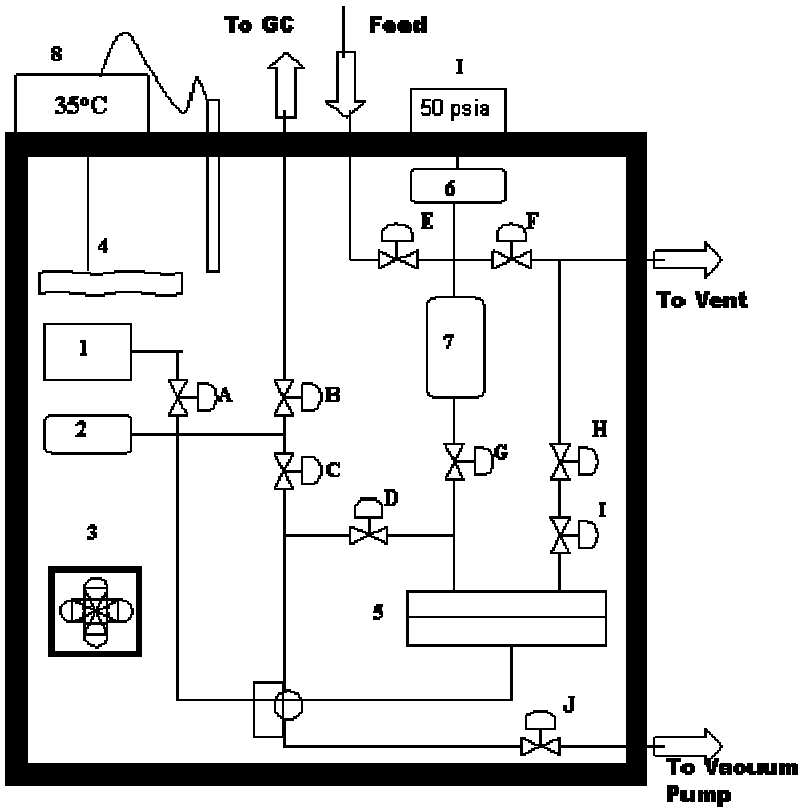

Figure 3.3: Schematic of the permeation system. Downstream pressure transducer(1), Downstream volume (2), Fan (3), Heating tape (4), Permeation Cell (5), Upstream pressure transducer (6), Upstream gas ballast (7), Temperature controller and readout (8)

Permeability is calculated from the steady state pressure rise in a constant volume at a constant temperature. A typical plot of the pressure vs. time data is shown in Figure 3.4. Data is collected using a data acquisition card (Keithley, KPCI-3107) and Labview program (National Instruments). As can be seen in Figure 3.4, when permeation first starts, there is some time (θ), at which the gas pressure on the downstream side of the membrane starts rising. This time is called the time lag. Along with the thickness (l) of

the film, θ can be used to evaluate the diffusivity of the gas at the upstream pressure using Equation 3.1.

$$D = \frac{l^2}{6\theta} \qquad 3.1$$

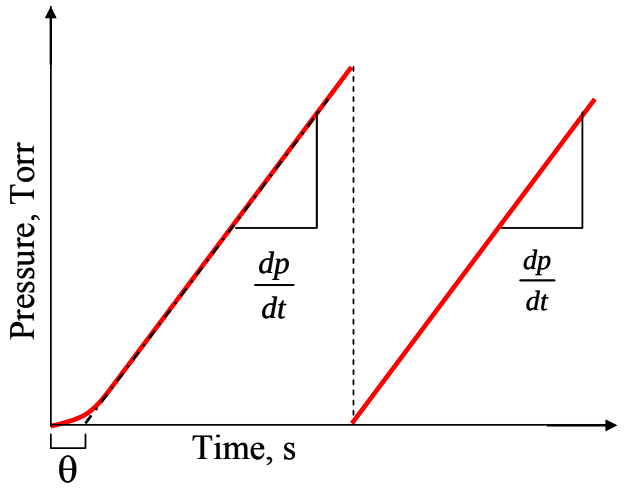

Figure 3.4: Typical plot of pressure vs. time obtained during permeability measurement

Steady state is achieved after 10 time lags and the slope dp/dt is used to calculate the permeability. Thus, pure gas permeation experiments have been used to obtain both, diffusivity and permeability. In the case of mixtures, only the steady state permeability of the components is calculated as the time lag can give no information about the diffusivity of the individual components. In both pure and mixed gas experiments, after permeation at steady state for some time, the downstream is evacuated and the permeate is collected again to obtain the slope. This procedure allows one to double check that steady state has been achieved.

In pure gas permeation, the upstream gas ballast is filled with the gas at constant pressure, and valves I and H in Figure 3.3 are closed off. In mixed gas permeation experiments, the feed stream flows past the film to ensure that the composition of the mixture in contact with the film does not change. The flow rates used are more than 100 times the permeation flux (stage cut of 1% or less), an essential condition to prevent concentration polarization in the upstream. The metering valve, H, in Figure 3.3 controls the flow rate, which is measured using a flow meter (MKS, model M10MB) connected to a power supply and readout (MKS, PR 4000). Permeate collected in the downstream is expanded across valve B into the sample loop of a gas chromatograph (model 6890N, Agilent Technologies, Palo Alto, CA) to characterize the composition of the permeate and calculate individual gas permeabilities. Details of the GC, its operating conditions, column calibration and a sample calculation are provided in Appendix A. The reader is also referred to several other reports of mixed and pure gas permeation systems [8-12].

3.2.1.1 Membrane masking

The design of typical permeation cells and membrane masking methods used for barrier materials has been described in detail by Moore et al [13]. The only difference in the permeation cell used in this work is that its downstream O-ring (Viton™, Dupont, Wilmington, DE) has a larger diameter than the upstream o-ring, as shown in Figure 3.5.. The film is sandwiched between two pieces of impermeable, adhesive backed aluminum tape (Fasson® 802, Avery Denison Specialty Tape Division; Pasadena, CA). This sandwich is then taped down onto the downstream surface using another piece of adhesive backed aluminum tape of diameter 3" (less than downstream o-ring groove I.D. and larger than upstream o-ring groove O.D.). The sintered metal (316 SS, Grade 1;

Metron Technology, Austin, TX) provides support to the film and can withstand hundreds of pounds of pressure. A piece of Whatman™ filter paper is used to help evenly distribute the permeate. A schematic is shown below.

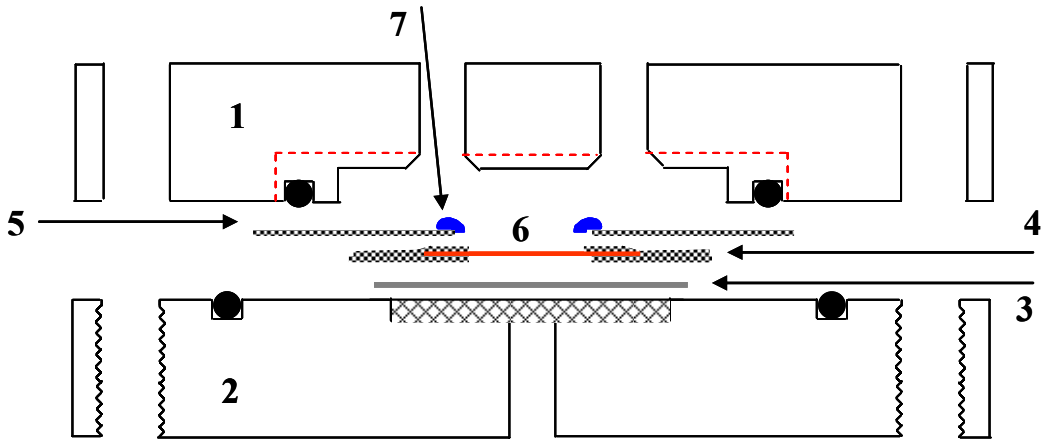

Figure 3.5: Permeation cell and schematic of the PET film masking method. Upstream half of the cell (1), Downstream half with sintered metal(2), Whatman™ filter paper (3), Sandwich of film between adhesive backed Aluminum tape (4), Ahdesive backed Aluminum tape to mount film on the downstream cell (5), Polymer film (6), Epoxy (7)

In the sandwich mask described by Moore et al [13], the upstream o-ring is larger in diameter than the downstream o-ring. Thus, while masking, the diameter of the tape (5 in figure 3.5) must be less than the I.D. of the downstream o-ring groove. The outer edge of this tape provides an alternate path for the gas to enter the downstream by traversing through the thin layer of the acrylate based adhesive. This additional flux is measurable only after 24 hrs due to the long path around the tape and is negligible in the case of high permeability materials. However, it can be significant for barriers. This leak can lead to an overestimation of the gas permeability when testing for extended periods. By using a

smaller upstream o-ring, the gas does not come into contact with the edge of the tape and the leak path is completely sealed off. Similarly, to seal off the inner edge of the Al tape, a 2-part epoxy (5 min- Devcon®, Andover, MA) is applied at the interface of the film and tape while pulling vacuum on the downstream. This allows the epoxy to flow into the gaps. The epoxy was cured in the permeation box at 35°C for at least 3-4 hrs before the cell was closed and evacuated. Film area was obtained by scanning the mask, and using imaging software (Scion Image) to measure the area. Leak rates obtained by this masking method are on the order of 10^{-8}ccSTP/s. For accuracy, the leak rate was measured before permeation at every pressure by shutting off valve C in Figure 3.3.

3.2.2 Gas/Vapor Permeation Equipment and Methods

For permeation of feeds consisting of vapors, some changes were incorporated in the permeation equipment described above. A feed preparation system was also set-up to prepare feeds at different activities of the vapor. Several control tests to check for adsorption of methanol and the response of epoxy under methanol were performed.

3.2.2.1 Feed Preparation

To prepare vapor laden feed streams, many researchers bubble pure gas through the liquid to reach saturation; and then, based on the desired activity, mix this stream with more pure gas [14-17]. This work took a different approach and made use of a highly accurate syringe pump (Model 100DM, Teledyne Isco, Lincoln, NE) to inject the liquid into the gas stream. Figure 3.6 below is a schematic of the feed preparation system that was designed. The syringe pump can precisely control flow rates as low as 0.01μL/minute. Liquid flow rates of 2-6 micro liters per minute have been used to obtain

different activities of methanol. Corresponding gas flow rates are within 200 sccm. For such low liquid flows, a 75 psia back pressure regulator (Upchurch Scientific, Oak Harbor, WA) has been used. The barrel of the pump is also wrapped in insulation to prevent over sensitivity to room temperature fluctuation which may lead to variations in the flow. Moreover, at these low liquid flow rates, surface tension at the tube-liquid-air interface at the exit leads to droplet formation. For larger tube O.D., droplet size is higher; and consequently, the drops fall into the surrounding gas medium very infrequently. Thus, instead of a continuous gas/vapor mixture stream, pulses of the vapor will be introduced into the gas stream, which is undesirable for permeation. To avoid this problem, a poly(ether ether ketone) capillary tubing, O.D. 300μm, and I.D. 50μm, has been used (Upchurch Scientific, Oak Harbor, WA). The capillary tubing is connected to a 1/16" tee using poly(ether ether ketone) sleeves of O.D. 1/16" and I.D. 350μm, also from Upchurch Scientific. The liquid and the gas come in contact at this t-junction (refer to Figure 3.6). The incoming gas is heated to 55^{o}C to increase the liquid vaporization rate. The mixture flows through a 500 cc, heated volume in which the feed stream has a residence time of 2.5-5 minutes, to ensure complete vaporization of the liquid. This mixture then flows through a 12" long piece of ¼" diameter, SS-316, static mixer tubing (KoFlo™, Cary, IL). This tubing has internal baffles that create turbulence, leading to complete mixing of the gas-vapor feed. All these lines are heated using Power Twin™, variable resistance heaters (GlasCol, Terra Haute, IN). The heated gas mixture is cooled down by passing it through a water bath at 40^{o}C. This feed then enters the permeation box, which is at 35^{o}C. Just before this feed comes in contact with the film, the

temperature is measured using K-Type thermocouple to be 34.7-35.2°C (Omega, Stamford, CT).

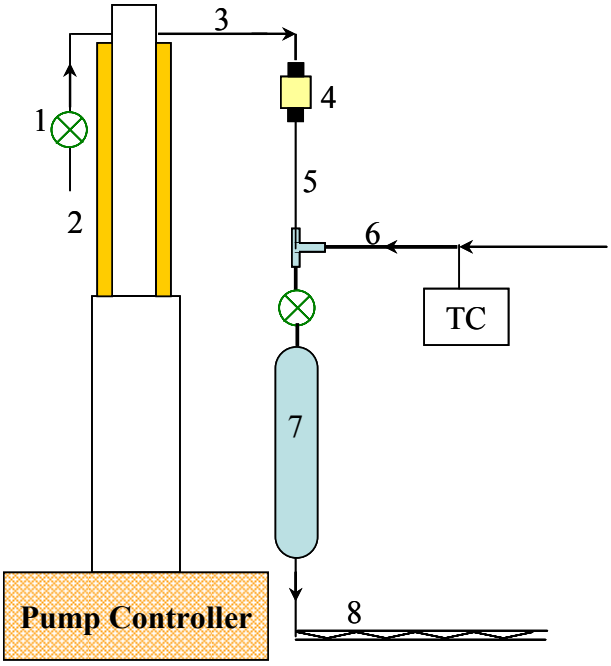

Figure 3.6: Schematic of Gas/Vapor Feed Preparation System. 1-Valve used to refill the pump; 2- Insulation around the pump barrel; 3- 1/16" SS316 Tubing; 4- 75 psia back pressure regulator; 5- 50µ ID PEEK capillary tubing; 6- Gas Inlet; 7- 500cc residence volume for liquid vaporization; 8- ¼" SS-316 KoFlo™ tubing with baffles for complete mixing; TC- Thermocouple

A complete schematic of the permeation system set-up is shown below in Figure 3.7. When the gas/vapor feed flow is first started, it flows through the bypass line without coming into contact with the film. The bypass line is connected to the GC and the composition of the feed can be analyzed. At least 2 hrs are needed after flow is first started before steady state composition of the feed is achieved and all the air is purged out of the lines. Once the desired methanol activity is achieved, the bypass valve is shut off and flow is started past the film. The total gas flow is measured with a MKS flow meter

and flow rate is regulated by a metering valve. The bypass line as well as all the transfer lines to the GC from both the upstream and the downstream are heated to 70°C or more to prevent adsorption of methanol during expansion into the GC sample loop. A detailed procedure of the characterization of methanol composition in the feed is described in Appendix A.

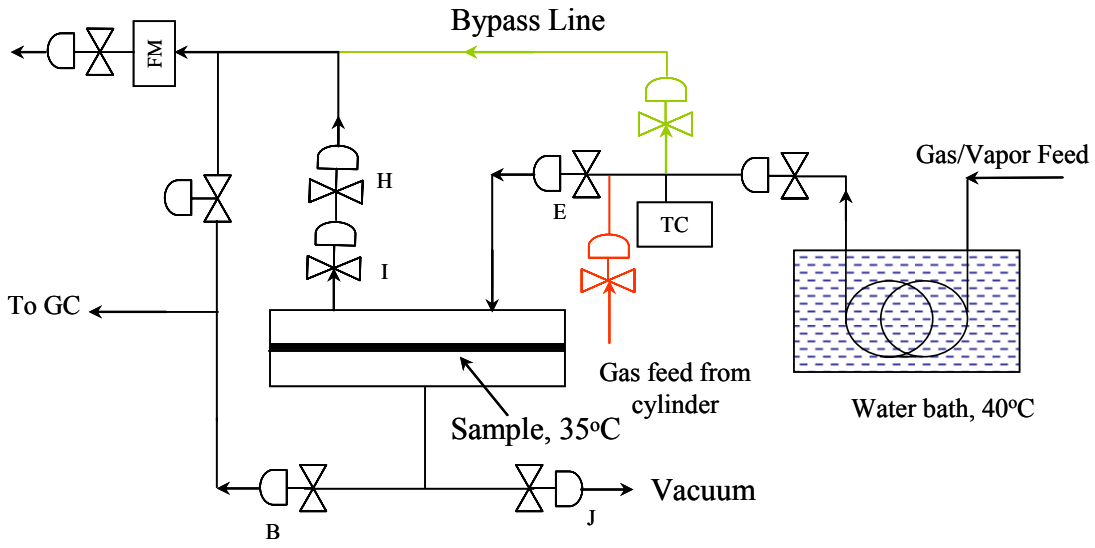

Figure 3.7: Schematic of mixed gas/vapor permeation system. The valves labeled B, E, H, I and J are the same as in Figure 3.3. The green lines indicate the by-pass line for gas/vapor feed flow. The red line shows the connection for pure gas feeds.

3.2.2.2 Methanol Adsorption

A major issue with using polar molecules such as methanol is that they adsorb on high energy surfaces such as SS-316. Since all the downstream fittings are made from this material, it is important to characterize and account for adsorption of methanol in the permeability calculations. Adsorption of water on SS-316 as well as glass has been

addressed by several researchers while performing both steady state and transient experiments [18-20]. Methanol adsorption must be characterized similarly to prevent underestimation of its permeability as a substantial fraction of the permeate may be lost to adsorption and hence, will not contribute to the measured dp/dt. To measure the extent of adsorption, the downstream half of the cell was attached to the system and sealed using a circular piece of adhesive backed aluminum tape with a filter paper beneath it. The leak rate was measured for 1-2 hrs. Thereafter, pure methanol vapor was introduced into the downstream and the pressure drop due to adsorption was observed until steady state was reached. Using the final and initial pressure information and accounting for leaks into the system, the total number of moles adsorbed was calculated. Initially, with the sintered metal and filter paper in place, nearly 50% of the methanol introduced was lost to adsorption. The sintered metal, which has a very high surface area, provides the majority of the adsorption sites. It was replaced with a SS 316 perforated disc which is able to withstand up to 200 psia. Further reduction in adsorption was achieved by replacing the Whatman™ filter paper with PTFE porous membrane (Zitex®, Saint-Gobain Performance Plastics). These changes reduced the adsorption to nearly 8% of the initial pressure. Two other methods were tried which did not lead to the desired reduction in adsorption. The first was deposition of a hydrophobic coating (Siltek™, Restek Co., Bellefonte, PA) on the inner surfaces of SS-316 fittings. A very small reduction in the adsorption was observed. Secondly, the sintered metal was replaced with a medium porosity glass frit whose surface was hydrophobized by reacting with a silane coupling agent, tridecaflouro-1,1,2,2-tetrahydrooctyl-triethoxy silane. However, significant reduction in adsorption was not observed.

Figure 3.8 shows the adsorption isotherm obtained at pressures equal to or less than 0.4 Torr. This pressure was chosen because of the need to maintain low downstream pressures of the permeate (less than 1% of the upstream pressure). As can be seen, the isotherm is linear at these low pressures. This loss of permeate due to adsorption is accounted for by correcting the methanol dp/dt with a correction factor of 1.08.

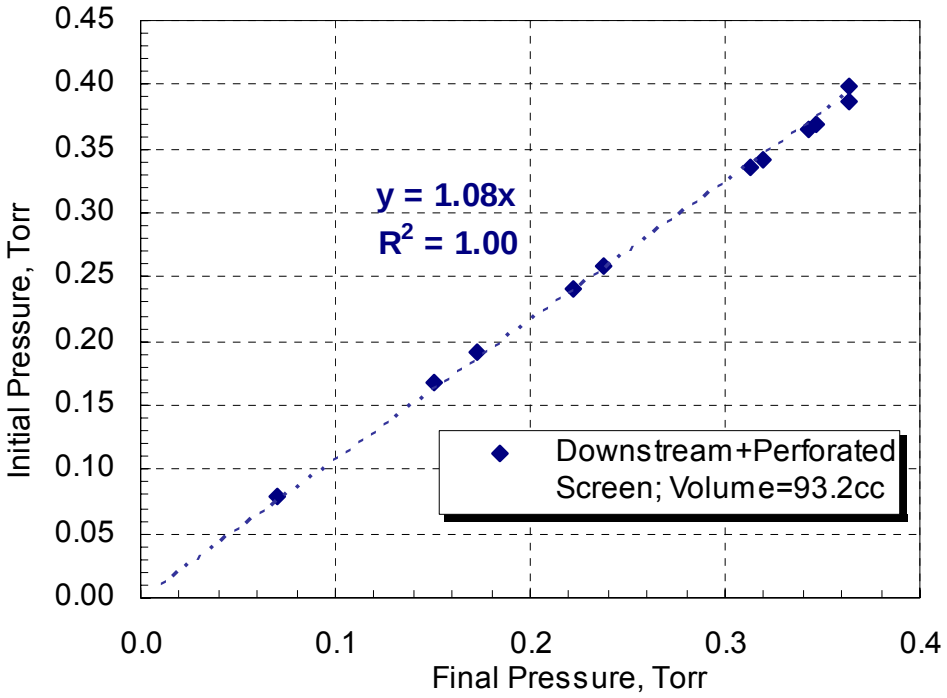

Figure 3.8: Methanol adsorption isotherm on the downstream of the permeation cell

3.2.2.3 Sample Mounting Method

Control tests on cured epoxy, immersed in liquid methanol at 25°C (p/p_o=1) for 24 hrs, showed that the epoxy swelled considerably due to methanol sorption and lost its sealant properties necessary for masking. This necessitated the elimination of epoxy from the permeation cell, which meant that the aluminum tape masking method could not be

used. Therefore, to mount the film for mixed gas/vapor permeation experiments, a larger film sample that was sealed with just the o-rings was used. A schematic is shown in Figure 3.9. This method has been used in the past and was replaced because of the difficulty in obtaining a larger, defect free area of the polymer. However, in this case, the polymer films are essentially free of defects. The large area actually helps to increase the permeation rate and reduce the time needed to collect a sufficient amount of permeate for expansion and injection into the GC.

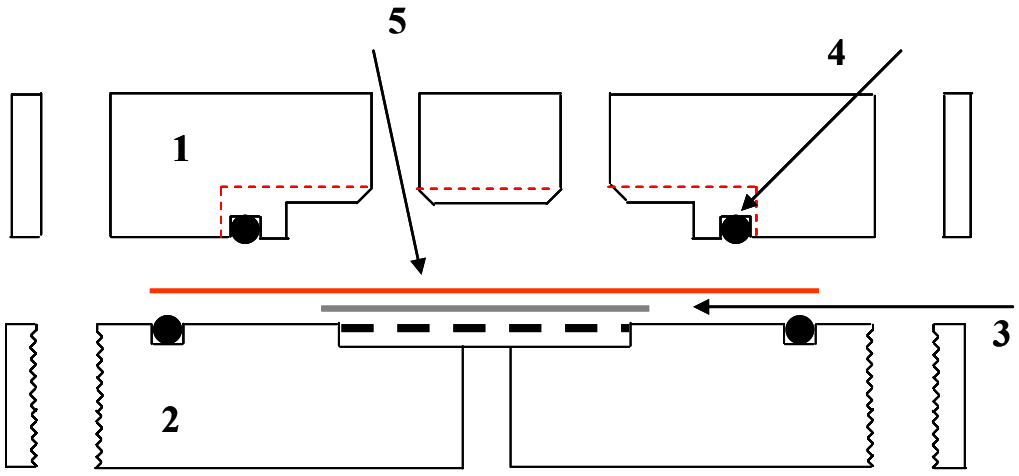

Figure 3.9: Schematic of permeation cell with sample film for mixed gas/vapor permeation. 1- Upstream; 2- Downstream; 3- Teflon™ filter membrane; 4- Viton™ O-ring; 5- Polymer film

The film is evacuated overnight and the leak rate in the downstream is measured before permeation is begun. Pure gas or CO_2/O_2 mixture permeability is measured, and then the gas/vapor feed is introduced in the upstream. For low activity methanol, the mixture is allowed to permeate for up to 24 hrs in order to reach steady state. At higher activities, permeation is maintained for 48-96 hrs to ensure steady state. The time is

determined based on sorption kinetics of pure methanol vapor. The feed is characterized 5 times to obtain the methanol activity in the upstream. Once the feed composition is found to be constant, the permeate is collected in the downstream. The total dp/dt is then measured and the permeate is expanded into the GC for composition analysis at least 5 times. This process usually takes 3-4 hrs during which the permeate is continuously collected. Care is taken to ensure that the downstream partial pressure of methanol does not exceed 1% of the upstream partial pressure. In the case of high activities, where one permeation run lasts for 3-4 days, the feed and permeate are characterized two days in a row to ensure that steady state has been achieved.

3.3 SORPTION TECHNIQUES

Sorption experiments are integral to this research, especially because of the ability to obtain both, diffusivity and solubility of the flavor simulant. The sorption isotherms are analyzed to evaluate the dual mode model parameters.

3.3.1 High Pressure Gas Sorption

The pressure decay method has been used to measure the sorption isotherm of gases at high pressures [21]. A schematic of the sorption system is shown in Figure 3.10. All measurements and calibrations have been made at 35^{o}C. Gas is filled in the reservoir and allowed to equilibrate. Then it is expanded into the cell by opening and shutting valve B quickly. The reduction in pressure in the cell, as the polymer absorbs the gas, is measured using highly accurate transducers. By doing a simple mole balance, the amount of gas

absorbed by the polymer is calculated. CO_2 and O_2 gas compressibilities have been taken from Appendix C in reference [22].

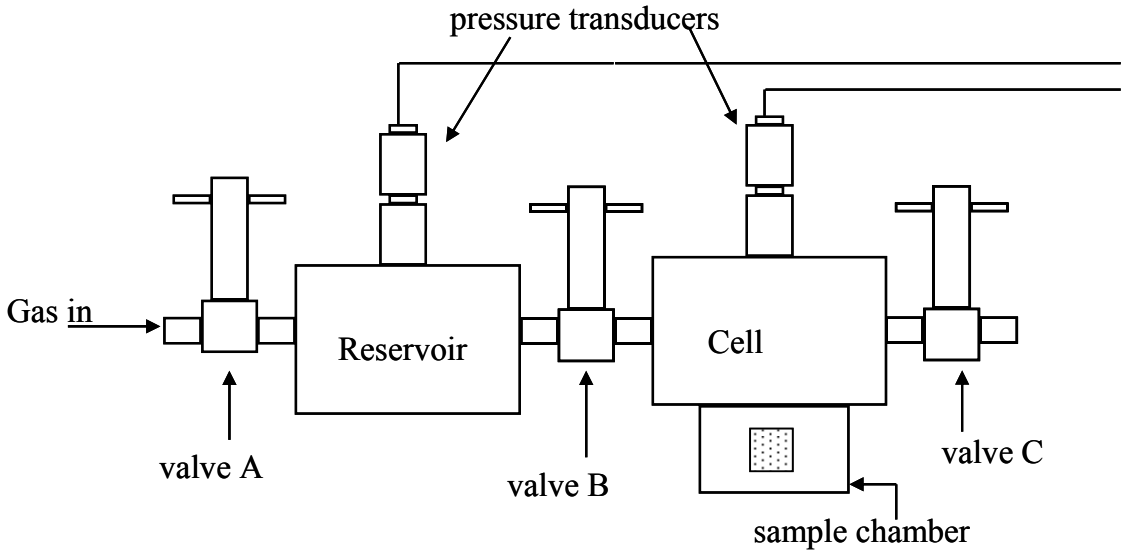

Figure 3.10: Pressure decay system used for high pressure sorption

3.3.2 Low Pressure Vapor Sorption

For sorption at sub-atmospheric pressures, the McBain quartz spring method has been used [23]. This is a gravimetric technique which involves the accurate measurement of mass of the sample using a quartz spring as it absorbs the penetrant. The extension of the spring with increasing sorption by the polymer is measured and converted into a change in mass. Sorption of lower alcohols including methanol has been done using this technique. Figure 3.11 shows a schematic of the equipment.

The sample is hung on a quartz spring (GE Sensing, Houston, TX). The spring has a maximum load of 50mg and a maximum extension of 200mm. Calibration with different masses of aluminum foil is done to obtain the spring constant. The spring hangs on a glass hook inside a chamber with a large volume. This volume is maintained at the

desired temperature (35°C in this case) by water circulation in the surrounding jacket. The rest of the manifold is heated to prevent condensation of the vapor on the side walls. The sample position is determined by focusing on a cross hair on the spring using a precision cathetometer. The smallest distance that can be read by the cathetometer is 0.0005 cm. Together, the cathetometer and the 50-200 spring provide a measurement accuracy of 1.25μg. A 1000 Torr transducer (MKS Type 622A), along with power supply and read out (MKS, PDR-C-1C), is used to measure the pressure in the chamber. The entire system is made from glass and all joints are o-ring type joints where solvent resistant Viton™ o-rings have been used. The valves have bakeable Teflon™ plugs and Viton™ o-rings. The entire system had a leak rate of less than 2 Torr/week.

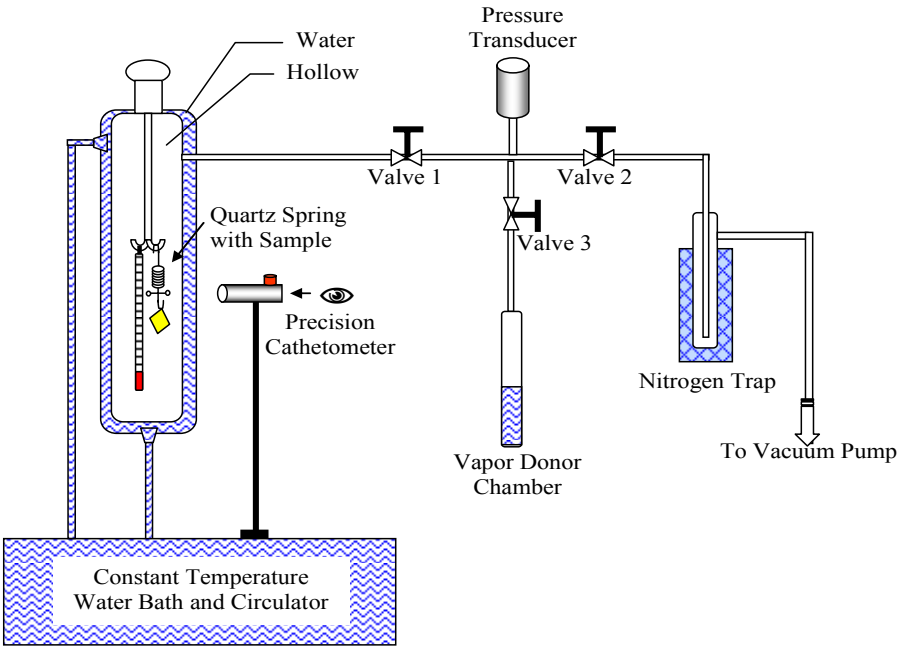

Figure 3.11: Set-up of the McBain quartz spring gravimetric sorption equipment [24]

The sample is loaded and evacuated overnight before sorption is started. During evacuation, a liquid nitrogen trap is used so that the pump oil does not back diffuse into

the chamber. Vapor is introduced from the vapor donor vial at a given pressure; however, before the vapor is introduced, all air in the headspace of the vial and air dissolved in the liquid are removed. For this, valve 1 in Figure 3.11 is shut off to isolate the sample. Then a freeze-pump-thaw cycle is carried out 5 times to evacuate the liquid headspace and remove all dissolved air. Valve 1 is then opened and valve 2 shut off. Valve 3 is opened to let the vapor into the sample chamber. Care is taken to ensure that the vapor is introduced very gradually so that the fragile spring does not oscillate too much. This can cause the spring to break or the sample to fall off from the spring. The same procedure applies when starting evacuation or venting of the system. To obtain the sorption kinetics, the spring position is recorded at different times. Equilibrium is assumed to be attained when the spring position does not change over the course of 24 hrs. Once equilibrium is reached, the pressure is increased by introducing more vapor. All experiments have been performed at 35^{o}C and up to a maximum activity of 96% for any liquid. Activities higher than this have been avoided due to the possibility of condensation. This type of step increase in pressure for sorption is called integral sorption. For desorption measurements, the chamber is evacuated gradually to reduce the pressure, again in decreasing steps of pressure.

3.4 COMPLEMENTARY CHARACTERIZATION METHODS

Complementary characterization methods have been used to obtain more information about the morphology of the polymer samples. Crystallinity, glass transition temperature, and density of all the films have been obtained.

3.4.1 Density Measurement

The density of the samples was measured using a density gradient column (Techne, Burlington, NJ). The column was filled with water-calcium nitrate solutions of two different densities to render a linear gradient in density. It was calibrated with small glass beads of known density. Small pieces of the samples were then floated into the column. Their position was visually determined and density was estimated using the calibration curve. Care was taken to ensure that there were no air-bubbles on the films as this can result in a lower apparent density. The crystalline weight fraction was calculated based on the sample density (ρ) using equation 3.2. The amorphous phase density (ρ_a) is taken to be 1.331 g/cc and the density of PET crystals (ρ_c) is taken to be 1.455 g/cc [25].

$$X_c = \left(\frac{\rho - \rho_a}{\rho_c - \rho_a} \right) \frac{\rho_c}{\rho} \qquad 3.2$$

Table 3.1: Density and crystallinity of all the samples

Sample	Density	% Crystallinity Density (w/w)	% Crystallinity DSC (w/w)	% Crystallinity WAXD(w/w)
Amorphous	1.3339	3	0.0	0.00
Semicrystalline annealed	1.3872	48	34	39
Semicrystalline non-annealed	1.3844	45	20	39
1.5μ biaxially oriented	1.3914	51	31	56

It must be noted here that there is not complete agreement in literature over the density of the ideal crystalline phase. Apart from 1.455g/cc reported by Daubeny et al [26], Fakirov et al calculated the density to be 1.515g/cc for many samples annealed between 120^{o}C and 260^{o}C and 1.484g/cc for one sample annealed at 100^{o}C [27]. The reader is referred to references in [27] for other reports of density of the crystal phase. Based on the ideal crystal density, the estimated crystallinity of the present films could vary substantially. For example, the X_c (w/w) for the annealed sample may be 47.5%, 39.3% or 33.4% depending on the ρ_c values of 1.455, 1.484 and 1.515 g/cc respectively. It was found that the value of 1.455g/cc is a well accepted value [25, 28]. Therefore, this value has been used for this work.

3.4.2 Differential Scanning Calorimetry

Another method commonly used to estimate crystallinity and the glass transition temperature is differential scanning calorimetry (DSC). The instrument used for these

measurements is model DSC 220C from Seiko Instruments (Horsham, PA). All the plots shown in Figure 3.12 below are first scans at a heating rate of 10^{o}C/min. Nitrogen flow at 50ml/min has been maintained during the heating step to prevent any oxidation of the polymer. Glass transition temperature and the ΔC_p for each film are shown in Table 3.2. These values are close to the T_g of PET, usually reported between 70-85^{o}C. A clear second order transition is not visible for the annealed sample. This could be due to crystallinity and orientation of these samples which reduce the ΔC_p of the films. Melting temperature is also shown in Table 3.2. These values match well with the typically reported T_m of 245-265^{o}C.

Table 3.2: Glass transition and melting temperature of all the samples

Sample	**T_g from DSC (^{o}C)**	**ΔC_p (J/g/^{o}C)**	**T_g from DMA (^{o}C)**	**T_m from DSC (^{o}C)**
Amorphous	74.5	0.19	85	246
Semicrystalline annealed	-	-	115	245
Semicrystalline non-annealed	75.0	0.09	116	246
1.5μ biaxially oriented	79.3	0.03	-	257

Based on the heat of fusion of the films (H_m), the specific heat of fusion of the crystals (H_f), and the heat of crystallization (H_c), the crystalline weight fraction can be calculated using equation 3.3. A specific heat of fusion value of 121.2 J/g has been used for this work [29, 30]. There are reports of heat of fusion values as high as 140 J/g but the

former value is more commonly used [31]. Unlike the amorphous film, a clear cold crystallization exotherm is absent for the semi-crystalline samples due to pre-existing crystallinity. However, the non-annealed film does show a broad exothermic peak with an onset temperature of 77^{o}C. Similarly, this broad peak occurs in the biaxially oriented film with onset at 80^{o}C. These onset temperatures are low when compared with crystallization peak in the unoriented, amorphous film at 150^{o}C with an onset temperature of 139^{o}C. Nevertheless, this peak can be due to cold crystallization of some oriented regions in the polymer which gain sufficient mobility at lower temperatures and crystallize. The lack of a cold crystallization exotherm in the annealed sample is likely to be due to prior annealing above T_g that leads to crystallization of such regions. Similar peaks are observed by Liu et al who studied various PET bottle samples [32]. The heat set bottle sample shows no exotherm while both, cold and hot blown bottle samples showed such an exotherm. Estimated weight percent crystallinities are shown in Table 3.1. Upon comparison, it is notable that the degree of crystallinity estimated from density and DSC measurements is substantially different. This will be discussed in section 3.4.5.

$$X_c = \frac{H_m - H_c}{H_f} \qquad 3.3$$

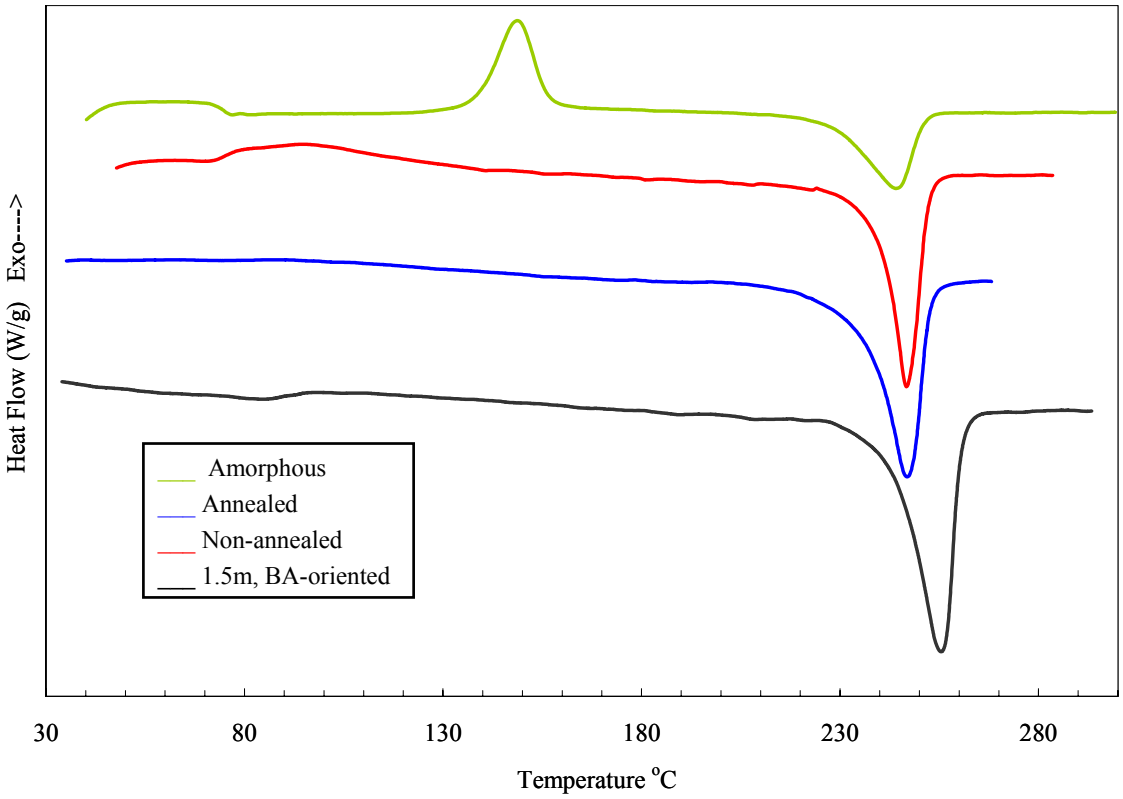

Figure 3.12: DSC plots of amorphous and semicrystalline samples

3.4.3 Wide Angle X-Ray Diffraction

Wide angle X-ray diffraction studies were performed on a Rigaku Micro Max 002 system. Cu K-α x-ray source with Ni filter was used. Figure 3.13 below shows the diffraction patterns obtained. The broad arcs corresponding to the crystal peaks are indicative of orientation in the semi-crystalline samples (Figure 3.13 b, c, d),. The crystalline fraction is calculated by plotting the intensity vs. 2θ and taking the ratio of the crystal peak area and total area. Results obtained are shown in Table 3.1. While the crystalline fraction evaluated from density and DSC measurements are dependent on the value of crystal density of its heat of fusion, x-ray diffraction has the advantage of being

independent of such variables. The estimated crystalline fraction is thus, likely to be quite accurate and has been used for comparisons later. It is still not clear why the crystallinity measurement for the non-annealed sample is so different from WAXD and DSC. At present, the WAXD value is considered more reliable and has been used for future comparisons.

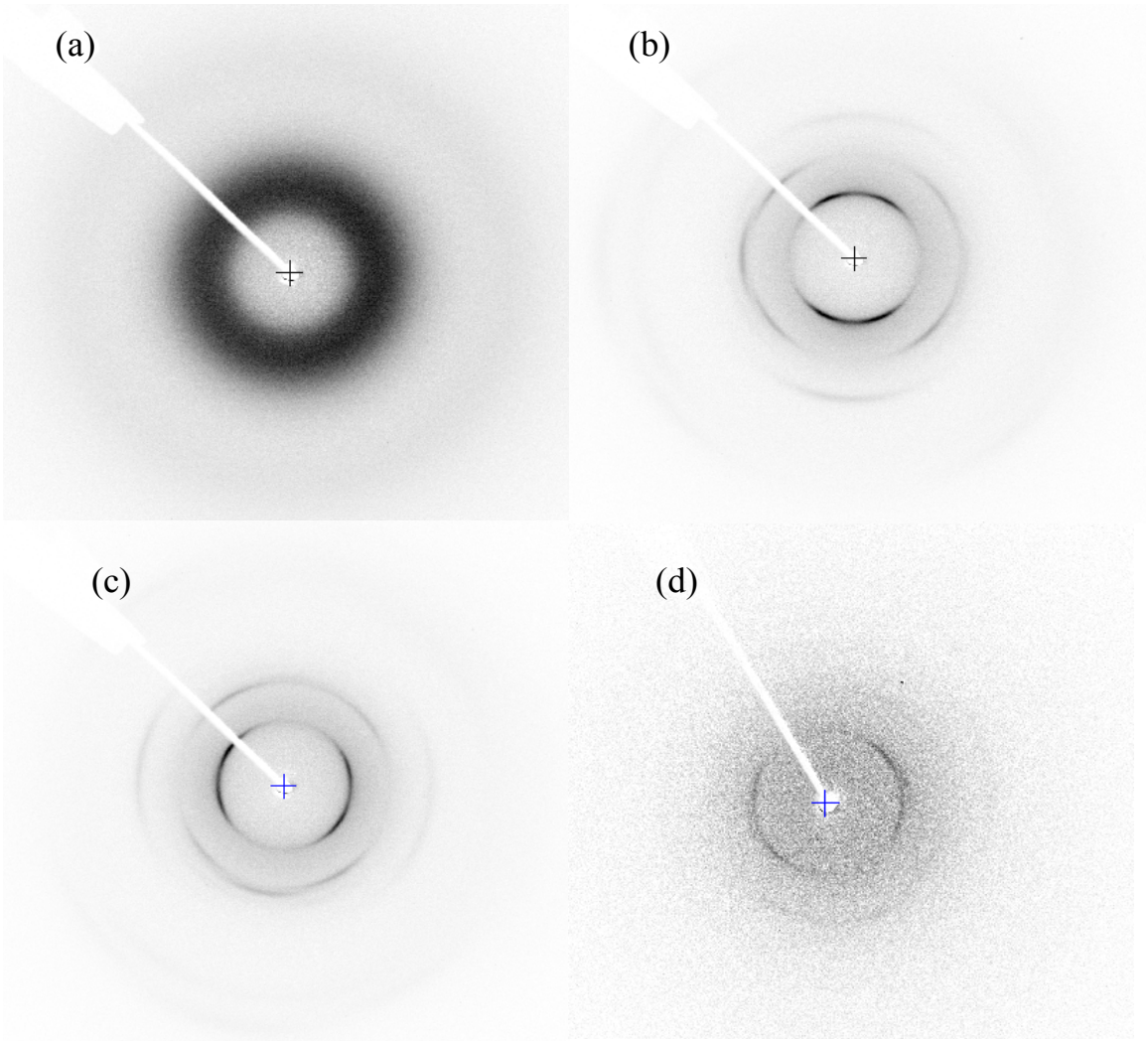

Figure 3.13: Wide Angle Diffraction Pattern of (a) Amorphous PET; (b) Oriented, Non-Annealed PET; (c) Oriented, Annealed PET; (d) Biaxially Oriented thin PET film

3.4.4 Dynamic Mechanical Analysis

Dynamic mechanical analysis measurements were performed on a RSA-III (Rheometric Instruments), at a scan rate of 2°C/min and a frequency of 1Hz, with the temperature starting from room temp up to a maximum of 200°C. The thin 1.5μ film was not tested as it was difficult to stretch out and clamp a strip on the sample holder without damaging the film and reducing its strength. The primary objective behind using DMA was to access the glass transition temperatures using an alternate method. As in the case of the annealed PET film, DSC may not show not a Tg, but DMA will always show a transition. The ratio of the storage modulus and the loss modulus is tanδ which is plotted vs. temperature. Glass transition occurs where tan δ goes through a maximum as shown in Figure 3.14. Results are shown in Table 3.2. As can be see, the T_g measured using DSC and DMA differ significantly. This has been discussed below.

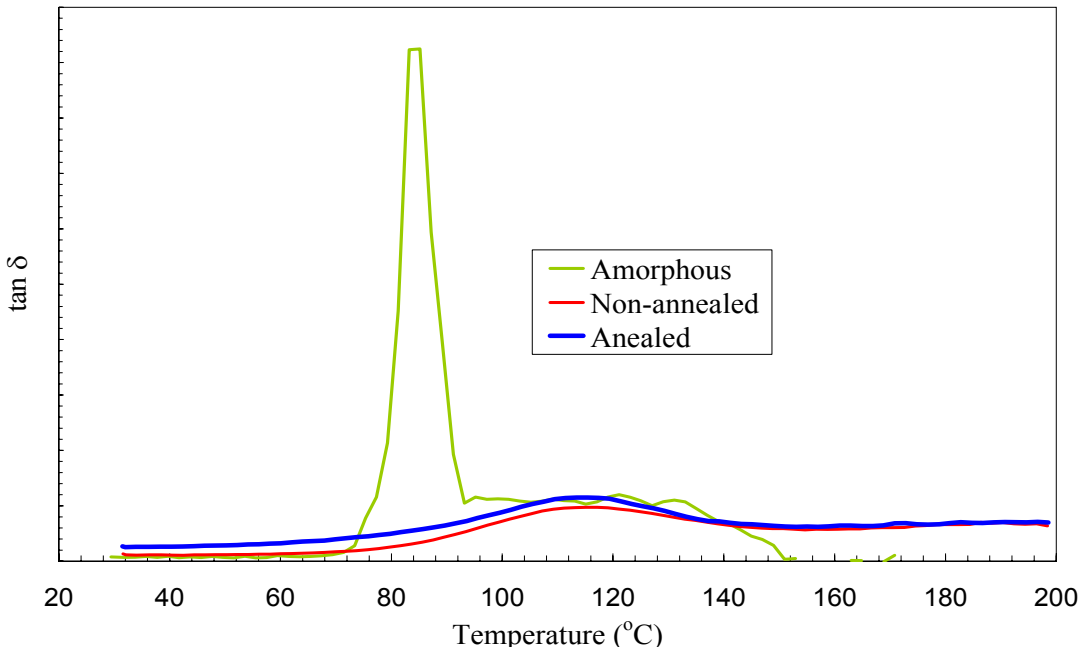

Figure 3.14: DMA of the amorphous, annealed and non-annealed PET samples

3.4.5 Discussion

It has been suggested that orientation and crystallization could lead to a third, intermediate phase around the crystals which may have different properties than the amorphous phase of a completely amorphous, unoriented sample[33, 34]. When crystallization occurs by heat treating or annealing at different temperatures, a rigid amorphous phase may form at interface of the crystalline and the regular amorphous phase [30, 31, 35]. Strain induced crystallization leads to a third, partially oriented mesophase which is a precursor to crystal formation [30, 36-38]. Depending upon the sample processing history, this intermediate phase may have different densities, which may lead to a higher overall density and a consequent overestimation of the crystalline fraction using the two phase model of equation 3.2. However, the exact processing conditions for the present samples are not known. Moreover, based on the x-ray diffraction pattern, shown in Figure 3.13, the amorphous phase does not seem have a high degree of orientation which could affect its density. These counter arguments make it difficult to conclude anything about the presence, morphology and fraction of the interphase. The small, broad exotherm in the DSC curve of the non-annealed film may also occur because beyond T_g, the increased cooperative motion of the polymer chains leads to relaxation of stresses that are present in an oriented material. Similar DSC plots were observed by Liu et al for studies with PET bottle samples [32].

Varying estimates of crystallinity, obtained from different methods such as DSC, density, infra-red spectroscopy and XRD, are very common in the polyester characterization literature. Ward et al [39] obtained X_c based on XRD, density and IR, and found them to be consistently different. Based on the characterization of a large

number of samples with crystallinity and orientational order, Abhiraman at al [40] concluded that none of these techniques, which measure fundamentally different physical properties, give similar phase estimations. Liu et al [32] also found that crystallinity determinations from DSC, IR and density do not match and attribute it to dependence on heat of fusion and crystal phase density. Many researchers have reconciled these differences by combining results from say, density, XRD and IR, to obtain the density of the third phase [30, 39, 41, 42]. However, given the fundamentally different measurements from each method and the need to use other data such crystal phase density or the heat of fusion, these estimations are fraught with uncertainty. The difference between the glass transition temperature measured using DSC and DMA can also be explained along similar lines. Both these methods measure different extensive properties and the transition in those properties may occur at different temperatures. In fact, DMA is usually reported to show PET glass transition temperatures in the range of 100-140^{o}C, which is much higher than the T_g reported using DSC.

Due to the uncertainties involved with the use of the three phase model, the two phase model for semi-crystalline polymers continues to be used for structure-property relations. Crystallinity estimate from XRD is considered to be most accurate. Even if a third phase is present, it will not have the long range order seen for crystals and will not contribute to the sharp diffraction peaks. Thus, based on the crystal peak areas, the degree of crystallinity can be determined accurately. These crystallinities have been found to correlate well with measured transport properties. Considering its simplicity and applicability, the two phase model has been used in this work, and as mentioned earlier, the crystalline weight fractions estimated from XRD have been used in later sections.

3.5 REFERENCES

1. Kriegel, R., W.J. Koros, Editor. 2004: Atlanta. p. Processing of the PET samples supplied to GT for testing in Preeti's research.

2. Natu, Y.S., P. Chandra and W.J. Koros, Editors. 2002: Atlanta.

3. Koros, W.J., *Sorption and transport of CO_2 above and below glass transition of poly(ethylene terephthalate).* Polymer Engineering and Science, 1980. **20**(1): p. 14-19.

4. Chiou, J.S., J.W. Barlow, and D.R. Paul, *Plasticization of glassy polymers by carbon dioxide.* Journal of Applied Polymer Science, 1985. **30**(6): p. 2633-42.

5. Bauer, K., D. Garbe, and H. Surburg, *Common Fragrance and Flavor Materials*. IIIrd ed. 1997, Weinheim: Wiley-VCH. 278.

6. Paul, E., *Technical information on product no. ES301009*, P. Chandra, Editor. 2003: Atlanta.

7. Koros, W.J. and C.M. Zimmerman, *Transport and barrier properties.* Comprehensive Desk Reference of Polymer Characterization and Analysis, 2003: p. 680-699.

8. O'Brien, K.C., et al., *A new technique for the measurement of multicomponent gas transport through polymeric films.* Journal of Membrane Science, 1986. **29**(3): p. 229-38.

9. Tanaka, K., et al., *Isotopic-transient permeation measurements in steady-state pervaporation through polymeric membranes.* Journal of Membrane Science, 2002. **197**(1-2): p. 173-183.

10. Slivon, L.E., et al., *Helium-purged hollow fiber membrane mass spectrometer interface for continuous measurement of organic compounds in water.* Analytical Chemistry, 1991. **63**(13): p. 1335-40.

11. Webb, J.A., et al., *The Effect of Drawing on Transport of Gases Through Polyethylene.* Journal of Polymer Science, Polymer Physics Edition, 1993. **31**: p. 743-757.

12. D. G. Pye, H.H.H.M.P., *: Measurement of gas permeability of polymers. II. Apparatus for determination of permeabilities of mixed gases and vapors.* Journal of Applied Polymer Science, 1976. **20**: p. 287.

13. Moore, T.T., et al., *Characterization of low permeability gas separation membranes and barrier materials; design and operation considerations.* Journal of Membrane Science, 2004. **245**(1-2): p. 227-231.

14. Ponangi, R.P. and P.N. Pintauro, *Separation of Volatile Organic Compounds from Dry and Humidified Nitrogen Using Polyurethane Membranes.* Industrial & Engineering Chemistry Research, 1996. **35**(8): p. 2756-2765.

15. Orchard, G.A.J., P. Spiby, and I.M. Ward, *Oxygen and water vapor diffusion through biaxially oriented poly(ethylene terephthalate).* Journal of Polymer Science, Part B: Polymer Physics, 1990. **28**(5): p. 603-21.

16. Moore, T.T., et al., *Effect of humidified feeds on oxygen permeability of mixed matrix membranes.* Journal of Applied Polymer Science, 2003. **90**(6): p. 1574-1580.

17. Madden, W.C., *Hollow Fibre Membranes for Gas Separation Applications*, in *School of Chemical and Biomolecular Engineering*. 2005, Georgia Institute of Technology: Atlanta.

18. Armstrong, A.A., Jr., J.D. Wellons, and V. Stannett, *Temperature effects during the sorption and desorption of water vapor in high polymers. II. Films with special reference to ethyl cellulose.* Makromolekulare Chemie, 1966. **95**: p. 78-91.

19. Schult, K.A. and D.R. Paul, *Techniques for measurement of water vapor sorption and permeation in polymer films.* Journal of Applied Polymer Science, 1996. **61**(11): p. 1865-1876.

20. Frank, H.S., *Low-pressure adsorption on a washed glass surface.* Journal of Physical Chemistry, 1929. **33**: p. 970-6.

21. Koros, W.J. and D.R. Paul, *Design considerations for measurement of gas sorption in polymers by pressure decay.* Journal of Polymer Science, Polymer Physics Edition, 1976. **14**(10): p. 1903-7.

22. Moore, T., *Effects of Materials, Processing, and Operating Conditions on the Morphology and Gas Transport Properties of Mixed Matrix Membranes*, in *Chemical Engineering*. 2004, The University of Texas: Austin, TX.

23. McBain, J.W. and A.M. Bakr, *A new sorption balance.* Journal of the American Chemical Society, 1926. **48**: p. 690-5.

24. Towidjaja, L. and M.A. Al-Juaied, *Quartz Spring Sorption*, P. Chandra, Editor. 2000: Atlanta.

25. Koros, W.J., *Sorption and transport of gases in glassy polymers*, in *Chemical Engineering*. 1977, University of Texas: Austin. p. 274 pp.

26. Duabeny, R.d.P., *Crystal Structure of Poly(ethylene terephthalate).* Proceedings of the Royal Society of London, Series A: Mathematical, Physical and Engineering Sciences, 1954. **226**: p. 531.

27. Fakirov, S., E.W. Fischer, and G.F. Schmidt, *The Unit Cell Dimensions of Poly(ethylene terephthalate).* Makromolekulare Chemie, 1975. **176**(8): p. 931.

28. Lapersonne, P., D.I. Bower, and I.M. Ward, *Benzene ring orientation in uniaxial-planar poly(ethylene terephthalate) films.* Polymer, 1992. **33**(6): p. 1266-76.

29. Roberts, R.C., *Poly(ethylene terephthalate) I- Heat of Fusion.* Polymer, 1969. **10**(2): p. 113-116.

30. Lin, J., S. Shenogin, and S. Nazarenko, *Oxygen solubility and specific volume of rigid amorphous fraction in semicrystalline poly(ethylene terephthalate).* Polymer, 2002. **43**(17): p. 4733-4743.

31. Kattan, M., E. Dargent, and J. Grenet, *Three phase model in draw thermoplastic polyesters: comaprison of differential scanning calorimetry and thermall stimulated depolarisation current experiments.* Polymer, 2002. **43**: p. 1399-1405.

32. Liu, R.Y.F., et al., *Crystallinity and oxygen transport properties of PET bottle walls.* Journal of Applied Polymer Science, 2004. **94**(2): p. 671-677.

33. Fu, Y., et al., *Analysis of structure and properties of poly(ethylene terephthalate) fibers.* Journal of Polymer Science, Polymer Physics Edition, 1994. **32**: p. 2289-2306.

34. Gupta, V.B. and S. Kumar, *Third phase in poly(ethylene terephthalate).* Polymer, 1978. **19**: p. 953-955.

35. Olson, B.G., et al., *Positron Annihilation Lifetime Spectroscopy of Poly(ethylene terephthalate): Contributions from Rigid and Mobile Amorphous Fractions.* Macromolecules, 2003. **36**(20): p. 7618-7623.

36. Mahendrasingam, A., et al., *Time resolved WAXS study of the role of mesophase in oriented crystallisation of poly(ethylene terephthalate-co-isophthalate) copolymers.* Polymer, 2005. **46**(16): p. 6044-6049.

37. Dargent, E., J. Grenet, and X. Auvray, *Thermal behaviour of drawn semi-crystalline poly(ethylene terephthalate) films.* Journal of thermal Analysis, 1994. **41**: p. 1409-1415.

38. Mahendrasingam, A., et al., *Influence of temperature and chain orientation on the crystallization of poly(ethylene terephthalate) during fast drawing.* Polymer, 2000. **41**(21): p. 7803-7814.

39. Farrow, G. and I.M. Ward, *Crystallinity in Poly(ethylene terephthalate): A comparsion of X-ray, Infra-red and density measurements.* Polymer, 1960. **1**: p. 330-339.

40. Sharma, V., P. Desai, and A.S. Abhiraman, *Crystallinity vis-a-vis two-phase models of oriented polymers: inferences from experimental study of poly(ethylene terephthalate).* Journal of Applied Polymer Science, 1997. **65**: p. 2603-2612.

41. Bove, L., et al., *Transport properties of the mesomorphic form of poly(ethylene terephthalate).* Polymer, 1996. **37**(23): p. 5309-5311.

42. Dlubek, G., et al., *Glass transition and free volume in the mobile (MAF) and rigid (RAF) amorphous fractions of semicrystalline PTFE: a positron lifetime and PVT study.* Polymer, 2005. **46**(16): p. 6075-6089.

CHAPTER 4 : SORPTION AND TRANSPORT OF METHANOL IN POLY(ETHYLENE TEREPHTHALATE)

Methanol has been chosen as the *flavor molecule simulant* for this research. The aim of this chapter is to estimate pure methanol transport properties, and to use sorption equilibrium and kinetics as tools to understand the effect of orientation and annealing. Low pressure vapor sorption equipment and methodology has already been described in section 3.3.2. The diffusivities estimated from these measurements have been used to determine the time needed to reach steady state in multi-component permeation experiments described in chapter 6. The dual mode model parameters estimated at low activities have been used in modeling and analysis of multi-component permeation.

4.1 EQUILIBRIUM SORPTION OF METHANOL

Sorption isotherms have been obtained for methanol in the amorphous, annealed, and non-annealed semi-crystalline samples. Interval sorption experiments on a single sample have been performed at 35^{o}C. Saturation pressure of methanol is 202.3mmHg at 35^{o}C.

4.1.1 Sorption at Low Activities

Sorption experiments at low activities were performed in small steps of increasing pressure to investigate the dual mode characteristics. Dual mode behavior, i.e. concavity of the isotherm to the x-axis, was evident until $p/p_o \approx 0.25$ in all the three samples. The isotherms are shown in Figure 4.1.

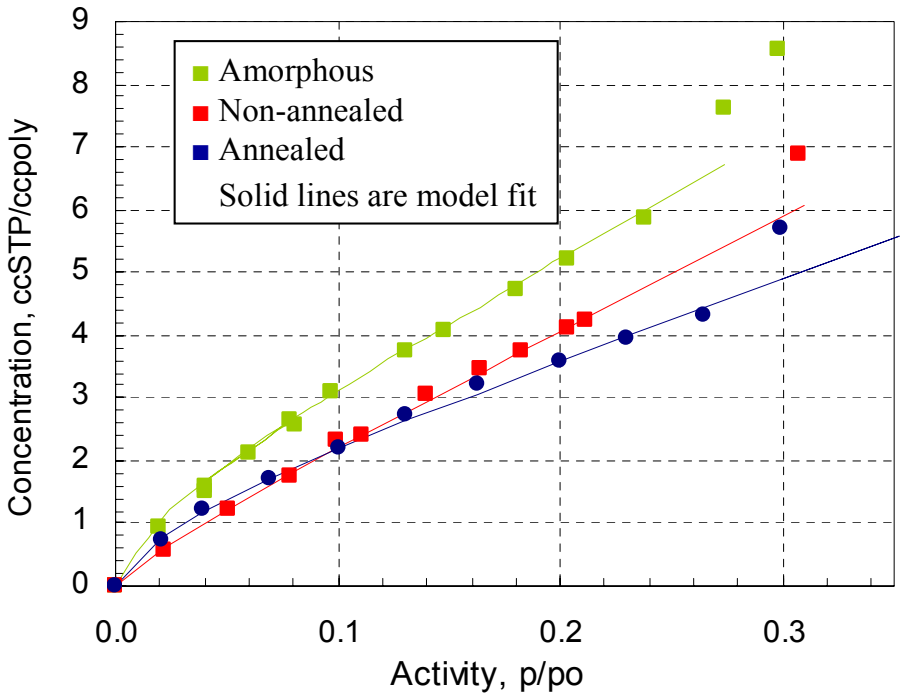

Figure 4.1: Sorption isotherm at low activities of methanol indicating the dual mode characteristics

Table 4.1: Dual mode model parameters for methanol

Parameter	**Amorphous**	**Annealed, semicrystalline**	**Non-annealed, semicrystalline**
b, (atm^{-1})	134 ± 35	124 ± 28	144 ± 15
C_H', (ccSTP/ccpoly)	1.37 ± 0.07	1.22 ± 0.06	0.7 ± 0.1
k_d, ccSTP/ccpoly/atm)	74 ± 5	48 ± 7	63 ± 2

Table 4.2: Dual mode model parameters predicted by the two phase model (WAXD data)

Parameter	**Annealed, semicrystalline**	**Non-annealed, semicrystalline**
$\phi_a C_H'$, (ccSTP/ccpoly)	0.88 ± 0.06	0.88 ± 0.11
$\phi_a k_d$, (ccSTP/ccpoly/atm)	47 ± 7	47 ± 2

The last point on each graph is plotted to show the activity at which deviation from dual mode occurs. The solid lines are the dual mode model fit of Equation 2.17(b). Parameters obtained are shown in the Table 4.1. As can be seen, the affinity constant, b, is the same within experimental uncertainty for all the three samples. This is to be expected because the affinity constant is representative of the polymer penetrant interaction. Morphological differences between the samples will not change the molecular level interaction of the penetrant with the polymer chain. However, the Henry's Law solubility constant, k_d, and the Langmuir saturation capacity, C_H', will be affected by morphological changes because these are dependent on the number of sorption sites available in the polymer, which in turn will depend on the fraction and morphology of the amorphous phase. As discussed in section 2.1.4, based on the two phase model, these values should be proportional to the crystallinity. For the semicrystalline samples, Equation 2.17(b) then becomes

$$C = \frac{\phi_a C_H' bp}{(1+bp)} + \phi_a k_D p \qquad 4.1$$

where α is the amorphous volume fraction, and the dual mode model parameters are those evaluated for a completely amorphous sample. Based on the crystallinity levels determined by x-ray diffraction, the estimated values for C_H' and k_d are shown in Table 4.2. The actual k_d for the annealed sample is within the error of the prediction. This suggests that the crystals are well formed after the orientation and annealing process, and the morphology of segments in equilibrium with each other in the amorphous phase is similar to that of the completely amorphous sample. In this case, after biaxial orientation, the sample is annealed at 210^{o}C. This temperature is high enough to allow substantial

rearrangement of the orientation of the non-crystalline regions [1]. On the other hand, the observed C_H' is higher than predicted. C_H' is determined by the non-equilibrium Langmuir sites in the polymer, which in turn will be influenced by the rate of quenching after annealing above the T_g. A very fast quench will create more non-equilibrium sites than a slower quench where segmental mobility is retained for a longer period and allows the chains to come closer to an equilibrium packing. Micheals et al also observed that the C_H' for an annealed, semi-crystalline sample was higher than predicted by the two phase model based on the amorphous film value [2].

In the case of the oriented, non-annealed sample, the C_H' which is closer to the predicted value. On the other hand, the k_d value is higher than predicted. The factors which determine the final morphology of this sample are its starting morphology, sample history, draw temperature, axial and transverse draw ratios, and the sequence of drawing (i.e. whether drawing in the machine direction and transverse direction was done sequentially or simultaneously) [1]. However, in the present study, the drawing conditions are unfortunately not known. Nevertheless, from the k_d values, it is quite clear that the biaxial orientation has created more free volume in the Henry's Law domains of the amorphous phase than in the completely amorphous sample. Ward et al observed that in the case of simultaneously drawn films with equal draw ratios in both directions, the oxygen permeability increased with increasing draw ratios and was always more than prediction based on crystallinity [3]. With regard to C_H', the temperature of draw becomes crucial. If the draw temperature is above T_g, as is usually the case, the C_H' will depend on the quench rate. On the other hand, if the drawing temperature is below T_g, C_H' will depend only on the draw ratios and the strain rates. Not knowing these conditions makes

it difficult to arrive at definite conclusions regarding the observed and predicted C_H' values. Vieth et al observed that the C_H' for a crystalline, oriented sample was actually more than the C_H' observed in the amorphous [4]. Similarly, Ward et al determined the C_H' in two semicrystalline PET samples, one highly oriented and one with a low degree of orientation. In both samples, the C_H' was more than the saturation capacity observed for the isotropic film with 5-6% crystallinity. Therefore, solubility and permeability predictions based on the two phase model were much lower than the actual values [5]. These reports suggest that with limited information about sample processing, specific conclusions about the effect of orientation on the number of non-equilibrium sites in the non-annealed, oriented film may not be drawn. Various researchers have also investigated such results using the three phase model, where the amorphous phase density is decreased and the sorption occurs in both, the bulk amorphous phase and the rigid amorphous interphase. This, somewhat complicated morphology may also be used to explain the results that are observed here. However, as mentioned earlier, exact fractions of the three phases are difficult to estimate in the present case [6].

After exposing the samples up to a maximum $p/p_o = 0.30$, integral desorption was performed by decreasing the pressure in a step wise manner. The complete sorption-desorption isotherm is shown in Figure 4.2. Considerable hysterisis is observed even after exposure to these low activities where mass uptake is less than 0.63wt%. Hysteresis in these isotherms is indicative of a conditioning effect. Koros et al observed hysterisis in desorption isotherms of CO_2 in PET after exposure to CO_2 at 20 atm [7]. Similar effects have been observed in the polycarbonate-CO_2 system as well [8, 9]. Berens observed hysteresis during desorption of vinyl chloride from poly(vinyl chloride). The hysteresis

was larger in samples exposed to higher activities of the vapor [10]. In this case, the hysteresis is least in the annealed, oriented sample. This result is due to the annealing process which reduces the free volume and improves the chain packing, which therefore enhances the resistance to conditioning effects. The amorphous and the non-annealed films have not gone through such a thermal stabilization step and show much greater susceptibility to conditioning.

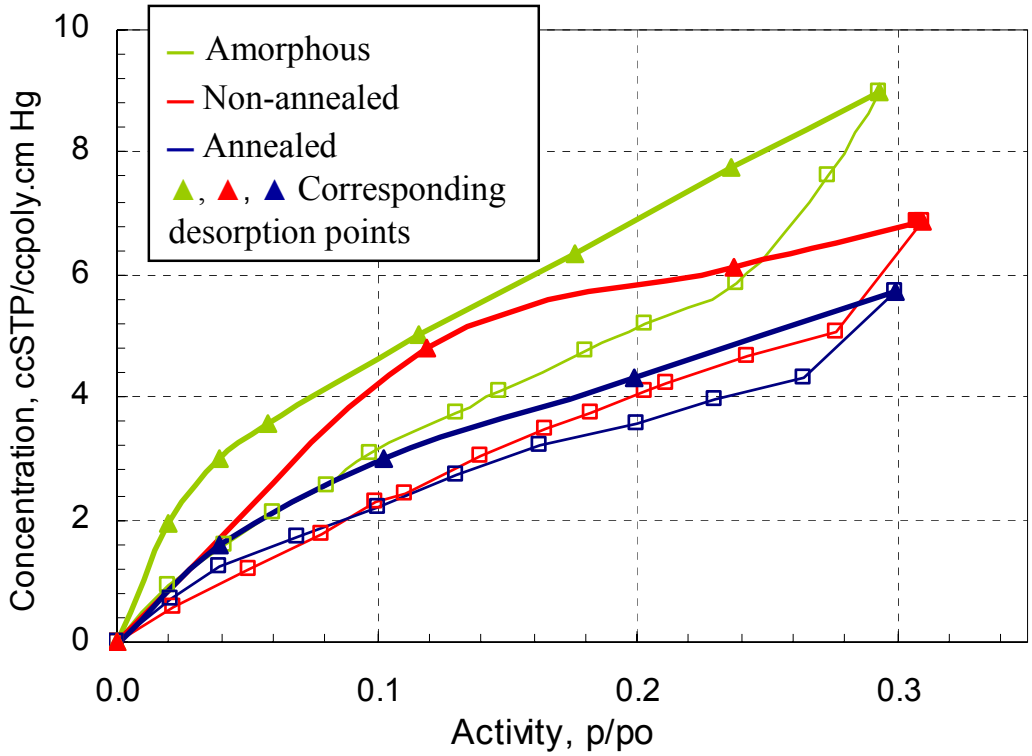

Figure 4.2: Methanol sorption and desorption isotherms of 'as received' samples exposed to a maximum activity of 0.30.

Conditioning effects on the polymer matrix caused by the presence of methanol can lead to increased gas permeability during multi-component permeation and loss of barrier efficacy due to an increase in the free volume of the system. Many literature reports

confirm an increase in free volume through resorption in conditioned polymers. Connelly et al found that pre-swelling of PMMA with organic molecules such as methanol led to a higher initial solubility of water, methanol, and ethanol at low pressures [11]. Similarly, in PET, sorption of low pressure acetaldehyde increased by a factor of 3.5 after exposure to high activity vapor [12]. Increased and faster propane sorption was observed in polystyrene microspheres pre-swollen with propane [13]. Similar results are seen in this work in the case of PET-methanol. Even after complete removal of methanol by evacuation, the polymer morphology does not return to the original 'as received' state. This was confirmed through resorption of methanol on the amorphous sample and observing a higher level methanol sorption. After complete desorption of methanol, the film was again exposed to methanol in increasing steps of pressure. The conditioned sample showed higher uptake than the 'as received' film as is shown in Figure 4.3. It is possible that the consolidation of the polymer matrix requires more time, and the 2 days of evacuation were insufficient to allow the chains to relax back to their original state. The gradual consolidation of a pre-swollen polymer matrix was studied by Hopfenberg et al using polystyrene microspheres pre-swollen with n-hexane at 90% activity and 15^{o}C. The relaxation back to the final equilibrium sorption state was dependent on the cumulative time under vacuum. The final equilibrium was the same as that reached by long term relaxations in an as received sample [14]. It is likely that after sufficiently long time under vacuum, the amorphous PET films in this work will reach a 'global' equilibrium state. However, in barrier packaging applications, the interacting flavor molecule will not be removed from the polymer matrix, and increases in free volume could assist the transport of gas molecules.

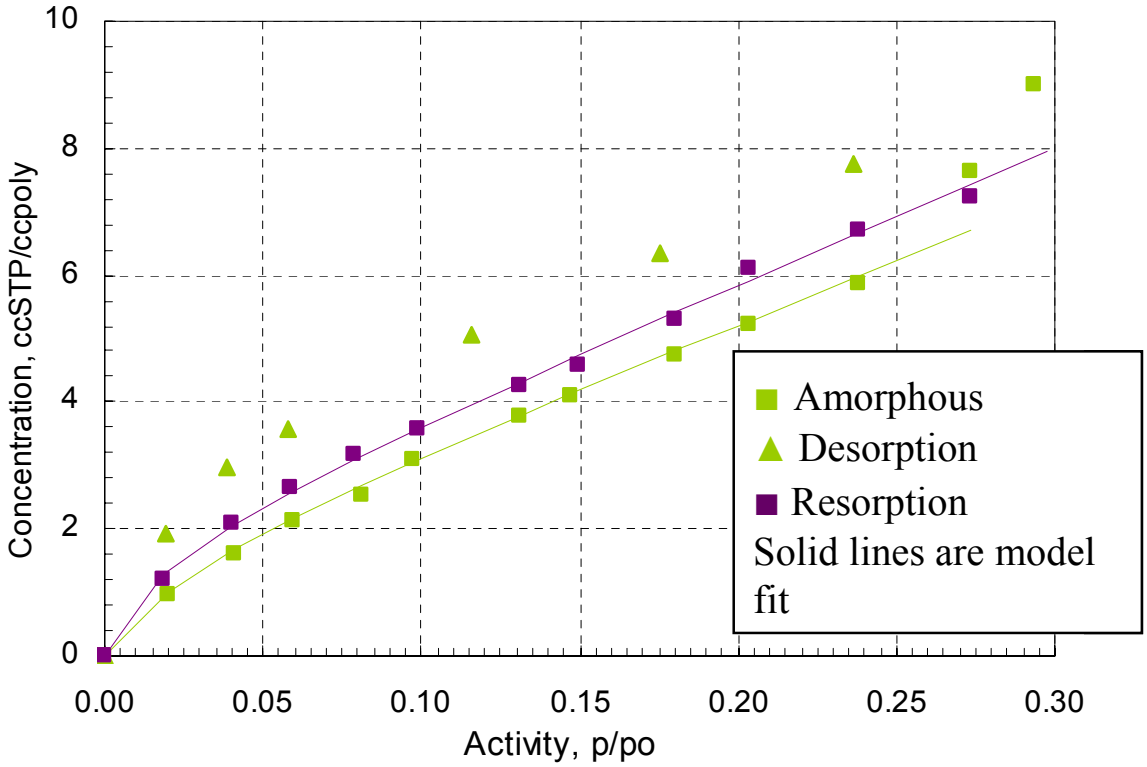

Figure 4.3: Resorption isotherm of methanol in amorphous PET. The first sorption and desorption isotherms are shown for reference.

4.1.2 Sorption at High Activities

The complete sorption isotherm of methanol was obtained on as-received films, with activities ranging from 0.10 to 0.96. Figure 4.4 shows the isotherms of the three PET samples. At 30% activity and beyond, the isotherm clearly has Flory-Huggins characteristics as it becomes convex to the x-axis. Below the 30% activity level, it is difficult to discern from Figure 4.4 that there is, indeed, a concavity to the x-axis in the isotherm. However, Figure 4.1 shows that at low activities, the isotherm does follow dual mode behavior. The solid lines in Figure 4.4 are obtained by curve fitting the experimental data to equation 2.29 with a constant Flory-Huggins interaction parameter (χ). Table 4.3 below shows the parameter values obtained.

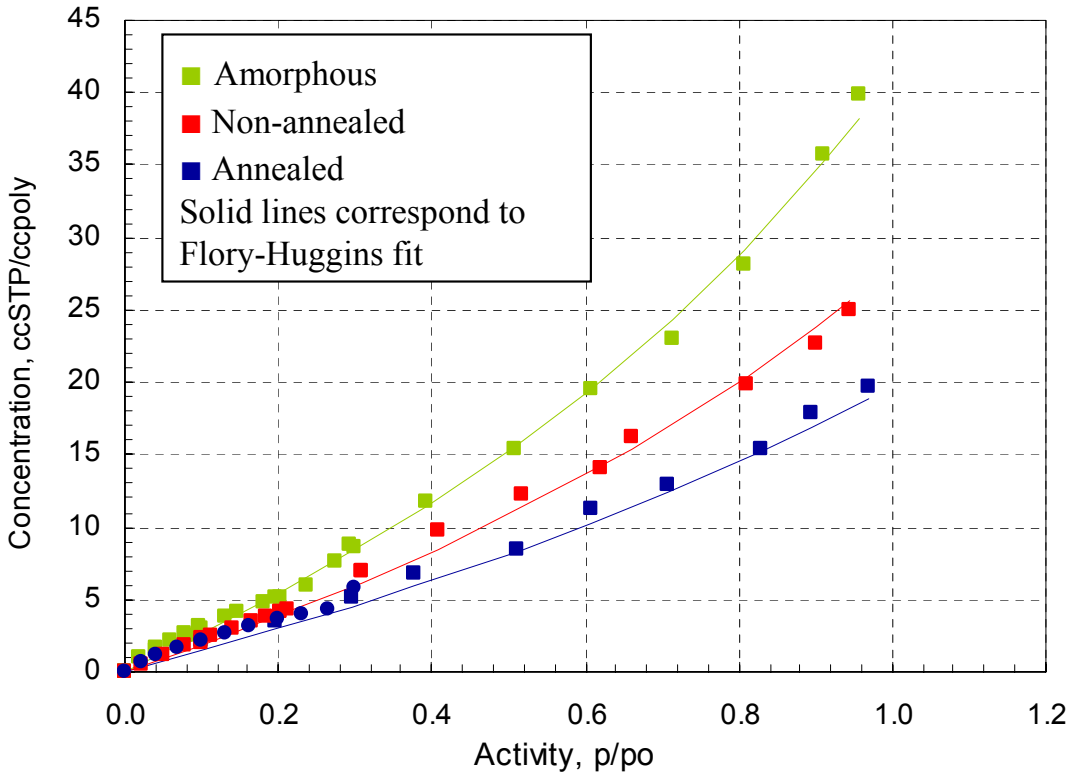

Figure 4.4: Methanol sorption isotherm in PET at 35°C

Table 4.3: Flory-Huggins interaction parameter and the mass uptake at p/p_o=0.96 for methanol in PET

	Amorphous	**Annealed, Semi-crystalline**	**Non-annealed, Semi-crystalline**
χ	2.03±0.01	2.57±0.02	2.33±0.01
Uptake at p/p_0=0.96 (g/100g poly)	4.3	2.0	2.5

The total uptake as weight percent at 96% activity by each sample is also mentioned in Table 4.3. It is evident that the amorphous sample swells considerably. 4.3 %wt methanol absorption corresponds to a volume fraction of 0.067 in the polymer. This value agrees well with the uptake of 0.06 volume fraction, reported by Durning et al. for liquid methanol (p/p_o=1) [15]. However, for the annealed film with 63.1% amorphous volume fraction, the uptake of 2.0 wt% corresponds to only 46.5% of the amorphous PET film. In the non-annealed, oriented film with amorphous volume fraction of 62.6%, the uptake is 58.1% of the amorphous PET. Lesser swelling than expected in the annealed semi-crystalline sample can be explained by the fact that the annealing leads to a stabilization of the polymer morphology and reduces the free volume, making it more difficult to swell. The restraining effect of the crystals also reduces the chain mobility in the amorphous phase. Zhou et al observed increased resistance to swelling and plasticization after sub-T_g thermal annealing of Matrimid™ hollow fibers due to decreased free volume and charge transfer complexes [16]. Wind et al observed that annealing stabilized the amorphous polyimide and increased the plasticization pressure [17]. In the non-annealed, semi-crystalline sample, the actual uptake is only slightly less than what is predicted. Assuming that the film extrusion and orientation processes are the same for both samples, the only difference between them is annealing. This data suggests that annealing is the dominant factor, and not the restraining effect of the crystals, that causes a reduction in the swelling of the amorphous regions. Moreover, Micheals suggested that segmental motion in glassy polymers is already very low to be significantly influenced by the crystals [18]. Therefore, in the present work, evidence points to limited influence of the crystals on the amorphous phase swelling. However, it

must be kept in mind that at higher solubility, the amorphous regions will swell more, the segmental motion will increase, and the chain immobilization due to crystallinity will become more important.

4.2 SORPTION KINETICS OF METHANOL IN PET

4.2.1 Kinetics at Low Activities

Sorption kinetics of methanol at various activities were obtained using interval sorption to estimate the diffusion coefficient and to assess the mode of transport (Fickian vs. non-Fickian). At low activities, with small increases in the methanol pressure, Fickian kinetics were observed. Diffusion coefficients were calculated by curve fitting the data to equation 2.36, and they were found to be concentration dependent. A few representative kinetics, obtained for the amorphous, non-annealed and annealed PET films, are shown in Figure 4.5, Figure 4.6, and Figure 4.7 respectively. The kinetics are Fickian up to p/p_o= 0.20 in the amorphous film, p/p_o= 0.24 in the non-annealed, oriented film, and p/p_o= 0.30 in the annealed film. Thereafter, some long term glassy state relaxation effects are visible in the sorption kinetics.

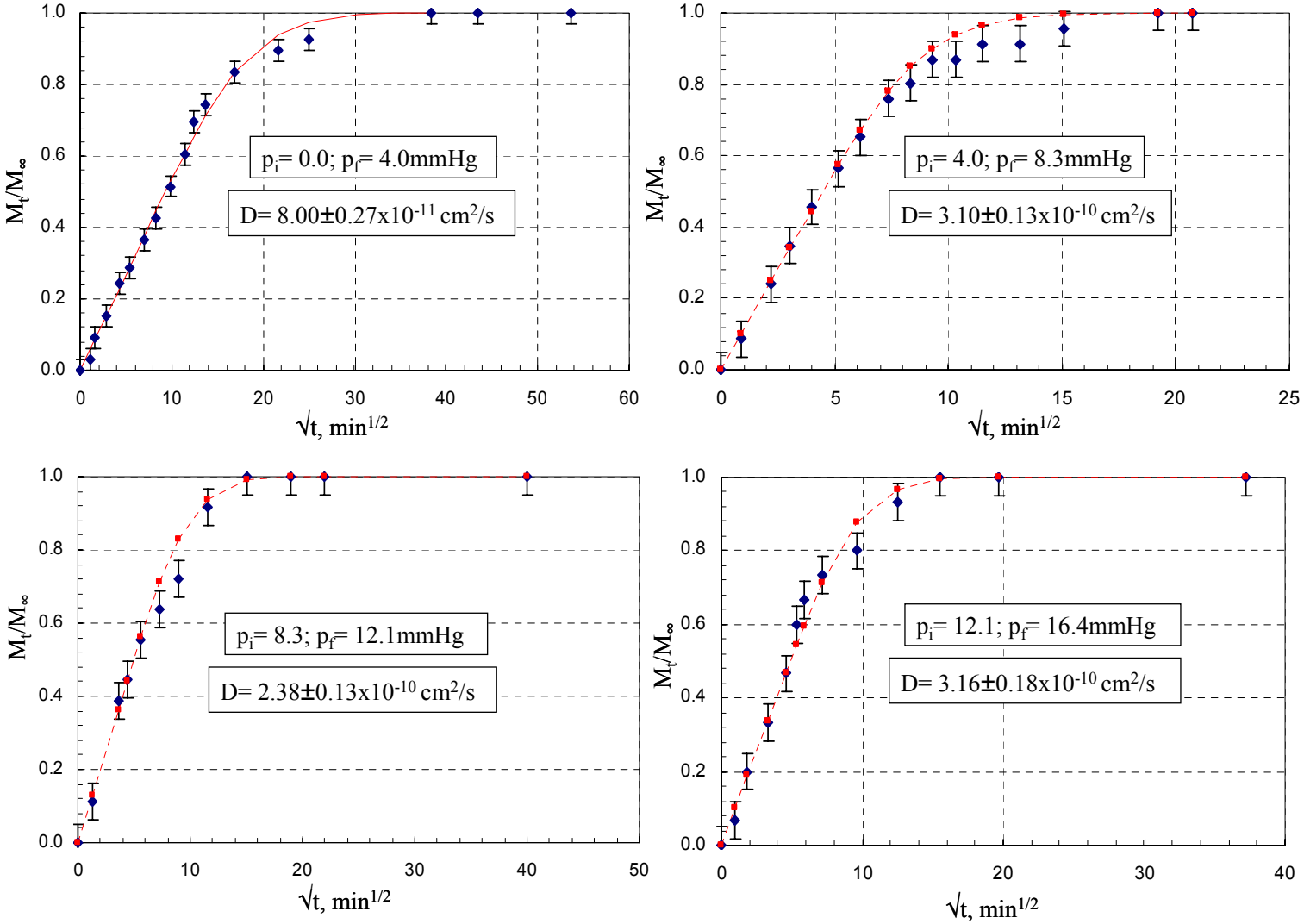

Figure 4.5: Sorption kinetics at low activities in amorphous PET at 35°C. Experimentally measured points (♦); Fickian fit (--□--)

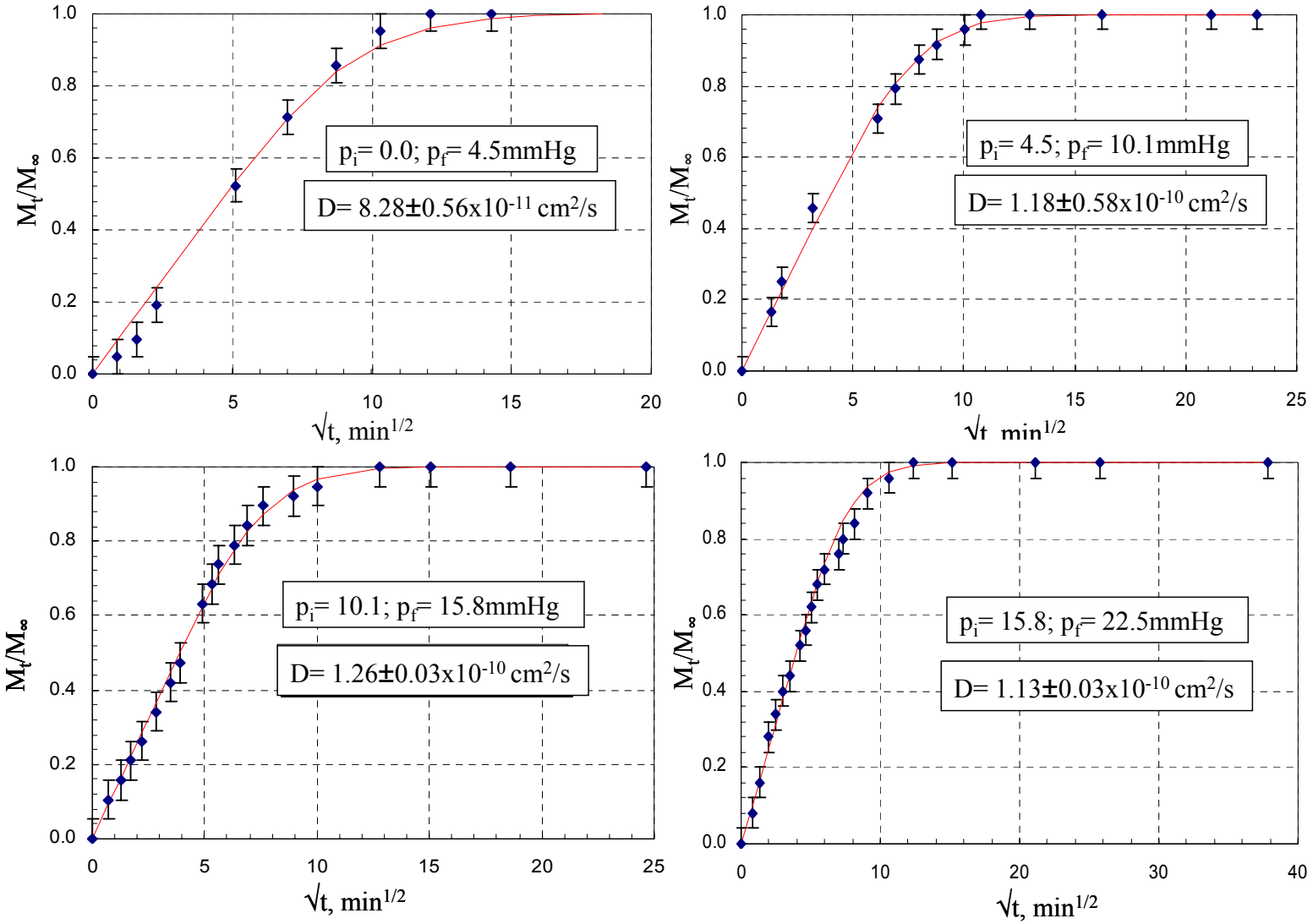

Figure 4.6: Fickian kinetics for the non-annealed film at 35°C. Experimentally measured points (♦); Fickian fit (__)

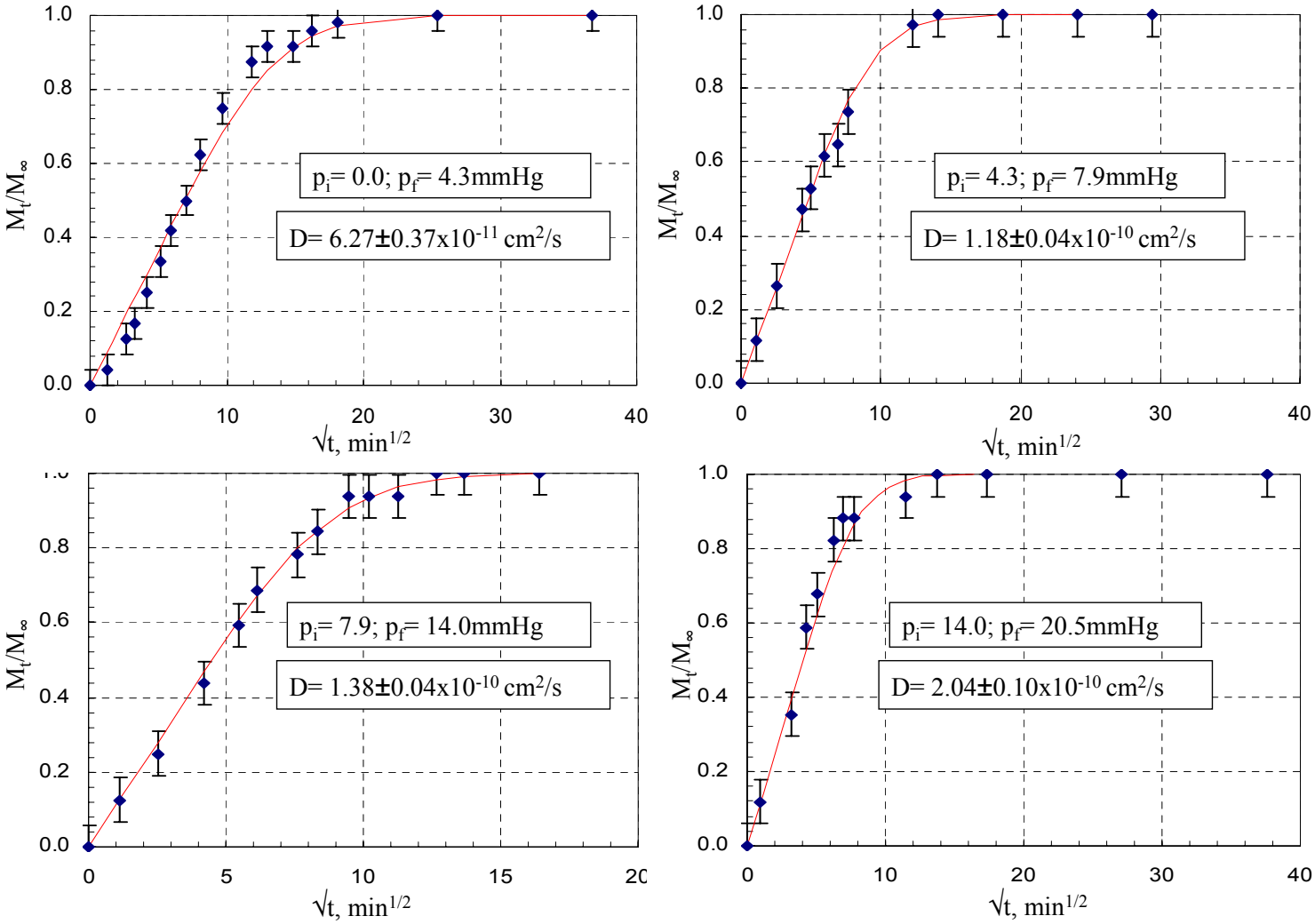

Figure 4.7: Fickian kinetics for the annealed film at 35°C. Experimentally measured points (♦); Fickian fit (___)

It is well known that in the case of concentration dependent diffusion coefficients, the average diffusivity in a concentration interval depends on the initial and final pressure of the vapor [19]. If the kinetics are Fickian, average diffusivity vs. pressure will yield the functional form of D(C). Using this functional form, kinetics for different initial and final concentration conditions can be evaluated. However, this is not possible if there are long term relaxation effects in the concentration interval of interest due to the additional time dependence of D and, therefore, lack of steady state diffusivity information. In such cases, knowledge of the exact kinetics in the concentration interval of interest becomes important. Berens et al observed diffusion controlled kinetics at small concentration intervals [19]. However, when a large concentration gradient is imposed, the polymer chains are unable to relax fast enough and anomalous kinetics are observed. In the PET-methanol system being studied here, when the 'as received' amorphous film was exposed directly to 40mmHg (p/po=0.20), some non-Fickian effects occurred. The same measurement was also done in 2 steps. The film was first exposed to 20 mmHg for equilibration, and then, the pressure was increased to 40 mmHg. Fickian kinetics was seen in both steps. The non-annealed sample showed Fickian kinetics in the first 0-20mmHg step. Relaxation, seen in the 20-40mmHg step, disappeared when the pressure was increased in smaller increments. The kinetics are shown in Figure 4.8 (a) and (b) for the amorphous and non-annealed films respectively. In contrast, the annealed sample showed Fickian kinetics in both cases- direct and step wise exposure to 40mmHg. Thus, apart from being morphology dependent, the kinetics are also history dependent. These observations emphasize the importance of the concentration gradient imposed on the polymer and have implications for transport measurements and various applications also.

For example, during permeation, the amorphous film is directly exposed to p/p_o=0.20 after evacuation. Even though, based on interval sorption, an average D can be calculated and used to predict the time lag, true equilibrium will not be reached after 5 time lags due to long term relaxation under the large concentration difference. Therefore, care needs to be taken to ensure that the steady state transport has been achieved before permeabilities are measured in permeation experiments.

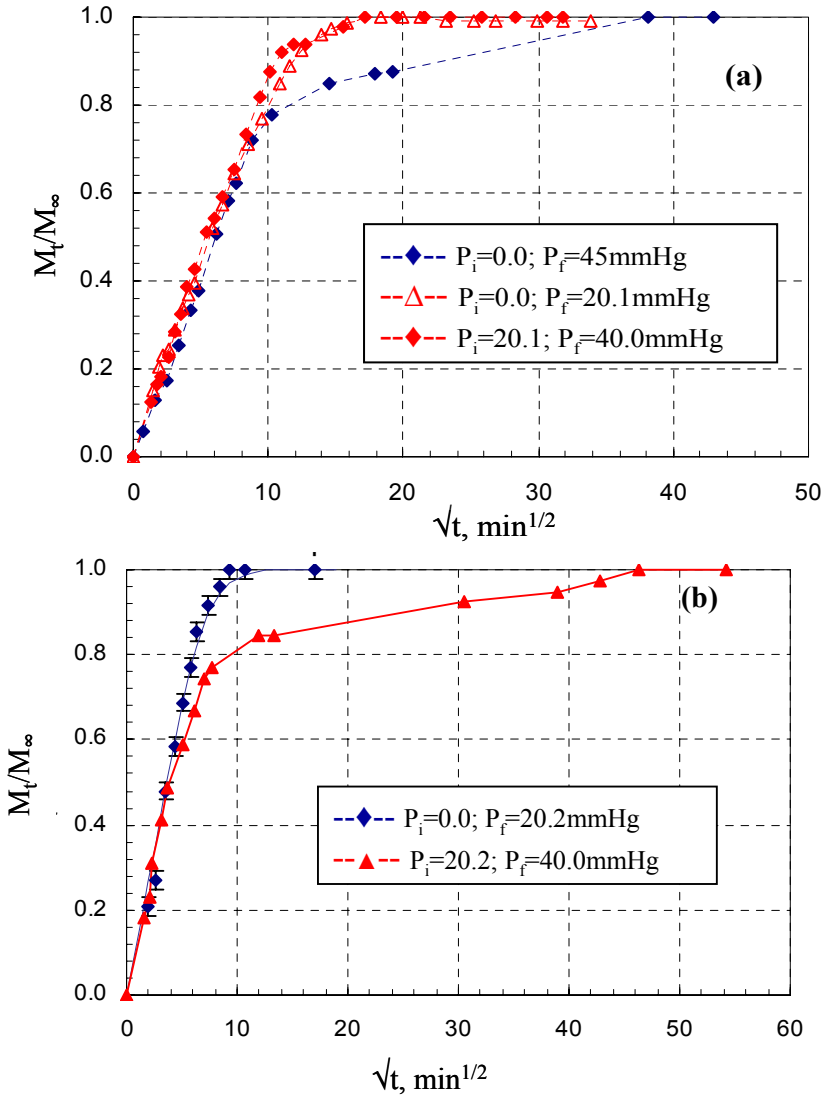

Figure 4.8: (a) Amorphous PET up to p/p_o=0.20; (b) Non-annealed PET up to p/p_o=0.20

As mentioned earlier, the methanol diffusion coefficient in PET is concentration dependent. At low concentrations, D(C) increases with increasing C in all the three samples. Average D values calculated for kinetics shown in Figures 4.5, 4.6, and 4.7 show this trend. This increase is further confirmed by the desorption kinetics. For diffusion coefficients that increase with concentration, desorption is slower than sorption [20]. The desorption diffusion coefficients have been measured by interval desorption with the film having seen a maximum of p/p_o=0.30 during interval sorption. Selected examples of sorption and desorption diffusion coefficients are shown in Table 4.4. In the case of the annealed, semi-crystalline film, two steps were taken during interval sorption. The average diffusivity for the 0→7.9mmHg range, evaluated using equation 2.4, is 8.55×10^{-11} cm^2/s. Desorption in a single step yielded a lower diffusion coefficient of 4.35×10^{-11} cm^2/s.

Table 4.4: Sorption and desorption diffusion coefficients in different PET films

Sample	**Sorption step**	**Sorption Diffusivity cm^2/s**	**Desorption step**	**Desorption Diffusivity, cm^2/s**
Amorphous	3.8→ 8.1 mmHg	3.49×10^{-10}	7.9→ 3.9 mmHg	1.20×10^{-10}
Non-annealed	0.0 → 20.2 mmHg	1.40×10^{-10}	24.2 → 0.0 mmHg	5.42×10^{-11}
Annealed	0.0 → 4.3 mmHg	6.27×10^{-11}	8.0 → 0.0 mmHg	4.35×10^{-11}
Annealed	4.3→ 7.9 mmHg	1.23×10^{-10}		

It has already been established that the sorption isotherm follows the dual mode model in the vapor pressure range being considered above. For diffusion, the dual mode model also predicts effective diffusion coefficients, which increase with increasing concentration to reach an asymptotic value. The data shown above suggests that the concentration dependence observed here could be due to the difference in the diffusion coefficients in the two sorption domains- the 'holes' and the 'dissolved regions'. At low concentrations, dissolution is favored in the 'holes', which results in a low diffusivity. As concentration increases, both diffusivity and the fraction of molecules in the equilibrium region increase. Figure 4.9 shows diffusion coefficients at different activities and the dual mode model fit using equation 2.25. The ratio $F= D_D/D_H$ is very small in each case (~0.004), and can be assumed to be negligible. This implies that methanol is practically immobilized in the non-equilibrium sites.

Table 4.5: Comparison of the ratio of diffusivities, F, of various molecules

Gas Molecule	Collision Diameter, Å	Critical Temperature, K	$F= D_D/D_H$
O_2 [this work]	3.0	154.35	0.140
CO_2 [21]	3.4	304.15	0.078
CH_3OH	4.5	513.15	0.004

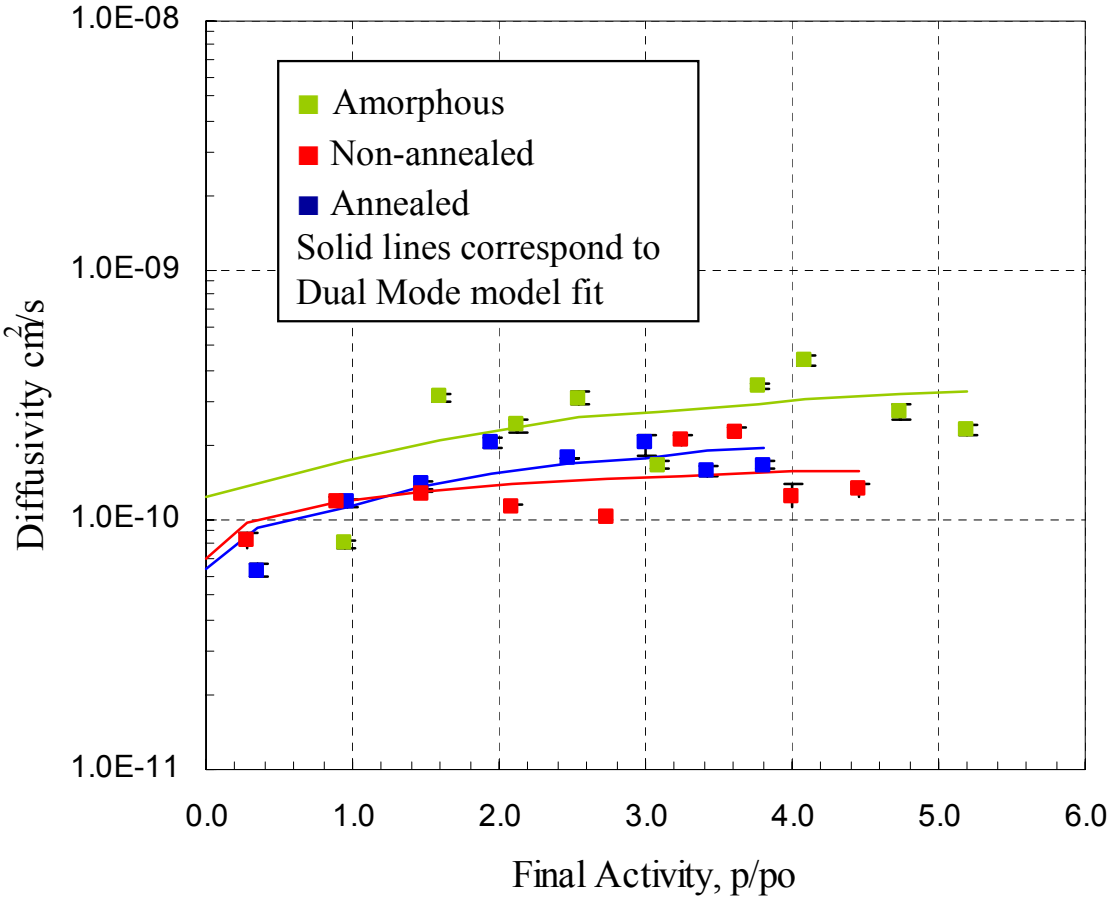

Figure 4.9: Diffusivity of different PET samples, obtained at different activitiy

Table 4.6: Methanol diffusivity in the equilibrium regions of PET

PET sample	**D_D, cm^2/s**	**Infinite dilution diffusivity, cm^2/s**
Amorphous	$4.21 \pm 0.50 \times 10^{-10}$	1.23×10^{-10}
Annealed, semi-crystalline	$2.68 \pm 0.38 \times 10^{-10}$	6.35×10^{-11}
Non-annealed, semicrystalline	$1.83 \pm 0.19 \times 10^{-10}$	8.28×10^{-11}

Table 4.5 compares the values of F obtained for CO_2 and O_2 with that of methanol. With increasing penetrant size and critical temperature, F decreases. Critical temperature is a measure of the condensability of the molecule. With increasing condensability, the non-equilibrium sites become more energetically favorable, and it is difficult for the molecule to jump out into the dissolved region. The diffusivity in the equilibrium domains, D_D, and the infinite dilution diffusion coefficient are shown in Table 4.6. The infinite dilution diffusivity is evaluated using equation 2.25 at $p \rightarrow 0$ or $C_D \rightarrow 0$.

4.2.2 Berens- Hopfenberg Model

Anomalous kinetics occurs when the polymer chain relaxation rate is comparable to that of penetrant diffusion. Several attempts have been made to model these effects using concentration and time dependent diffusion coefficients. While none of these models predict all the features observed so far, they do apply to specific cases. Crank and Windle separately provide brief reviews of these theories [20, 22].

Two-stage kinetics has been observed in this work. The first stage, which occurs at small times, is diffusion controlled, and the uptake is linear with the square root of time. The second stage, at long times, is a relaxation controlled regime. The second stage persists for a long time and pertains to the slow polymer chain relaxations. Berens and Hopfenberg proposed a parallel model for two stage sorption that allowed separation of the relaxation and diffusion parameters [23]. The total uptake (M_t) at any time t, can be written as

$$M_t = M_{t,R} + M_{t,F} \qquad 4.2$$

$M_{t,R}$ and $M_{t,F}$ are the amounts absorbed due to relaxation (subscript R) and Fickian diffusion (subscript F) respectively. For Fickian diffusion in plane sheets, equation 2.36 can be modified to yield:

$$M_{t,F} = M_{\infty,F}\left\{1-\frac{8}{\pi^2}\sum_{n=0}^{\infty}\frac{1}{(2n+1)^2}\exp\left[-\frac{(2n+1)^2\pi^2 Dt}{4l^2}\right]\right\} \qquad 4.3$$

$M_{\infty,F}$ is the equilibrium uptake due to Fickian diffusion. The relaxation uptake is assumed to be first order in the driving force, which is the concentration difference between relaxation uptake at time t ($M_{t,R}$) and the equilibrium uptake due to relaxation ($M_{\infty,R}$). The relaxation rate constant is k_R. Equation 4.4 can be integrated to obtain an expression for $M_{t,R}$ as shown in equation 4.5.

$$\frac{dM_{t,R}}{dt} = k_R\left(M_{t,R} - M_{\infty,R}\right) \qquad 4.4$$

$$M_{t,R} = M_{\infty,R}\left(1-\exp(-k_R t)\right) \qquad 4.5$$

The total uptake can then be written as:

$$M_{t,F} = \phi_F\left\{1-\frac{8}{\pi^2}\sum_{n=0}^{\infty}\frac{1}{(2n+1)^2}\exp\left[-(2n+1)^2 k_F t\right]\right\} + (1-\phi_F)\left(1-\exp(-k_R t)\right) \qquad 4.6$$

$$k_F = \frac{\pi^2 D}{4l^2} \qquad 4.7$$

$$\phi_F = M_{\infty,F}/M_{\infty} \qquad 4.8$$

The above expressions indicate that the relaxation is independent of the sample dimensions. It is only related to the relaxation of the swelling stresses created by a plasticizing penetrant. For thick films, k_F may be small, and if $k_F \leq k_R$, the two stages will not be very clearly discernible. Thus, the observed kinetics becomes dependent on the

dimensions of the sample. The use of a distribution of relaxation rates is more rigorous and provides a more accurate representation, but that will make it nearly impossible to evaluate the parameters separately. If fewer parameters were to be taken, it poses the difficulty of picking the number of parameters and therefore, adds a degree of ambiguity. The single parameter, k_R can be viewed as the average relaxation rate constant. Equation 4.4 indicates that as the penetrant reaches closer to equilibrium, the rate of uptake decreases, and true equilibrium is reached only at $t \rightarrow \infty$. Extremely long times are often experimentally inaccessible due to time constraints. Therefore, equilibrium is assumed to be reached once absorption does not increase within the error of measurement, or when the error in measurement will be at the most 1-2%. Thus, to be theoretically exact, the measured M_∞ is more likely to be 98-99% of the actual equilibrium value.

4.2.3 Kinetics at High Activities

Significant non-Fickian effects have been observed in the sorption kinetics of methanol at intermediate and high activities. Interacting penetrants at high activities, such as benzene, acetone, dimethyl formamide, methlyene dichloride, acetaldehyde, methyl ethyl ketone and methyl acetate have also shown non-Fickian kinetics in PET [15, 24-27]. Kinetics obtained at intermediate activities of $p/p_o=0.40$ and $p/p_o=0.50$ have been shown in Figure 4.10 and Figure 4.11. As is evident from both the figures, the diffusion rate and relaxation rate are slower in the non-annealed, semi-crystalline PET film than the amorphous and annealed films. The slower relaxation is contrary to what was observed by Hopfenberg et al in polystyerene-n-pentane. They found that relaxation rate was higher in the uniaxially oriented glassy films than the annealed samples [28]. Orientation leads to residual stresses in the polymer. Even though the non-annealed film has a higher

final uptake than the annealed film, the residual stresses seem to slow down the relaxation process In other words, the activation energy of the process seems to be higher. Moreover, due to a greater degree of polymer chain stability in the annealed sample, a larger fraction of the uptake is contributed by Fickian diffusion in the annealed sample than the amorphous and non-annealed samples. Less stress and lower susceptibility to swelling result in lower uptake due to relaxation in the annealed film. A more systematic study with samples of different elongations and tested at different temperatures is needed to understand the rate of relaxation in the non-annealed, oriented polymers.

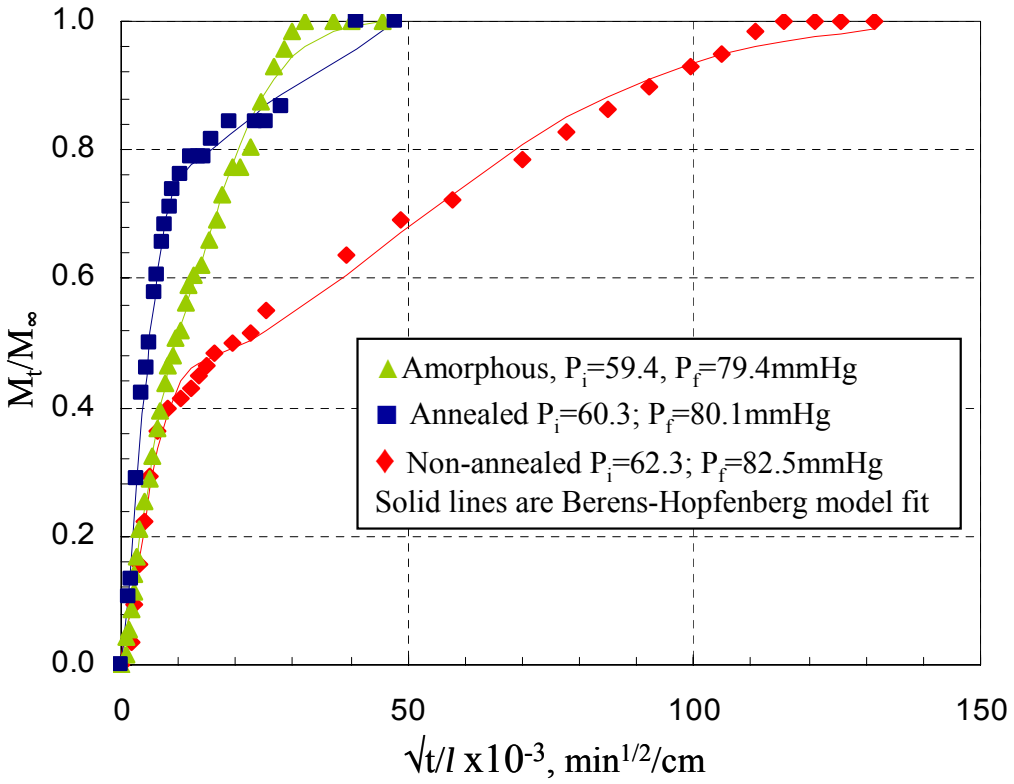

Figure 4.10: Sorption kinetics of different PET samples at 35°C at p/p_o=0.40.Amorphous: D= 2.64±0.33 x10^{-10} cm^2/s, k_R=2.13±0.10x10^{-5} s^{-1}, Φ_F=0.37±0.02; Annealed PET: D=2.48±0.15x10^{-10} cm^2/s , k_R=2.02±0.32 s^{-1}, Φ_F=0.74±0.01; Non annealed PET- D= 1.84±0.20 x10^{-10} cm^2/s, k_R=0.62±0.03 x10^{-5} s^{-1}, Φ_F=0.45±0.01

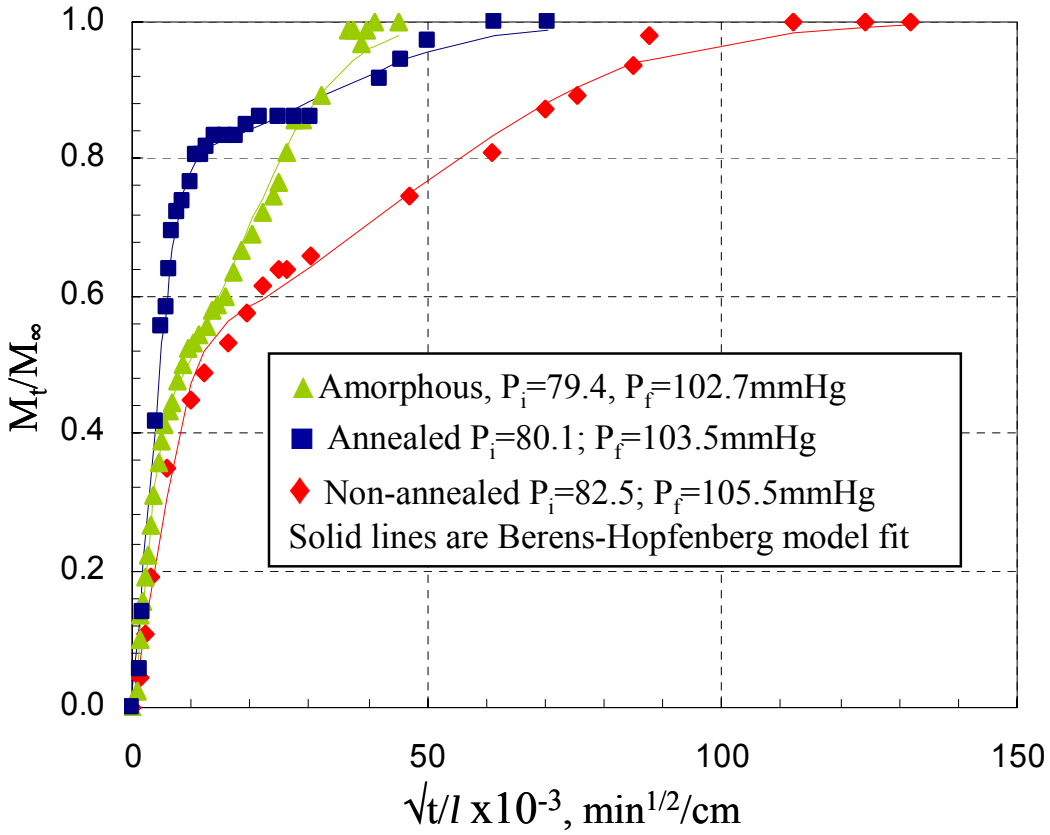

Figure 4.11: Sorption kinetics of different PET samples at 35°C at p/p_o=0.50. Amorphous PET- D= 4.86±0.44 x10^{-10} cm^2/s, k_R= 1.31±0.05 x10^{-5} s^{-1}, Φ_F=0.42±0.01; Annealed PET- D= 2.16±0.14 x10^{-10} cm^2/s, k_R=1.16±0.22 x10^{-5} s^{-1}, Φ_F=0.80±0.01; Non-annealed PET- D= 1.15±0.14 x10^{-10} cm^2/s, k_R=0.80±0.06 x10^{-5} s^{-1}, Φ_F=0.54±0.01

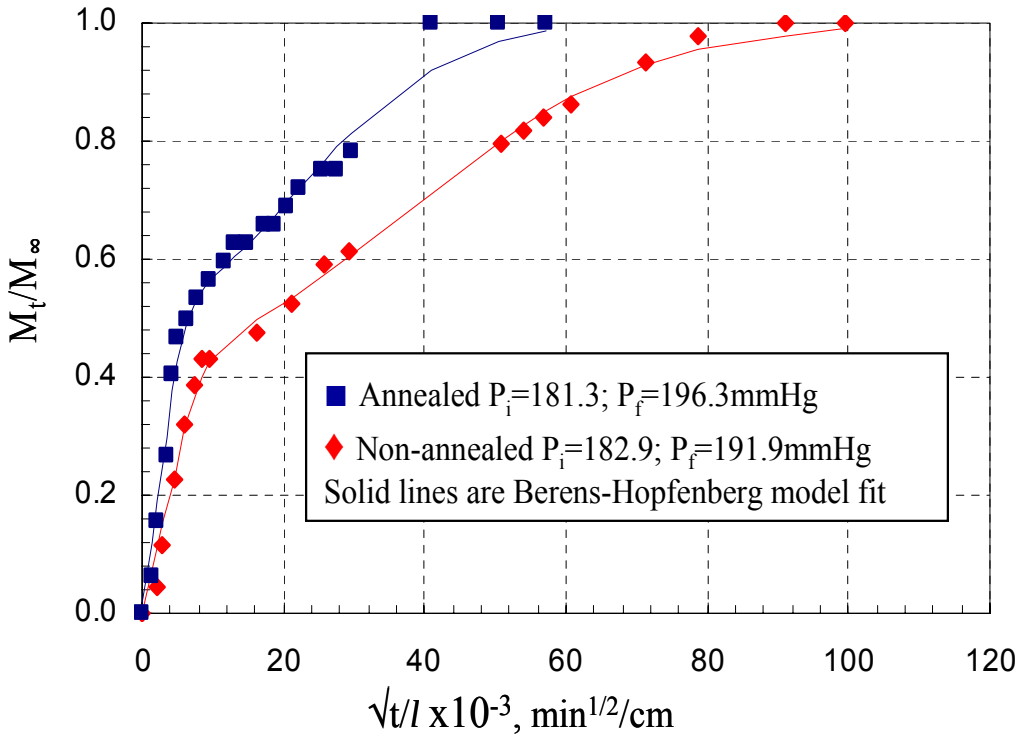

Figure 4.12: Kinetics of the semicrystalline samples at p/p_o=0.95 at 35°C. Annealed PET- D= 3.57±0.53 x10^{-10} cm^2/s, k_R=2.05±0.23 x10^{-5} s^{-1}, Φ_F=0.52±0.02; Non-annealed PET- D= 1.70±0.24 x10^{-10} cm^2/s, k_R=1.15±0.08 x10^{-5} s^{-1}, Φ_F=0.44±0.02

At high activities, both semicrystalline samples show two-stage kinetics. As at intermediate activities, the non-annealed film relaxes much more slowly that the annealed film. The kinetics are shown in Figure 4.12. However, kinetics for amorphous PET, shown in Figure 4.13, have some interesting and unusual features. Two things stand out: (a) there is an induction period of nearly 1.0 minute in each of the three cases; (b) the sorption shows Fickian characteristics with the diffusivity increasing with activity or concentration. The occurrence of these features together represents a dichotomy.

It is believed that this induction is statistically significant. A comparison with Fickian kinetics at lower activities in Figure 4.5 shows that sorption is measurable after 1 minute

of vapor introduction. The total mass uptake in these low activity cases is actually less than at the higher activities being considered here. Thus, at small times, the mass change is also correspondingly small. Nevertheless, it is measurable and correlates well with the Fickian prediction. Therefore, it is believed that the induction period observed here is not the result of error. Durning and coworkers studied sorption of methanol in annealed, semi-crystalline PET by dipping it in liquid methanol (p/p_o=1) at various temperatures [26]. They also observe an induction time followed by uptake that is linear with square root of time in the temperature range of 35-62^oC. However, they choose to ignore the induction time as an artifact because of the dominantly Fickian nature of the kinetics [15]. An induction time is the fingerprint of non-Fickian effects, commonly observed with Case II kinetics. Hopfenberg et al. and Windle et al. observed an induction time in the PMMA-n-propyl alcohol and PMMA-methanol systems respectively [29, 30]. However, once mass uptake starts, the kinetics is clearly Case II as it is linear in time (n = 1 in equation 2.38). At higher temperatures, they observed that the features of anomalous kinetics appeared and approached Fickian behavior ($\frac{1}{2} \leq n < 1$) [30, 31]. The induction time also disappeared in these cases. Hopfenberg suggested that this could be happening due to an increase in the diffusion resistance in the swollen regions of the polymer, which slowed further sorption and swelling. Hopfenberg also observed that samples with different characteristic dimensions show completely different kinetics due to the dimensional dependence of diffusion rate. N-hexane sorption in polystyrene was Case II in 3mil thick films, Super Case II in 1.5 mil thick films, and anomalous in 0.534 micron diameter spheres [32]. There are no reports of the uptake kinetics showing Fickian features together with an induction time. The present observations of anomalous kinetics

up to p/p_o= 0.70, coupled with an induction time, suggest that the amorphous PET at p/p_o= 0.80 and above most likely undergoes significant relaxations. An alternate way of looking at the kinetics would be to recognize the presence of an inflection point in the M_t/M_∞ plots at, approximately, 1.2 minutes. An inflection point can never occur in a completely Fickian curve. Hopfenberg and Peterlin have observed such kinetics and show that this is predominantly relaxation driven [32, 33]. Both the analyses seem to suggest that relaxation effects are involved here.

To confirm this, completely amorphous films of different thicknesses should be studied. As mentioned in section 2.4, the fool proof test of Fickian characteristics is the collapse of all kinetics on to a master curve when plotted against $\sqrt{t}/l$. In PET-methanol case, there is a strong possibility that the relaxation and Fickian components will be separable when the characteristic dimensions are different. Moreover, the swelling of the sample and concentration dependent diffusion coefficients can be understood for this system.

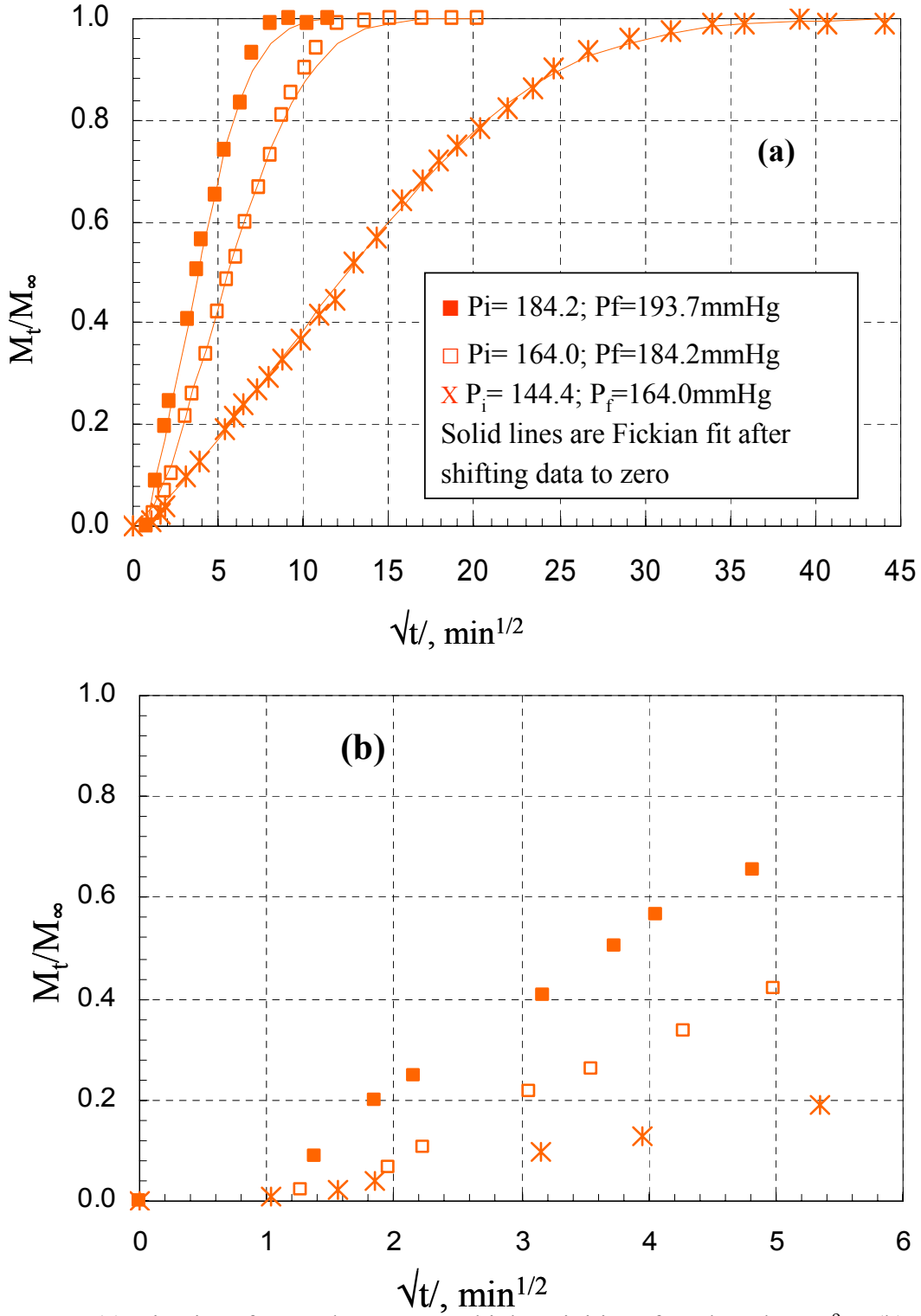

Figure 4.13: (a) Kinetics of amorphous PET at high activities of methanol at 35°C; (b) Inset showing the kinetics at small times with a clear induction time

4.3 METHANOL TRANSPORT USING DUAL MODE MODEL

Permeability of methanol in the PET samples has been evaluated based on the diffusion coefficients and equilibrium concentration at low activities. At high activities, due to relaxation effects, the diffusion coefficient at the steady state is unknown. This prevents evaluation of the permeability at steady state from sorption experiments alone. Permeability has been calculated using equation 2.10. The average D for a given concentration range is known from sorption experiments, and piece-wise integration is used to calculate the permeability that will be obtained in a typical permeation experiment when the film, after being evacuated, is exposed to a certain pressure on the upstream with the downstream at vacuum. Thus, C_1 in equation 2.10 is equal to zero, and C_2 corresponds to the equilibrium concentration at the upstream pressure.

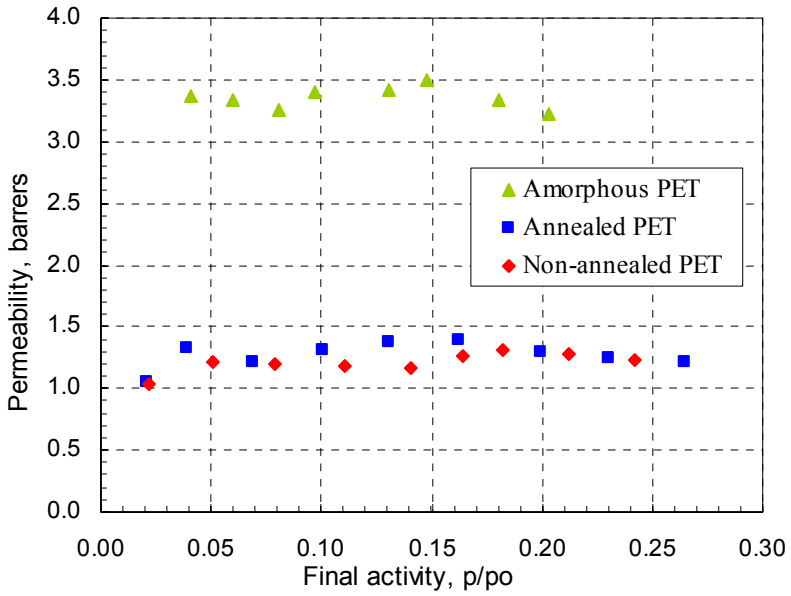

Figure 4.14: Permeability of methanol in PET at low activities at 35°C (P_{sat}= 202.3mmHg) estimated from sorption kinetics and equilibrium uptake.

Figure 4.14 shows the plot of permeability vs. activity. The permeability is constant with activity. This is to be expected because $F \rightarrow 0$, as evaluated from the dual mode model for effective diffusivity. $F \rightarrow 0$ in equation 2.26 results in a constant permeability. Thus, the predicted permeability is consistent with the dual mode model at low activities. The average values are shown in Table 4.7. Based on the amorphous film permeability and the amorphous fraction of the semi-crystalline samples, permeability of the annealed and non-annealed films is predicted using equation 2.14. Given the complexities of the semi-crystalline samples, the prediction matches the experimental results very well.

Table 4.7: Permeability of methanol in PET at low activities at 35^{o}C

	Amorphous	**Annealed**	**Non-annealed**
Average permeability (Barrers)	3.36±0.11	1.30±0.11	1.23±0.08
Predicted permeability using X_a & amorphous PET value (Barrers)	-	1.34±0.11	1.32±0.08

4.4 SUMMARY

The major conclusions of this chapter are summarized below:

1. Sorption isotherms show dual mode characteristics at low activities of methanol at 35^{o}C, and Flory-Huggins features at high activities. In the low activity regime, the diffusion coefficients followed concentration dependence predicted by the dual mode model. Permeability was predicted and model parameters evaluated.

Clustering phenomenon is not believed to be occurring in the methanol-PET system because diffusion coefficients increase as opposed to the decrease that may be expected with increasing concentration if clustering were to occur.

2. Even at low methanol activities, hysterisis in desorption and increased resorption suggest methanol induced conditioning effects. This conditioning may have detrimental effects on the barrier efficacy due to increased gas transport.
3. Unusual kinetics are observed in the amorphous film at high activities. It is hypothesized that these are strongly relaxation related and may be verified using films of different thicknesses.
4. At high activities, significant relaxation and swelling effects are observed despite crystallinity and orientation. Such swelling may deteriorate the barrier properties of the polymer.

4.5 REFERENCES

1. Gohil, R.M. and D.R. Salem, *Orientation distribution in the noncrystalline regions of biaxially drawn poly(ethylene terephthalate) film: a chain-intrinsic fluorescence study.* Journal of Applied Polymer Science, 1993. **47**(11): p. 1989-98.

2. Michaels, A.S. and H.J. Bixler, *Solubility of gases in polyethylene [and rubbery polymers].* Journal of Polymer Science, 1961. **50**: p. 393-412.

3. Slee, J.A., et al., *The transport of oxygen through oriented poly(ethylene terephthalate).* Journal of Polymer Science, Part B: Polymer Physics, 1989. **27**(1): p. 71-83.

4. Vieth, W.R., H.H. Alcalay, and A.J. Frabetti, *Solution of gases in oriented poly(ethylene terephthalate).* Journal of Applied Polymer Science, 1964. **8**(5): p. 2125-38.

5. Brolly, J.B., D.I. Bower, and I.M. Ward, *Diffusion and sorption of CO2 in poly(ethylene terephthalate) and poly(ethylene naphthalate).* Journal of Polymer Science, Part B: Polymer Physics, 1996. **34**(4): p. 769-80.

6. Hiltner, A., et al., *Oxygen transport as a solid-state structure probe for polymeric materials: A review.* Journal of Polymer Science, Part B: Polymer Physics, 2005. **43**(9): p. 1047-1063.

7. Koros, W.J. and D.R. Paul, *Carbon dioxide sorption in poly(ethylene terephthalate) above and below the glass transition.* Journal of Polymer Science, Polymer Physics Edition, 1978. **16**(11): p. 1947-63.

8. Jordan, S.M. and W.J. Koros, *Characterization of carbon dioxide-induced conditioning of substituted polycarbonates using various \"exchange\" penetrants.* Journal of Membrane Science, 1990. **51**(3): p. 233-47.

9. Jordan, S.M., M.A. Henson, and W.J. Koros, *The effects of carbon dioxide conditioning on the permeation behavior of hollow fiber asymmetric membranes.* Journal of Membrane Science, 1990. **54**(1-2): p. 103-18.

10. Berens, A.R., *Solubility of Vinyl-Chloride in Polyvinyl-Chloride).* Angewandte Makromolekulare Chemie, 1975. **47**(OCT21): p. 97-110.

11. Connelly, R.W., et al., *The effect of sorbed penetrants on the aging of previously dilated glassy polymer powders. I. Lower alcohol and water sorption in poly(methyl methacrylate).* Journal of Applied Polymer Science, 1987. **34**(2): p. 703-19.

12. Serad, G.E., et al., *Gas and vapor sorption and diffusion in poly(ethylene terephthalate).* Polymer, 2001. **42**(16): p. 6929-6943.

13. Stewart, M.E., et al., *The effect of sorbed penetrants on the aging of previously dilated glassy polymer powders. II. n-Propane sorption in polystyrene.* Journal of Applied Polymer Science, 1987. **34**(2): p. 721-35.

14. Enscore, D.J., et al., *Effect of prior sample history on n-hexane sorption in glassy polystyrene microspheres.* Polymer, 1977. **18**(11): p. 1105-10.

15. Billovits, G.F. and C.J. Durning, *Penetrant transport in semicrystalline poly(ethylene terephthalate).* Polymer, 1988. **29**(8): p. 1468-84.

16. Zhou, F.B. and W.J. Koros, *Study of thermal annealing on Matrimid (R) fiber performance in pervaporation of acetic acid and water mixtures.* Polymer, 2006. **47**(1): p. 280-288.

17. Wind, J.D., et al., *Relaxation dynamics of CO2 diffusion, sorption, and polymer swelling for plasticized polyimide membranes.* Macromolecules, 2003. **36**(17): p. 6442-6448.

18. Michaels, A.S., *Diffusion of gases in polyethylene terephthalate.* Journal of Applied Polymer Science, 1963. **34**(1): p. 13.

19. Berens, A.R., *Induction and measurement of glassy state relaxations by vapor sorption techniques.* Journal of Polymer Science, Part B: Polymer Physics, 1979. **17**(10): p. 1757-70.

20. Crank, J., *The Mathematics of Diffusion. 2d Ed*. 1975. 414 pp.

21. Koros, W.J., *Sorption and transport of gases in glassy polymers*, in *Chemical Engineering*. 1977, University of Texas: Austin. p. 274 pp.

22. Windle, A.H., *Case II Sorption*, in *Polymer permeability*. 1985.

23. Berens, A.R. and H.B. Hopfenberg, *Diffusion and relaxation in glassy polymer powders. 2. Separation of diffusion and relaxation parameters.* Polymer, 1978. **19**(5): p. 489-96.

24. Patton, C.J., R.M. Felder, and W.J. Koros, *Sorption and transport of benzene in poly(ethylene terephthalate).* Journal of Applied Polymer Science, 1984. **29**(4): p. 1095-110.

25. McDowell, C.C., B.D. Freeman, and G.W. McNeely, *Acetone sorption and uptake kinetics in poly(ethylene terephthalate).* Polymer, 1999. **40**(12): p. 3487-3499.

26. Durning, C.J., L. Rebenfeld, and W.B. Russel, *Integral sorption with induced crystallization.* Polymer Engineering and Science, 1986. **26**(15): p. 1066-78.

27. Dhoot, S.N., B.D. Freeman, and M.E. Stewart, *Sorption and Transport of Linear Esters and Branched Alkanes in Biaxially Oriented Poly(ethylene terephthalate).* Industrial & Engineering Chemistry Research, 2004. **43**(12): p. 2966-2976.

28. Baird, B.R., H.B. Hopfenberg, and V. Stannett, *The effect of molecular weight and orientation on the sorption of n-pentane by glassy polystyrene.* Polymer Engineering and Science, 1971. **11**(4): p. 274.

29. Hopfenberg, H.B., L. Nicolais, and E. Drioli, *Relaxation controlled (case II) transport of lower alcohols in poly(methyl methacrylate).* Polymer, 1976. **17**(3): p. 195-8.

30. Thomas, N. and A.H. Windle, *Transport of methanol in poly(methyl methacrylate).* Polymer, 1978. **19**(3): p. 255-65.

31. Nicolais, L., et al., *Diffusion-controlled penetration of polymethyl methacrylate sheets by monohydric normal alcohols.* Journal of Membrane Science, 1978. **3**(2-3-4): p. 231-45.

32. Hopfenberg, H.B., *The effect of film thickness and sample history on the parameters describing transport in glassy polymers.* Journal of Membrane Science, 1978. **3**: p. 215-230.

33. Peterlin, A., *Type II diffusion.* Organic Coatings and Plastics Chemistry, 1978. **39**: p. 121-2.

CHAPTER 5 : SORPTION AND TRANSPORT OF LOWER ALCOHOLS IN PET

This chapter presents equilibrium sorption and kinetics of lower alcohols in the 1.5 micron thick, biaxially oriented PET film. Methanol, ethanol, n-propanol and iso-propanol have been studied for the solubility and sorption kinetics in this film to understand how these properties change with increasing size of the penetrant and how branching may influence them as well. Sorption isotherms and kinetics are discussed in sections 5.1 and 5.2 respectively. Correlations of the penetrant solubility with various thermodynamic constants have been investigated to understand which quantities have the best correlation and may be used for prediction purposes.

5.1 EQUILIBRIUM SORPTION OF LOWER ALCOHOLS

Equilibrium uptake and kinetics were measured at 35^{o}C using the McBain quartz spring apparatus described in section 3.3.2 [1]. Table 5.1 shows some relevant properties of the penetrants.

5.1.1 Dual Mode Sorption

In the low activity region, methanol, ethanol and iso-propanol show dual mode behavior (i.e. the isotherm is concave to the x-axis). MeOH, EtOH and i-PrOH deviate positively from dual mode uptake predictions at activities of 0.25, 0.18 and 0.35 respectively. N-propanol shows dual mode characteristics all the way up to p/p_o= 0.91, which was the maximum activity tested. The methanol data for the low activity region

has been taken from the non-annealed, semicrystalline PET sample discussed in chapter 4 since the overall isotherms of methanol in the thin biaxially oriented film are very similar to those obtained for the thicker, non-annealed film. The dual mode isotherms of the lower alcohols are shown in Figure 5.1. Table 5.2 shows the dual mode parameters. Solubility of a penetrant generally increases with increasing condensability. This trend is seen in the case of lower alcohols since the sorbed concentration and k_d are highest in propanol (p_{sat} = 36 mmHg) and lowest in methanol. There is very little difference between the sorption isotherms of ethanol and iso-propanol, probably as a result of very similar saturation pressures (103.3 and 80.0 mm Hg respectively). This has been discussed further later in this section. It is also possible that owing to shape of i-propanol, the enthalpy of sorption is less which causes a lower overall uptake.

Table 5.1: Properties of lower alcohols and PET solubility parameter

Property → Penetrant ↓	**Saturation vapor pressure at 35°C, mmHg [2]**	**Molar Volume, cc/mol**	**Critical Temperature, K**	**Solubility Parameter, $MPa^{1/2}$**			
				δ_d	δ_p	δ_h	δ
Methanol [3]	202.3	40.7	518	15.1	12.3	22.3	29.7
Ethanol[3]	103.3	58.5	521	15.8	8.8	19.4	26.6
n-Propanol[3]	36.0	75.2	513	16.0	6.8	17.4	24.6
i-Propanol [3]	80.0	68.4	541.7	15.8	6.1	16.4	23.5
PET [4]	-	-	-	19.4	3.5	8.6	21.5

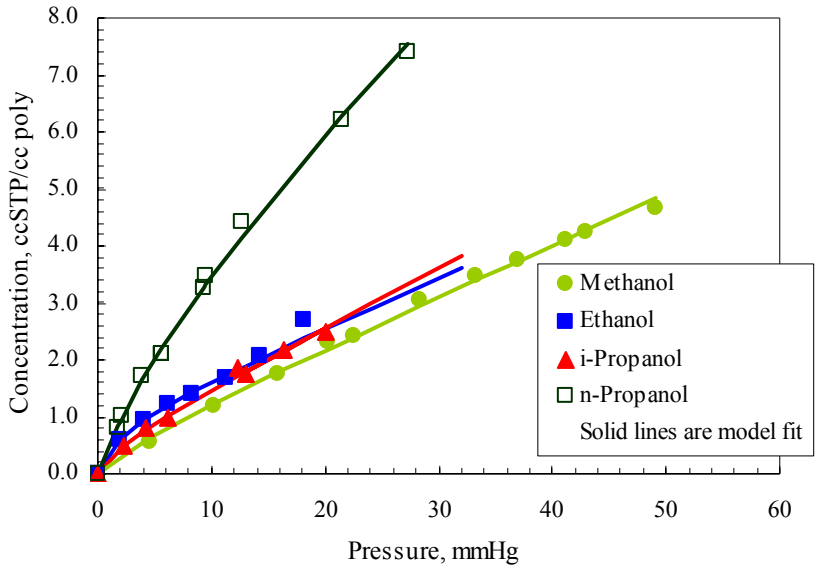

Figure 5.1: Dual mode region of the sorption isotherm of MeOH, EtOH, i-PrOH and n-PrOH

Table 5.2: Dual mode model paramaters for lower alcohols

Penetrant → Parameter ↓	**C_H', ccSTP/ccpoly**	**b atm^{-1}**	**k_d, ccSTP/ccpoly/atm**
Methanol	0.71 ± 0.11	144.4 ± 15.2	63.1 ± 2.1
Ethanol	0.95 ± 0.31	308.5 ± 177.6	64.6 ± 11.6
n-Propanol	2.33 ± 0.12	104.46 ± 21.89	159.8 ± 53.0
i-Propanol	0.47 ± 0.25	415.3 ± 51.2	80.56 ± 8.71

Since the objective of this work is to provide further insight into the prediction of sorption properties of larger compounds, it is important to compare the solubility of the alcohols with that of other available penetrants. As was mentioned in section 2.1.2, solubility of a penetrant depends on many factors including its condensability. Critical temperature and boiling temperature are very good measures of the penetrant condensability and, hence, are often used to compare the solubility of different penetrants. Figure 5.2 shows the correlation between penetrant critical temperature and its infinite dilution solubility, similar to what was proposed by Dhoot et al. Data generated in this work has also been added [5]. Based on the dual mode model described in equations 2.17 and 2.19, at low pressures, with $p \rightarrow 0$, the solubility is the sum of k_d and $C_H'b$. This sum is the infinite dilution solubility (S_a). Whenever the dual mode parameters are available, S_a is evaluated using equation 2.19. In other cases such as water, CH_2Cl_2 and CH_3CHO, S_a is evaluated from the data at low activities by assuming Henry's Law. For the purposes of comparison with various literature values, all the solubility values have been normalized by the amorphous fraction of the PET sample. Dhoot et al propose a power law fit between the infinite dilution solubility and critical temperature. As can be seen from the solid line (exponential fit) in the figure, a broad correlation exists between solubility and T_c. However there are significant deviations, especially for molecules with polar functional groups. For example, though CH_2Cl_2 and CH_3COOCH_3 have similar T_c values of 510 K, their S_a values are quite different. On the other hand, the solubility of the permanent gases correlates very well with T_c. Thus, the predicted solubility may be quite accurate using the exponential dependence on critical temperature for permanent gases. However, for large, condensable, polar penetrants, the error of the prediction may

be large. Micheals et al. showed that solubility of permanent gases also correlates very well with the Lennard-Jones force constant (ε/k) [6]. However, for larger, polar penetrants, even that correspondence shows significant deviations. Therefore it becomes important to understand the factors which may lead to a better prediction of the solubility of polar molecules.

A quantity which is often used to establish mutual solubility of two solvents and to choose a good solvent for a particular polymer is the Hildebrand's solubility parameter, which depends on the cohesive energy density of the solvent molecule. This solubility parameter has been decomposed into dispersive (δ_d), permanent dipole-dipole interaction (δ_p) and hydrogen bonding parameters (δ_h) [3]. These are called Hansen's solubility parameters. For alcohols and PET, these values have been shown in Table 5.1. The overall solubility parameters δ may be written as:

$$\delta^2 = \delta_d^2 + \delta_h^2 + \delta_p^2 \qquad 5.1$$

Despite the presence of the polar ester (–COO–) group in PET, the dipole-dipole interaction and hydrogen bonding parameters are not very large. The largest contribution comes from the dispersive solubility parameter, indicating that this, and not hydrogen bonding might be the dominant factor in PET. This is also evidenced by the water solubility in PET, which is much lower than the solubility in other polymers with polar groups such as ethylene vinyl alcohol, poly(methyl methacrylate), polyimides and poly(acrylonitrile) [7-13]. Figure 5.3 shows the infinite dilution solubility of various classes of penetrants such as alcohols, ketones and hydrocarbons plotted against the penetrants' dispersive solubility parameter (δ_d). δ_d values for the organic species have

been taken from the Polymer Handbook [3], and the $\delta_{d,PET}$ is more than all of these values. The solubility shows an excellent exponential correlation with the dispersive solubility parameter within the same group of penetrants. Since only two data points are known for the esters, an exponential fit has not been made. It must be pointed out that even water solubility in PET lies on the same line as the alcohols. Water has very different overall properties with a very high value of δ_h =42.7 $MPa^{1/2}$ and cannot be associated with organic molecules in the strict sense. Yet, the δ_d of water is similar to that of the alcohols. Structurally it may be considered that one of the hydrogen atoms in water has been replaced with a CH_3- group in methanol. It is, therefore, encouraging to find that even water fits the correlation drawn with the dispersive solubility parameter.

Since different functional groups lie along different lines, the dipole-dipole interaction and hydrogen bonding ability play an important role in determining the solubility even though δ_d may be the dominant factor,. Even for similar dispersive solubility parameter values, the trend of solubility is:

Esters > Ketones > Alcohols > Hydrocarbons

As a general rule, closer matching of the solubility parameters of species 1 and 2 (i.e. lower $(\delta_1-\delta_2)^2$ values) leads to greater solubility of 1 in 2. However, this general thumb rule may not be directly applicable in the case of polymers. The solubility of the esters is higher than the ketones due to differences in the polar and hydrogen bonding characteristics, with the esters having a stronger hydrogen bonding nature [14]. Similar trends have also been reported for acetone and methyl acetate sorption in poly(n-butyl methacrylate) [15]. Alcohols also have a very high hydrogen bonding character. However, their solubility in PET is only slightly more than that of the hydrocarbons,

which have no polar groups, and is less than the esters and ketones. Hopfenberg et al. studied sorption of lower alcohols including n-PrOH and i-PrOH in PMMA at different temperatures and evaluated the enthalpy of sorption. They concluded that while hydrogen bonding may control the penetrant-penetrant interactions, it plays a smaller role to play in the penetrant-polymer interactions [16]. Similarly, for PET-lower alcohol systems, it seems that hydrogen bonding has a smaller, still significant role to play in the solubility of the penetrants. As shown in Figure 5.4, $(\delta_h-\delta_{h,PET})^2$ of the different functional groups influences the solubility of the penetrant. Solubility of C-3 and C-4 molecules with different functionalities such as ketone, ester or alcohol groups decreases with increasing $(\delta_h-\delta_{h,PET})^2$. This difference is lowest for esters and results in their increased solubility over alcohols, even though the δ_d is similar for the penetrants. Such a correlation can become a useful tool for larger flavor molecules which usually have more than one functional group. However, to develop this correlation completely, two things are needed: (a) some other functionalities such as –COOH, -CHO, -O- and –C= need to be studied and plotted in a similar manner and, (b) flavor molecules are often cyclic compounds; therefore a few small cyclic molecules should also be added to this data base [17]. These investigations may lead to the identification of an additional dependence on δ_p which is not evident in this case. Therefore, depending on the functional groups present and the number of carbon atoms, a penetrants' solubility may be predicted using Hansen solubility parameters. Of course, it must be emphasized that, all throughout, only infinite dilution solubility is being correlated. At higher activities, conditioning and swelling effects and solvent induced crystallization will be dependent on the Flory-Huggins parameter that determines the penetrant uptake. Consequently, the sorbed concentration

of the swelling penetrant will cause enhancement in the polymer chain mobility, and a reduction in the glass transition temperature.

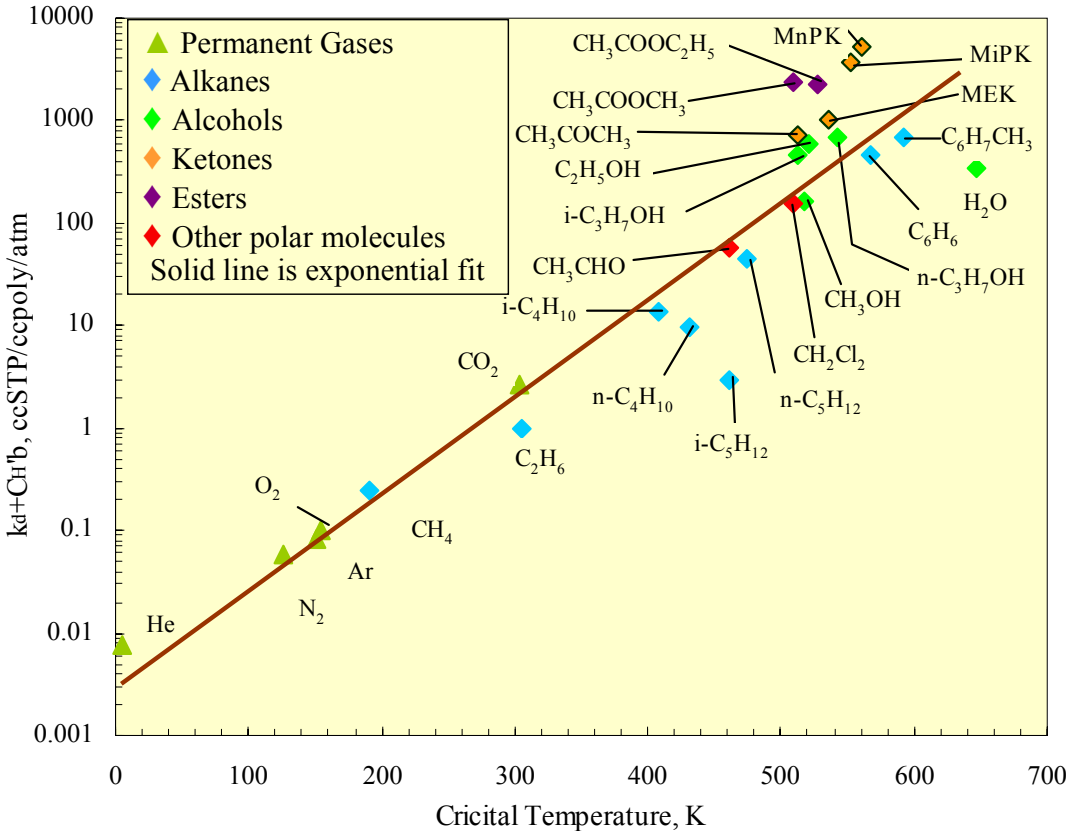

Figure 5.2: Infinite dilution solubility of various penetrants in PET, normalized with respect to the amorphous fraction. Data for He, N_2, O_2, Ar, CH_4 and C_2H_6 has been taken from [6], CO_2 data from [18], acetone data from [19], CH_3COOCH_3, i-C_4H_{10}, $CH_3COOC_2H_5$, i-C_5H_{12} data from [20], MEK, MiPK, MnPK data from [14], n-C_4H_{10}, n-C_5H_{12} data from [5], C_6H_6 from [21], H_2O from [22], CH_2Cl_2 from [23] and CH_3CHO from [24]. All except water have been measured at 35°C. Water was measured at 25°C.

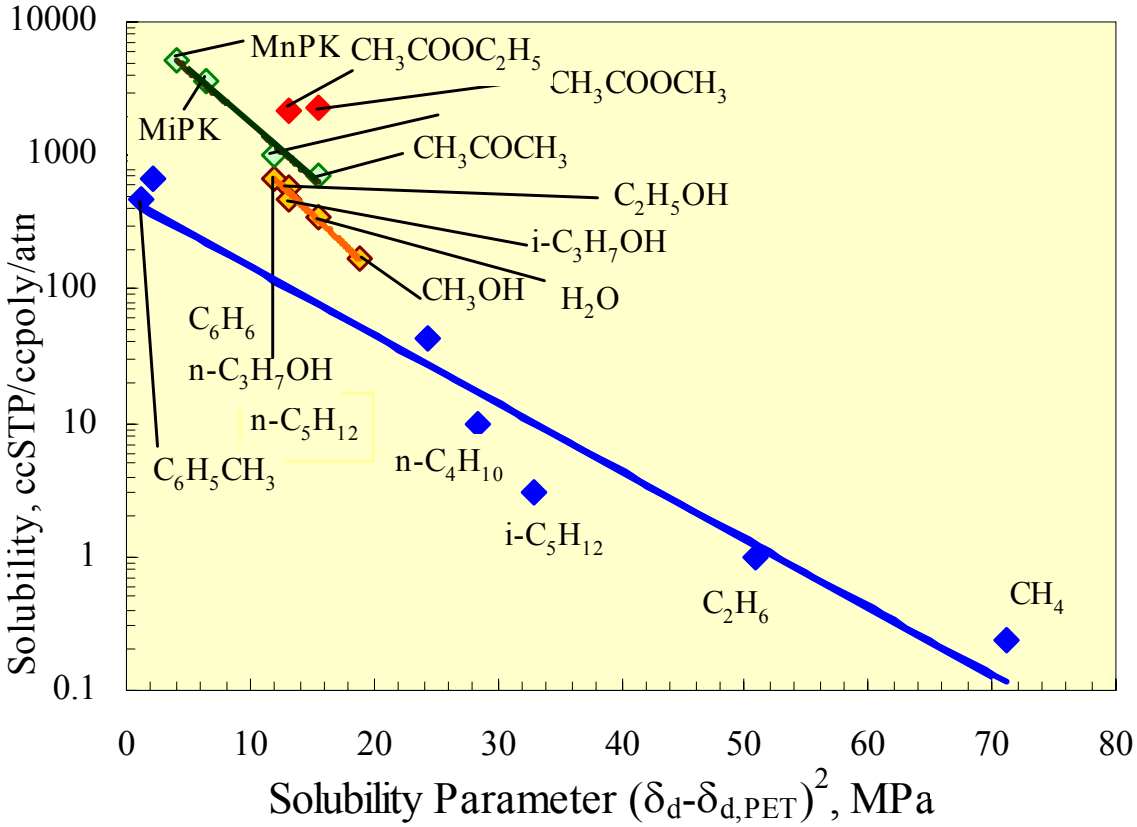

Figure 5.3: Relationship of solubility with the dispersive solubility parameter. PET δ_d is 19.4MPa$^{1/2}$. References are the same as in figure 5.3.

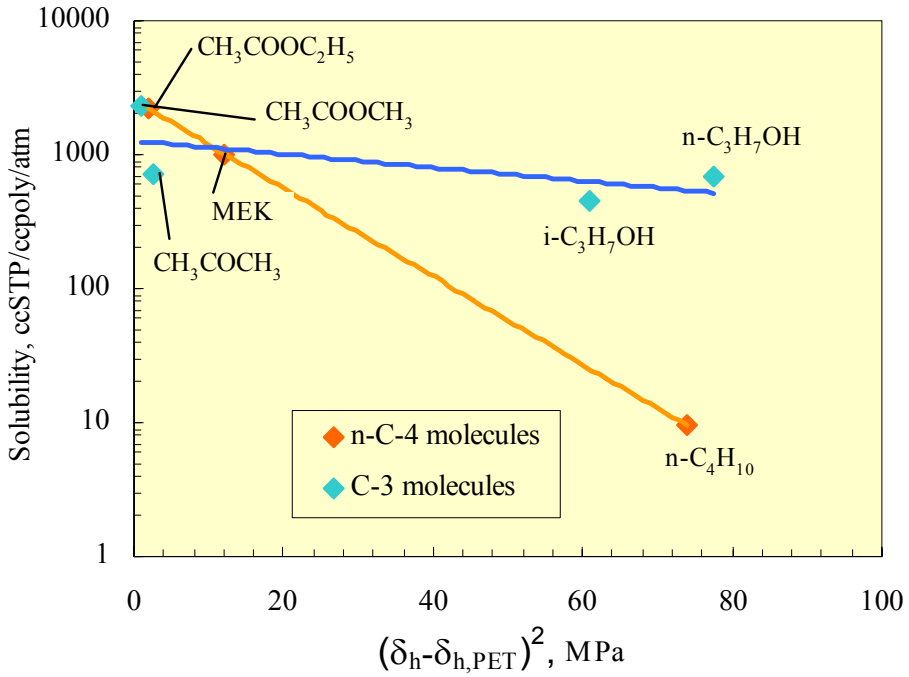

Figure 5.4: Relationship of solubility of penetrants with different functional groups with hydrogen bonding solubility parameter

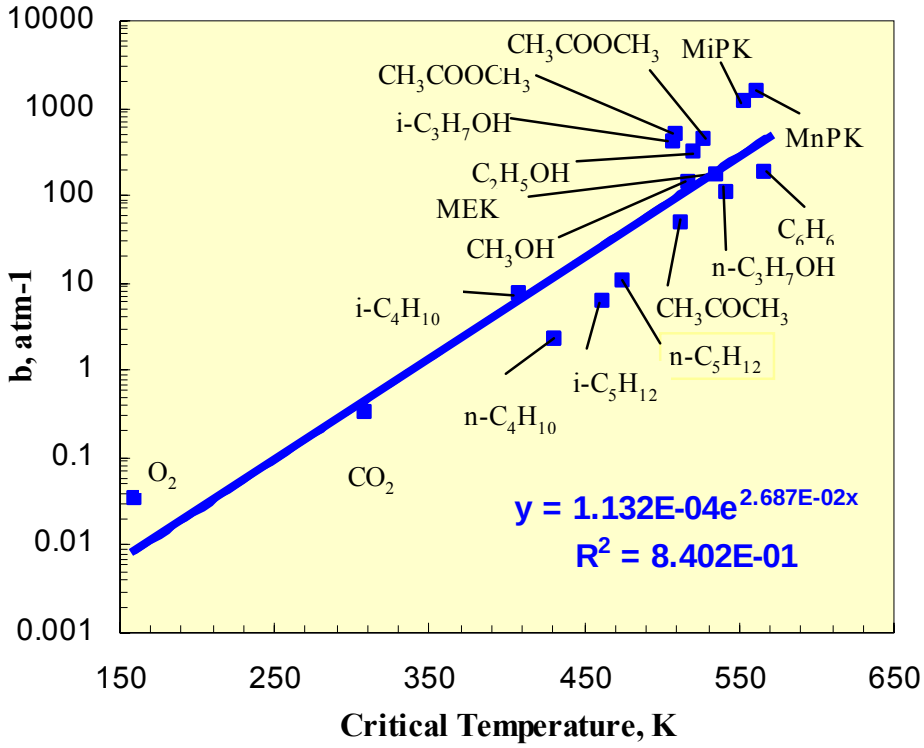

Figure 5.5: Correlation of affinity constant of various penetrants in PET with their critical temperature

Attempts have also been made to correlate the affinity constant, b, with various thermodynamic quantities such as critical temperature and the Lennard-Jones force constant (ε/k) [19]. For the permanent gases such as He, O_2, Ar, etc, the ε/k vs. log b has been shown to be linear for various polymers [25]. However, when all the polar molecules are also included, correlating with critical temperature seems to give a better fit. This is shown in Figure 5.5 above. The critical temperature for the penetrants has been obtained from [26].

5.1.2 Sorption at High Activities

Sorption isotherms of methanol, ethanol and iso-propanol showed Flory-Huggins characteristics at higher activities. The complete sorption isotherms, plotted with respect to activity of the penetrant, are shown in Figure 5.6. n-Propanol has been included in the figure for comparison even though it shows dual mode characteristics up to p/p_o=0.90. Flory-Huggins parameters are shown in Table 5.3. At similar activity levels, methanol has the highest sorption among the four penetrants and may be expected to swell the polymer more than the other molecules. Ethanol sorption is less than methanol but more than n- and i-propanol. It is interesting to note that the uptake of the propyl alcohols is very similar in the high activity range despite significantly different saturation pressures or volatility (80 mm Hg for i-propanol vs. 36 mm Hg for n-propanol). % Weight uptake at the highest activity of the penetrant is also shown in Table 5.3. These values are on a total polymer weight basis. Even though the sorbed concentration is higher for MeOH due to a smaller molecular weight, the weight % uptake is very similar for all the penetrants.

Table 5.3: Flory-Huggins interaction parameter and % weight uptake for lower alcohols

Penetrant	**Methanol**	**Ethanol**	**n-propanol**	**Iso-propanol**
Interaction parameter, χ	1.95 ± 0.01	2.10 ± 0.02	-	2.06 ± 0.03
Uptake at the highest activity measured, g/100g poly	2.47	2.08	1.72	1.98

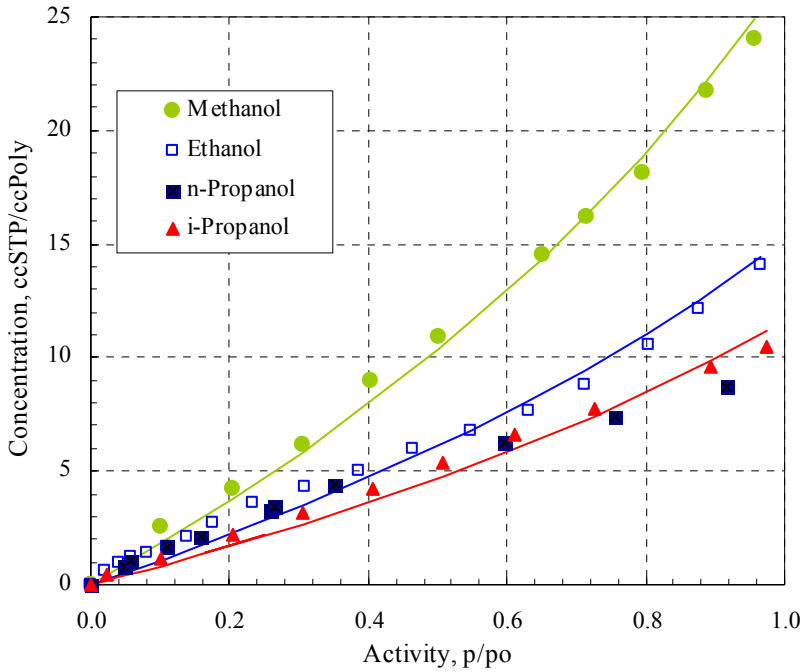

Figure 5.6: Sorption isotherms of lower alcohols in PET. Solid lines are Flory-Huggins model fit with a constant interaction parameter χ.

5.2 SORPTION KINETICS

As in the case of the methanol and amorphous PET system where Fickian diffusion was observed at low activities and small concentration intervals, the thin, biaxially oriented film shows Fickian characteristics at low activities methanol, ethanol and n- and i-propanol. However, significant relaxation effects are observed at higher activities. Figure 5.7 shows the kinetics of EtOH, i-PrOH and n-PrOH at low partial pressures. Methanol sorption in the 1.5μ thick film at low activities is not shown here because sorption equilibrium is reached very fast when the kinetics are Fickian which leads to a higher diffusion coefficient of the order of 10^{-10}cm^2/s as shown in chapter 4. Based on the M_t/M_∞ vs. $t^{1/2}$ plots, diffusion coefficients have been evaluated for all the penetrants using

equation 2.36. As is to be expected with increasing penetrant size, the diffusion coefficients decrease in the following order in the low pressure range being considered.

MeOH (10^{-10}cm^2/s) > EtOH (10^{-12}cm^2/s) > n-PrOH (10^{-13}cm^2/s) > i-PrOH (10^{-14} cm^2/s)

The difference in the position of the –OH group in i- and n-PrOH causes an order of magnitude decrease in the diffusion coefficient. The van der Waal's diameter and the dimensions of these molecules are shown below in Table 5.4. The van der Waal's diameter (units of nm) has been calculated using equation 5.1. The constant *b* (units of liter/mol) is the molar volume that is used in van der Waal's equation of state [27], and may be calculated using the critical temperature and pressure [26].

$$d_{vdW} = 1.184 b^{1/3} \qquad 5.2$$

Though the van der Waal's diameters of the i-PrOH and n-PrOH have been calculated to be very similar, the changes in the dimensions of the two molecules clearly explain the reduction in the diffusivity of i-PrOH. The decreased diffusion coefficient is a result of the molecular shape of i-PrOH. Despite being shorter than n-PrOH, iso-propanol is a much fatter molecule as is suggested by its greater width and height. This means that the molecule needs to expend more energy as its makes an activated jump. A higher energy penalty will result in decreased frequency of the jumps and, hence, a lower diffusion coefficient. Dhoot observed that for hydrocarbons, i-butane has a lower diffusion coefficient than even n-pentane. They conclude that branching influences the diffusivity more than an increase in the chain length by one carbon atom. It seems that the increase in the width and height of i-butane molecule with respect to the n-butane structure is responsible for the lower diffusion coefficient than n-butane and n-pentane. Berens and Hopfenberg suggest that anisometric molecules, which have different orthogonal

dimensions and are either flattened (e.g. benzene) or long (e.g. n-hexane), have greater mobility than the nearly spherical molecules. They conclude that the diffusivity of such molecules is governed by a dimension smaller than the mean penetrant diameter. This could explain why, despite very similar van der Waal's diameter, i- and n-propanol have different diffusivities. They also propose the concept of a 'diffusion diameter', which is the diameter of a hypothetical spherical molecule that has the same diffusion coefficient. Though this approach takes into account the shape effect, as opposed to other correlations that may be drawn with the mean diameter estimated from liquid density and the critical or molar volume of the penetrant, it suffers from the disadvantage that the 'diffusivity diameter' is not known for all penetrants. Moreover, the diameter evaluated by Berens and Hopfenberg for the same species in different glassy polymers often has different values [27]. Therefore, it appears that the correlation with critical or mean diameter may be more useful despite the possibility of a large error in the predicted diffusivity of polar molecules [24] [27].

Table 5.4: Dimensions of lower alcohols

Penetrant	**Methanol**	**Ethanol**	**n-Propanol**	**i-Propanol**
van der Waal's diameter, (Å)	4.78	5.25	5.65	5.69
Dimensions, $l \times w \times h$ (Å)	4.6×3.8×3.5	6.0×3.8×4.0	6.3×5.4×4.9	7.5×3.8×4.2

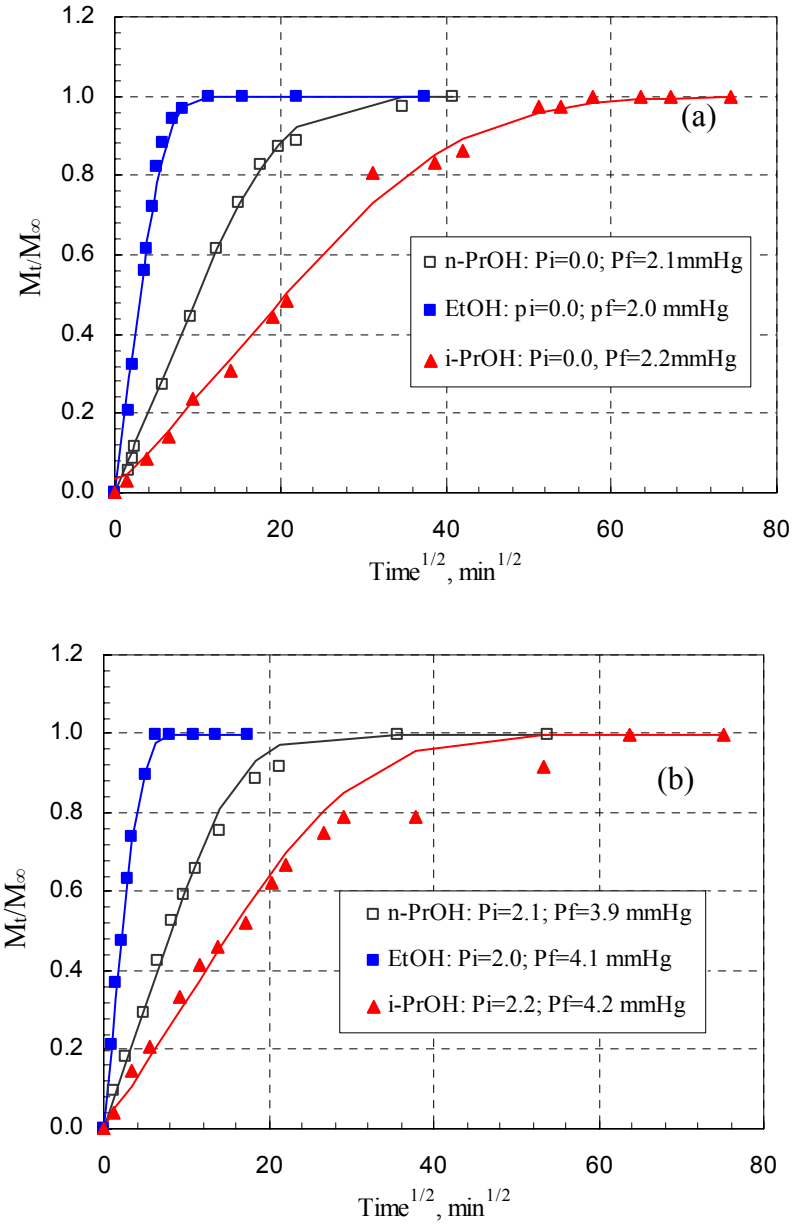

Figure 5.7: Fickian diffusion of ethanol, i-propanol and n-propanol in the low pressure regime. (a) $D_{EtOH}=1.91 \pm 0.07x10^{-12}cm^2/s$; $D_{i\text{-}PrOH}= 4.31 \pm 0.18x10^{-14}cm^2/s$; $D_{n\text{-}PrOH}= 1.79 \pm 0.05x10^{-13}cm^2/s$. (b) $D_{EtOH}=3.41 \pm 0.10x10^{-12}cm^2/s$; $D_{i\text{-}PrOH} = 7.83 \pm 0.18x10^{-14}cm^2/s$; $D_{n\text{-}PrOH}= 2.64 \pm 0.13x10^{-13}cm^2/s$

At intermediate and high activities, relaxation effects have been observed in the kinetics of all the penetrants. Figure 5.8, Figure 5.9, Figure 5.10 and Figure 5.11 show representative kinetics for methanol, ethanol, n-propanol and i-propanol. Such kinetics have also been observed for sorption of other penetrants such as benzene, acetone and methyl acetate etc in PET. Other polymer penetrant systems which show such a behavior include polystyrene- n-hexane, poly(vinyl alcohol)-vinyl chloride and many others [28, 29]. Even sorption of d-limonene in oriented, rubbery poly-propylene shows such non-Fickian characteristics which suggest that sorption kinetics of large aroma flavors is influenced by the polymer chain relaxation. These two stage effects in the PET-lower alcohols system have been modeled as before using the Berens-Hopfenberg model (equations 4.6-4.7), and the relaxation rate constant, diffusion coefficient and fractional Fickian uptake can be obtained. Diffusion coefficients thus obtained as a function of concentration are plotted in Figure 5.12. There is a general trend of increase in the diffusivity with concentration. The most pronounced effect is in the case of isopropanol, where the diffusion coefficients actually increase by two orders of magnitude over the entire activity range. Methanol diffusion coefficients cannot be obtained for the thin film because nearly 90% of the Fickian uptake happens within the first minute during which many data points cannot be taken. For comparison, therefore, diffusion coefficients from the non-annealed, semicrystalline film have been shown in the plot. A common form of the concentration dependence of the diffusivity is an exponential relationship as is shown in equation 5.2.

$$D = D_O \exp(\beta C) \qquad 5.3$$

C is the average concentration of the penetrant in the polymer that has been calculated

using equation 2.5. D_o represents the infinite dilution diffusion coefficient, and β is a constant. The concentration dependence of β is strongest for isopropanol, the largest penetrant, and weakest for methanol, the smallest penetrant. This would suggest much stronger concentration dependences for larger molecules. Reported values of the parameter β for linear and branched alkanes, esters and ketones suggests that the concentration dependence of the diffusion coefficient is highest for the alkanes (iso-butane, n-pentane and iso-pentane), with β being greater than 1. On the other hand, as in the case of alcohols, the esters and ketones have relatively weaker concentration dependence with β being in the range of 0.3 and 0.5. This is somewhat surprising, as a more interacting penetrant would be expected to have higher concentration dependence, which, in the case of PET, would be molecules with polar groups and not the hydrocarbons. Solubility trends reinforce this expectation as the solubility of the penetrants with polar groups is higher than that of the hydrocarbons. At present, however, values reported in the literature seem to support the reverse trend of concentration dependence. It must be kept in mind that the diffusion coefficients reported here are based on the initial uptake of the penetrant, which is Fickian. Relaxation of the polymer chains thereafter implies that the diffusion coefficient of the penetrant, apart from being concentration dependent, will also be time dependent. The penetrant diffusion coefficient obtained using the Berens-Hopfenberg model is not the steady state diffusivity. Apart from being a measure of the initial diffusivity, this value is also indicative of the penetrant mobility of the polymer matrix [30]. In that sense, deviation from dual mode behavior of the sorption isotherm and swelling are consistent with the increasing diffusivity that has been measured.

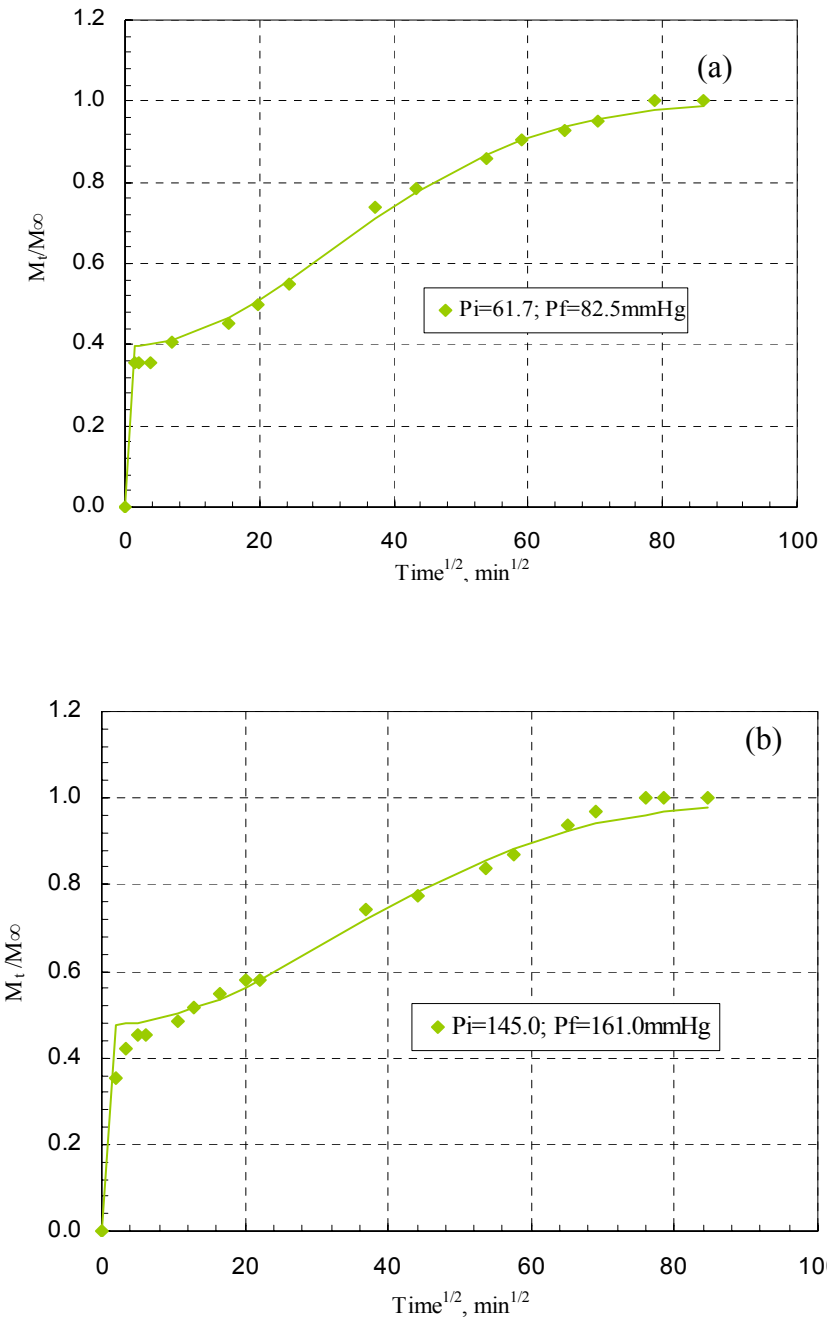

Figure 5.8: Non-Fickian sorption kinetics of methanol in 1.5m biaxially oriented PET. Diffusion coefficient is not obtained due to very quick Fickian uptake. (a) k_R= 8.77x10^{-6} s^{-1}, ϕ_f= 0.40; (b) k_R= 7.59x10^{-6} s^{-1}, ϕ_f= 0.48;

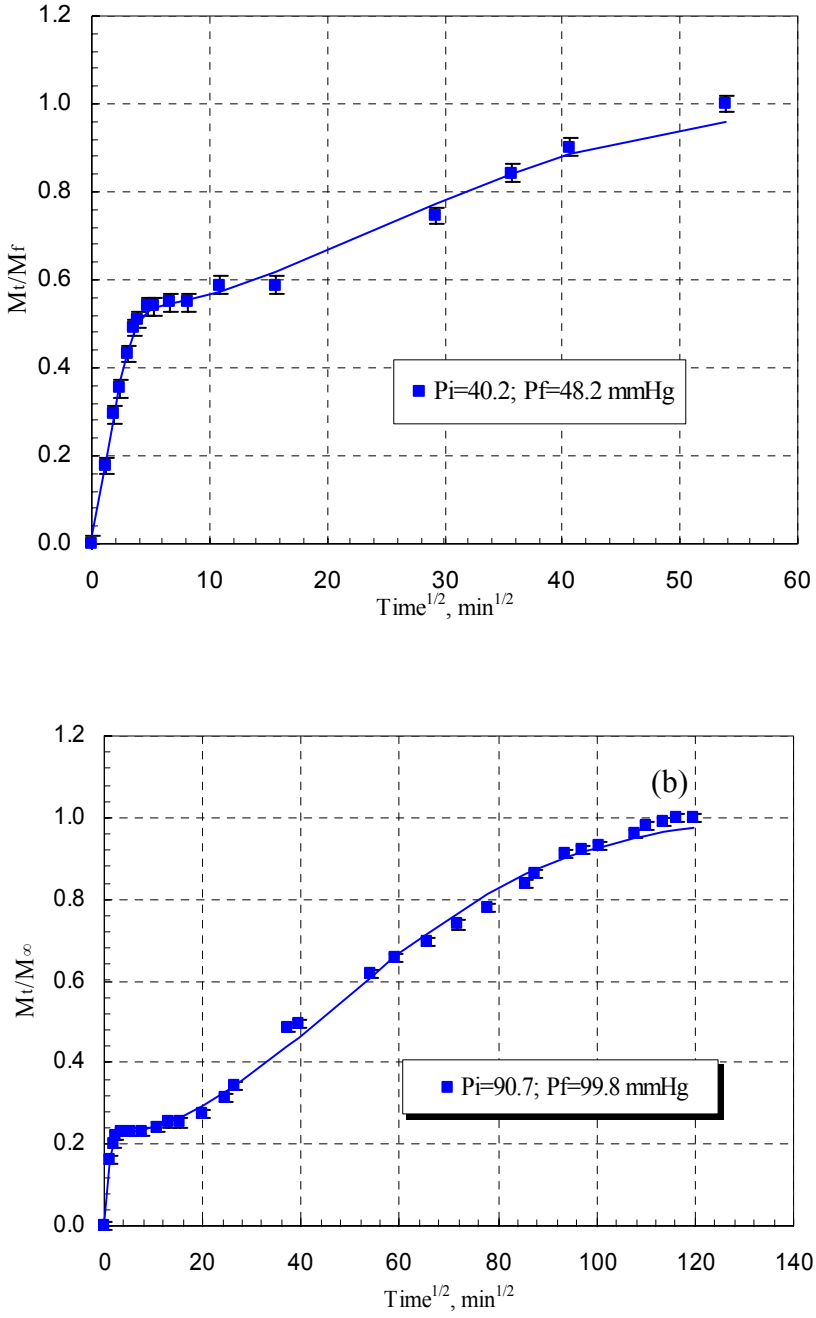

Figure 5.9: Non-Fickian sorption kinetics of ethanol in 1.5m biaxially oriented PET. (a) $D = 6.16 \pm 0.5 \times 10^{-12}$ cm^2/s, $k_R = 1.43 \pm 0.09 \times 10^{-5}$ s^{-1}, $\phi_f = 0.53 \pm 0.009$; (b) $D = 2.53 \pm 0.64 \times 10^{-11}$ cm^2/s, $k_R = 3.91 \pm 0.1 \times 10^{-6}$ s^{-1}, $\phi_f = 0.24 \pm 0.007$

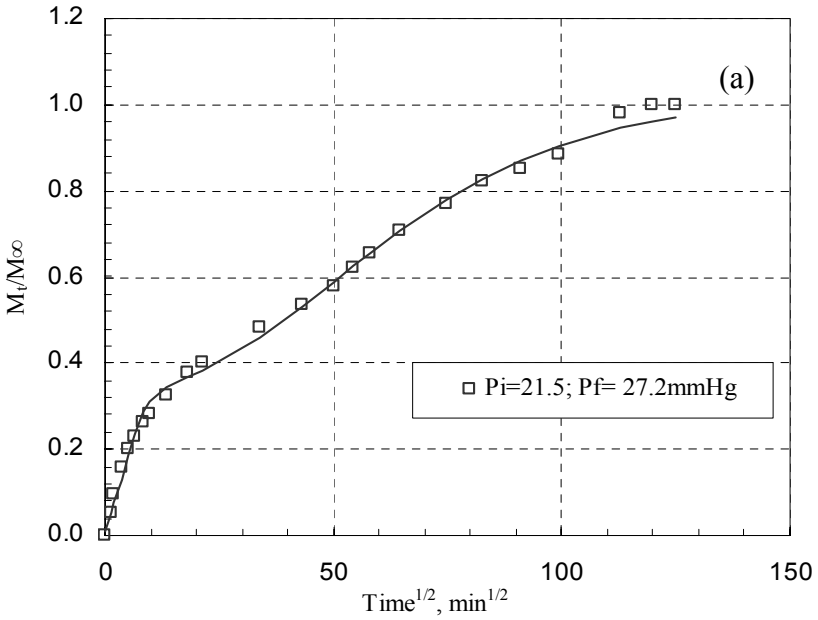

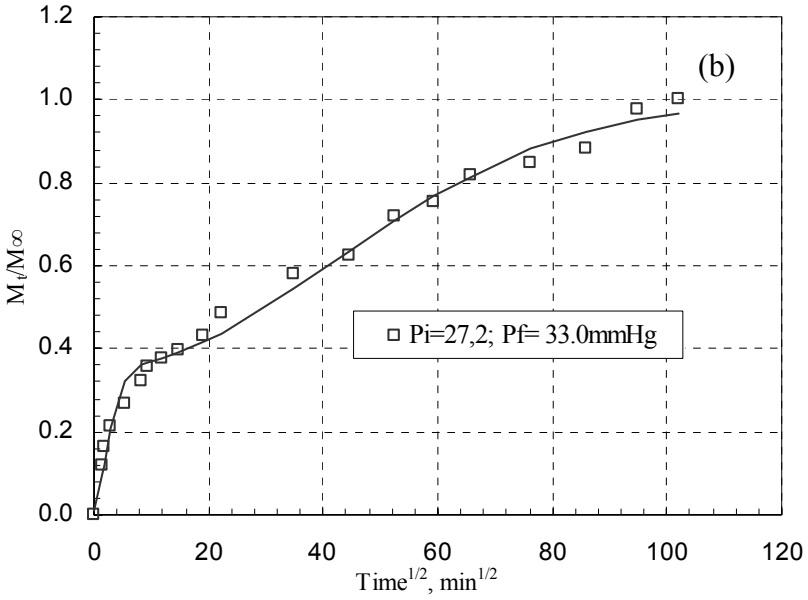

Figure 5.10: Non-Fickian sorption kinetics of n-propanol in 1.5m biaxially oriented PET.
(a) $D = 6.16 \pm 0.5 \times 10^{-12}$ cm^2/s, $k_R = 1.43 \pm 0.09 \times 10^{-5}$ s^{-1}, $\phi_f = 0.53 \pm 0.009$;
(b) $D = 2.53 \pm 0.64 \times 10^{-11}$ cm^2/s, $k_R = 3.91 \pm 0.1 \times 10^{-6}$ s^{-1}, $\phi_f = 0.24 \pm 0.007$

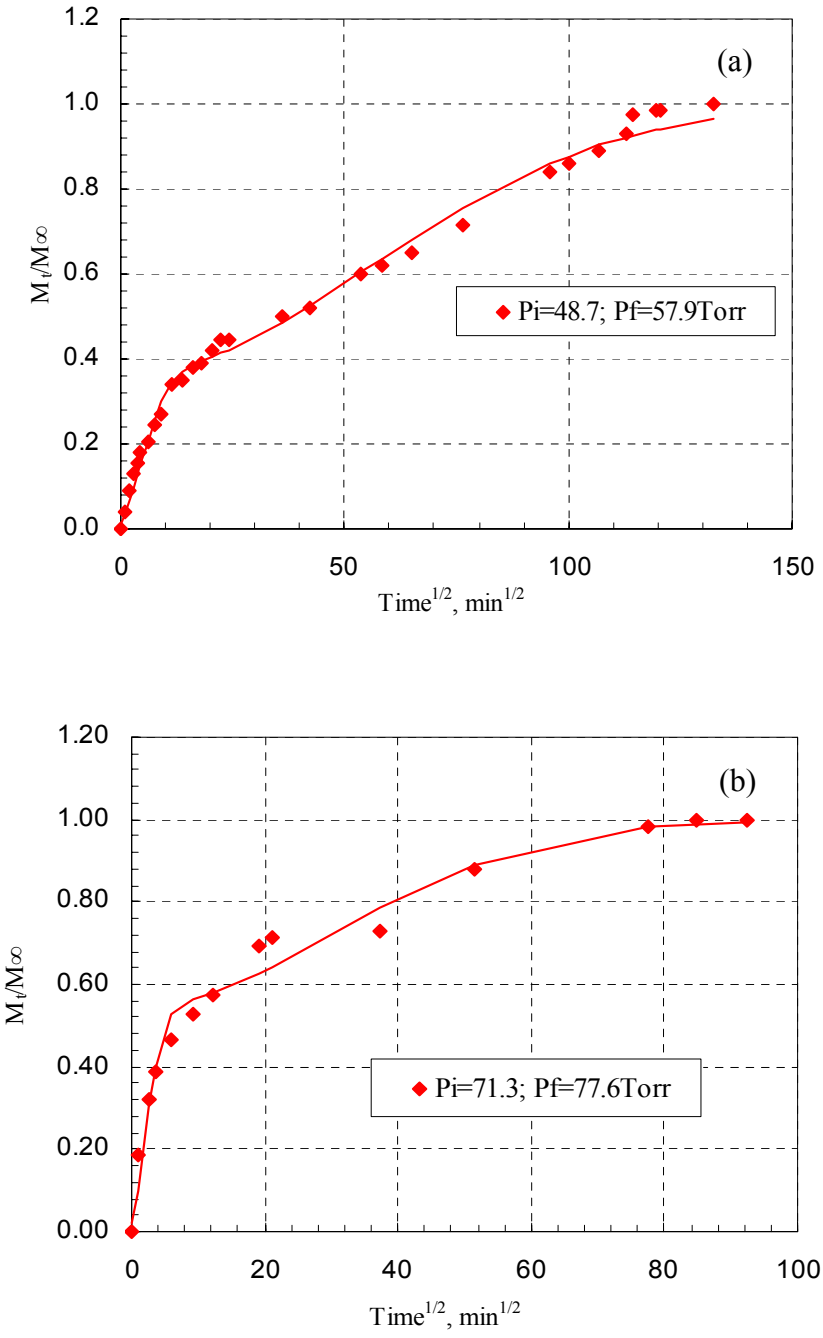

Figure 5.11: Non-Fickian kinetics of i-propanol in 1.5m biaxially oriented PET. (a) D= $6.32 \pm 0.94 \times 10^{-13}$ cm^2/s, $k_R = 2.73 \pm 0.13 \times 10^{-6}$ s^{-1}, $\phi_f = 0.36 \pm 0.01$; (b) D= $3.11 \pm 0.08 \times 10^{-12}$ cm^2/s, $k_R = 8.90 \pm 2.0 \times 10^{-6}$ s^{-1}, $\phi_f = 0.54 \pm 0.03$

Based on the parameters obtained from the Berens-Hopfenberg model, certain other observations may be made. The relaxation constant, k_R is a measure of the polymer chain motion during the sorption process. Most of the relaxation constant (k_R) values are lower for n-propanol and i-propanol. All values for the penetrants studied here are of the order of 10^{-5} and 10^{-6} s^{-1}. Patton et al report k_R of the order of 10^{-5} s^{-1} for benzene diffusion in PET [21]. Similarly, for ketones, the relaxation time constant is of the order of 10^{-5} [14]. Based on this evidence, it is difficult to draw any correlation between the relaxation rate constant and penetrant size. The fractional Fickian uptake decreases with increasing activity and concentration, and it often increases again at the high activities such as p/p_o=0.80 or 0.90 due to swelling which enhances the polymer chain mobility.

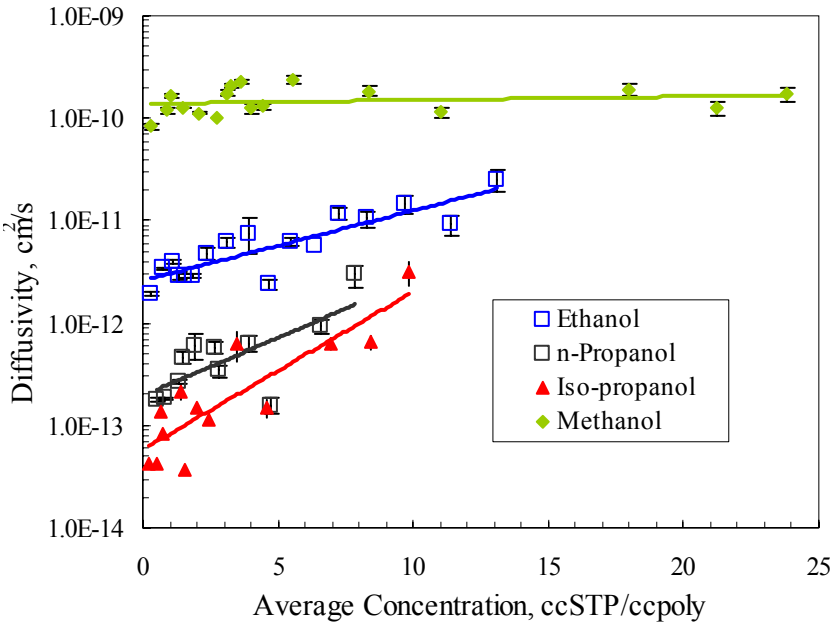

Figure 5.12: Diffusion coefficient of lower alcohols as a function of the average concentration

Table 5.5: Parameters defining the exponential dependece of diffusion coefficient on concentration

Constant	D_o, cm^2/s	β, $(ccSTP/ccpoly)^{-1}$
Methanol	1.39×10^{-10}	0.008
Ethanol	2.59×10^{-12}	0.158
n-Propanol	1.95×10^{-13}	0.261
i-Propanol	5.79×10^{-14}	0.355

5.3 SUMMARY

Solubility and diffusivity of methanol, ethanol, n-propanol and i-propanol have been measured in a thin biaxially oriented PET film. Results indicated that solubility increases with increasing penetrant size and diffusivity decreases with the same. Change in the position of the hydroxyl group in propanol appears to significantly affect the diffusivity of the molecule. As a result, the diffusivity of iso-propanol is an order of magnitude lower than n-propanol. Such behavior may be attributed to increased width and height of the i-propanol molecule.

It is proposed that the infinite dilution solubility of various species with the same chemical functionality correlates well with the dispersive solubility parameter. Functional groups with hydrogen bonding parameter (δ_h) closer to that of PET demonstrate a higher solubility in the polymer. The proposed correlation may be helpful in predicting the sorption properties of large flavor molecules using their solubility parameters estimated from group contribution methods [3].

5.4 REFERENCES

1. McBain, J.W. and A.M. Bakr, *A new sorption balance.* Journal of the American Chemical Society, 1926. **48**: p. 690-5.

2. Perry, R.H. and D.W. Green, eds. *Perry's Chemical Engineer's Handbook*. Sixth Edn ed. 1984, McGraw-Hill: New York. pp 3-55.

3. Immergut, E.H. and J. Brandrup, eds. *Handbook of Polymers*. 7th Edn. ed. 1989, Wiley and Sons: New York. pp 684.

4. Barton, A.F., ed. *CRC HAndbook of Polymer-Liquid Interaction Parameters and Solubility Paramaters*. 1990, CRC Press: Boca Raton, FL.

5. Dhoot, S.N., et al., *Sorption and transport of linear alkane hydrocarbons in biaxially oriented poly(ethylene terephthalate).* Journal of Polymer Science, Part B: Polymer Physics, 2001. **39**(11): p. 1160-1172.

6. Michaels, A.S., *Solution of gases in Polyethylene Terephthalate.* Journal of Applied Polymer Science, 1963. **34**(1): p. 1-12.

7. Lokhandwala, K.A., S.M. Nadakatti, and S.A. Stern, *Solubility and transport of water vapor in some 6FDA-based polyimides.* Journal of Polymer Science, Part B: Polymer Physics, 1995. **33**(6): p. 965-75.

8. Stannett, V.T., G.R. Ranade, and W.J. Koros, *Characterization of water vapor transport in glassy polyacrylonitrile by combined permeation and sorption techniques.* Journal of Membrane Science, 1982. **10**(2-3): p. 219-33.

9. Massey, L., K., ed. *Permeability Properties of Plastics and Elastomers, A Guide to Packaging and Barrier Materials*. 2nd Edn ed. Plastics Design LIbrary. 2002, William Andrew Publishing: Norwich. 601.

10. Connelly, R.W., et al., *The effect of sorbed penetrants on the aging of previously dilated glassy polymer powders. I. Lower alcohol and water sorption in poly(methyl methacrylate).* Journal of Applied Polymer Science, 1987. **34**(2): p. 703-19.

11. Ranade, G.R., V.T. Stannett, and W.J. Koros, *Kinetics of sorption and desorption for water vapor-glassy polyacrylonitrile (PAN) system.* Polymer Preprints (American Chemical Society, Division of Polymer Chemistry), 1981. **22**(2): p. 411-12.

12. Yang, D.K., et al., *Sorption and transport studies of water in Kapton polyimide. I.* Journal of Applied Polymer Science, 1985. **30**(3): p. 1035-47.

13. Orchard, G.A.J., P. Spiby, and I.M. Ward, *Oxygen and water vapor diffusion through biaxially oriented poly(ethylene terephthalate).* Journal of Polymer Science, Part B: Polymer Physics, 1990. **28**(5): p. 603-21.

14. Dhoot, S.N., B.D. Freeman, and M.E. Stewart, *Sorption and transport of linear and branched ketones in biaxially oriented polyethylene terephthalate.* Polymer, 2004. **45**(16): p. 5619-5628.

15. Wibawa, G., et al., *Solubilities of 11 Polar Organic Solvents in Four Polymers Using the Piezoelectric-Quartz Sorption Method.* Journal of Chemical and Engineering Data, 2002. **47**(4): p. 1022-1029.

16. Hopfenberg, H.B., L. Nicolais, and E. Drioli, *Relaxation controlled (case II) transport of lower alcohols in poly(methyl methacrylate).* Polymer, 1976. **17**(3): p. 195-8.

17. Bauer, K., D. Garbe, and H. Surburg, *Common Fragrance and Flavor Materials*. IIIrd ed. 1997, Weinheim: Wiley-VCH. 278.

18. Koros, W.J., *Sorption and transport of gases in glassy polymers*, in *Chemical Engineering*. 1977, University of Texas: Austin. p. 274 pp.

19. McDowell, C.C., B.D. Freeman, and G.W. McNeely, *Acetone sorption and uptake kinetics in poly(ethylene terephthalate).* Polymer, 1999. **40**(12): p. 3487-3499.

20. Dhoot, S.N., B.D. Freeman, and M.E. Stewart, *Sorption and Transport of Linear Esters and Branched Alkanes in Biaxially Oriented Poly(ethylene terephthalate).* Industrial & Engineering Chemistry Research, 2004. **43**(12): p. 2966-2976.

21. Patton, C.J., R.M. Felder, and W.J. Koros, *Sorption and transport of benzene in poly(ethylene terephthalate).* Journal of Applied Polymer Science, 1984. **29**(4): p. 1095-110.

22. Yasuda, H. and V. Stannett, *Permeation, solution, and diffusion of water in some high polymers.* Journal of Polymer Science, 1962. **57**: p. 907-23.

23. Bove, L., et al., *Transport properties of the mesomorphic form of poly(ethylene terephthalate).* Polymer, 1996. **37**(23): p. 5309-5311.

24. Serad, G.E., et al., *Gas and vapor sorption and diffusion in poly(ethylene terephthalate).* Polymer, 2001. **42**(16): p. 6929-6943.

25. Koros, W.J., A.H. Chan, and D.R. Paul, *Sorption and transport of various gases in polycarbonate.* Journal of Membrane Science, 1977. **2**(2): p. 165-90.

26. Reid, R.C., J.M. Prausnitz, and B.E. Poling, *The properties of gases and liquids*. 4th Edn. ed. 1987, New York: mcGraw Hill.

27. Berens, A.R. and H.B. Hopfenberg, *Diffusion of organic vapors at low concentrations in glassy PVC, polystyrene, and PMMA.* Journal of Membrane Science, 1982. **10**(2-3): p. 283-303.

28. Hopfenberg, H.B., R.H. Holley, and V. Stannett, *The effect of penetrant activity and temperature on the anomalous diffusion of hydrocarbons and solvent crazing in polystyrene.* Polymer Engineering and Science, 1969. **9**(4): p. 242.

29. Berens, A.R., *Diffusion and relaxation in glassy polymer powders. 1. Fickian diffusion of vinyl chloride in poly(vinyl chloride).* Polymer, 1977. **18**(7): p. 697-704.

30. Sfirakis, A. and C.E. Rogers, *Sorption and diffusion of alcohols in amorphous polymers.* Polymer Engineering and Science, 1981. **21**(9): p. 542-547.

CHAPTER 6 : MULTI-COMPONENT TRANSPORT OF GASES

The aim of this chapter is to study the transport properties of pure and mixed gas feeds containing methanol vapor. Based on the significant sorption of methanol, plasticization effects are possible which may lead to enhanced gas permeability and a consequent loss of barrier. The objective therefore is to investigate these potential enhancements and to analyze any such enhancements using the free volume theory. The larger goal is to provide a framework within which, through as few measurements as possible, the effect of other flavor molecules on the barrier capabilities of PET may be estimated. There are several studies on sorption of vapor laden gas feeds. Most of these focus on membrane based separations and hence, are with amorphous polymers that have high permeabilities [1-4]. There are several studies on flavor scalping in PET, which study removal of flavor molecules such as d-limonene and ascorbic acid from the packaged food [5-8]. Among the few studies that investigate the effect of flavor molecules on gas transport in PET is that of van Willige who reports oxygen transport in the presence of d-limonene. While loss in barrier capabilities is not observed with respect to the pure gas, the absence of reduction in oxygen flux which usually results due to competition effects in glassy polymers is also not observed [9]. This suggests that d-limonene may have some conditioning effects on the polymer. Additional observations with other barrier polymers also exist in [10] and [11-14], but most document effects, rather than analyze them. Specifically, none of these studies go into the detailed analysis of the morphological changes that might be occurring as well as consider the effect of the

different polymer morphologies. The current work, therefore, is the first to investigate loss of barrier due to model flavor compound as a step to understand the effect of different sample processing histories as well as to provide a sound basis for analysis with other materials.

6.1 PURE GAS TRANSPORT

Transport properties of pure oxygen and carbon dioxide were studied in the amorphous and semi-crystalline PET samples. The equipment and procedure for the permeation and sorption experiments has been described in sections 3.2.1 and 3.3.1 respectively. For all the studies, the samples have been use as-received. Figure 6.1 and Figure 6.2 below show the sorption isotherms of carbon dioxide and oxygen respectively. Since oxygen permeability is quite low, the percentage error in its measurement is higher than is observed for CO_2. Permeability plots for CO_2 and O_2 are shown in Figure 6.3 and Figure 6.4. The dual mode model parameters have been obtained by fitting the permeation and sorption isotherms to equation 2.36 and 2.37 respectively. Parameters obtained have been shown in Table 6.1. Methanol parameters already discussed in chapter 4, have also been shown for comparison.

The values of k_d and b for CO_2 are very similar to those reported in the literature [15-17]. However, the C_H' appears to be suppressed in the current samples. C_H' is dependent on the sample processing if any treatment is done below the glass transition temperature. In case of processing above glass transition, the quench rate will play an important role. Unfortunately, this information is not available for the samples considered here. Following a protocol similar to that adopted by Koros, CO_2 sorption isotherm was

obtained after pre-conditioning the non-annealed, semicrystalline sample at 19 atm. Interestingly, this isotherm coincided very closely with that reported by Koros [18]. The value of C_H' obtained was 4.75 ccSTP/ccpoly which is in good agreement with various literature reports. The lower sorption level of the as-received samples thus, reflects the morphological differences in the present samples. These differences are, of course, important in their relative barrier performance, so it was felt that the samples should not be pre-conditioned to 'homogenize' the morphologies of the various samples. For oxygen, no reports of its dual mode model parameters in PET were found. Micheals et al report the value of k_d^*, which is the sum of $C_H'b$ and k_d, equal to 0.100 ccSTP/ccpoly/atm in amorphous PET. The amorphous PET sample here has a k_d^* value of 0.093 ccSTP/ccpoly/atm, and agrees well with the previous report [19]. The values of F and D_D were obtained using transport measurements. The results obtained here are consistent with the report of Koros who calculated an F_{CO2} equal to 0.071 at 35°C in semi-crystalline PET. F_{O2} is higher by virtue of its higher critical temperature and smaller size. As was shown section 4.1.1, methanol, with a lower critical temperature and larger size, was nearly immobilized in the non-equilibrium sites. Similarly, Patton et al have shown that benzene, at 40°C is also nearly completely immobilized with F~0. At higher temperatures, the penetrant gain greater mobility and has a non-zero value for F [20].

Since CO_2 is an interacting penetrant, it was important to investigate the possibility of conditioning effects of CO_2 at 100 psia. Oxygen was used as the probe gas for this process. O_2 permeability was measured in an 'as received' amorphous film. Thereafter, CO_2 permeability was measured. The CO_2 was then replaced with O_2 by exchanging the upstream gas, without evacuating the film. Thus, any extra free volume created by CO_2

will be available for O_2 to sorb into, leading to increases in permeability. Similar effects have been observed for highly interacting gases such as CO_2 and in poly(4-methyl-1-pentene) by Pope et al and for CO_2 in substituted polycarbonate by Jordan et al [21-23]. However, in the case of amorphous PET, when CO_2 was exchanged with O_2, no change was observed in O_2 permeability. This leads to the conclusion that at 100 psia and below, CO_2 does not induce any changes in the polymer free volume.

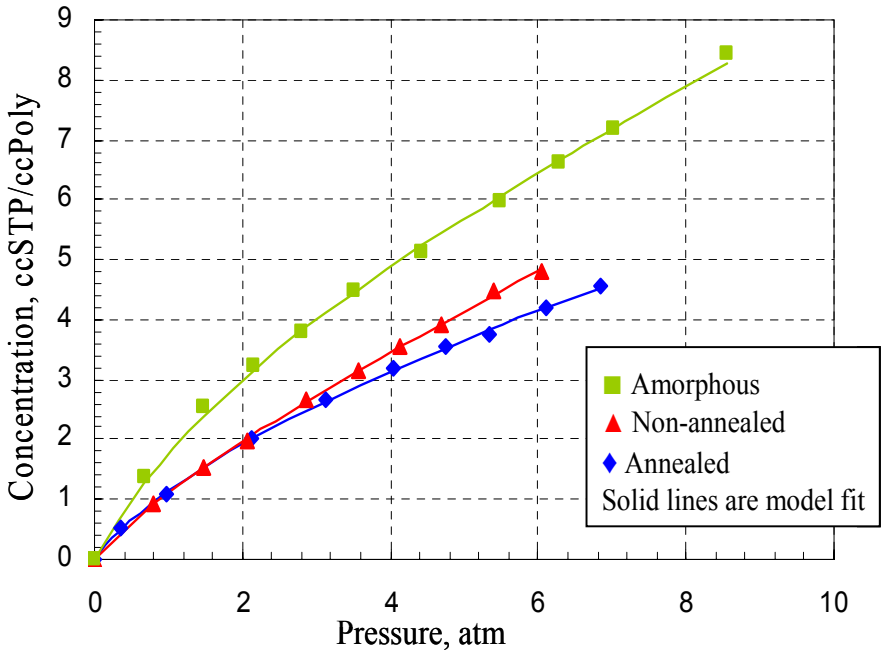

Figure 6.1:Carbon dioxide sorption isotherm in PET samples

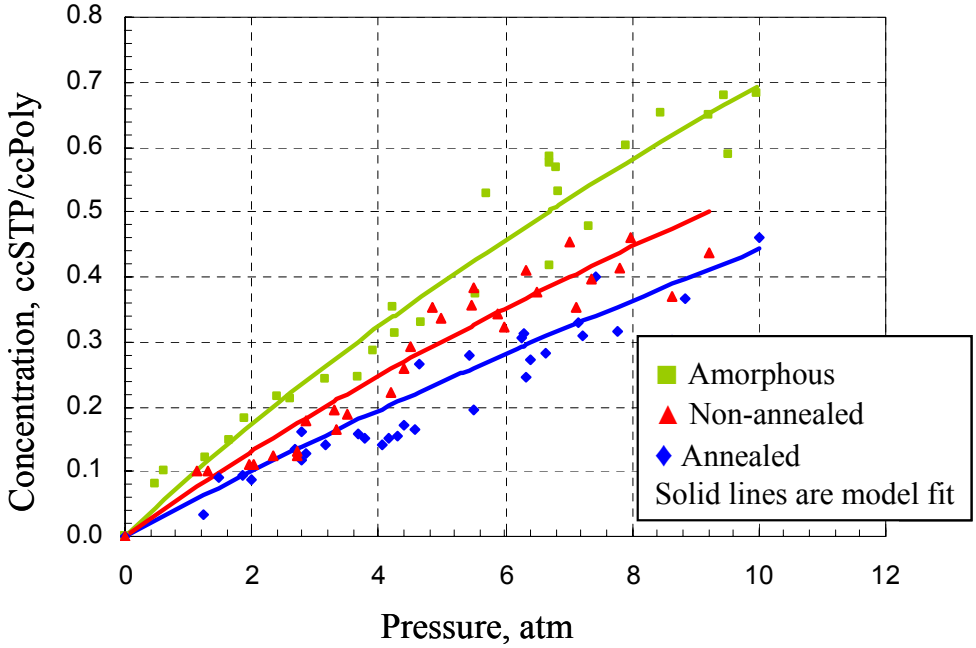

Figure 6.2: Oxygen sorption in PET

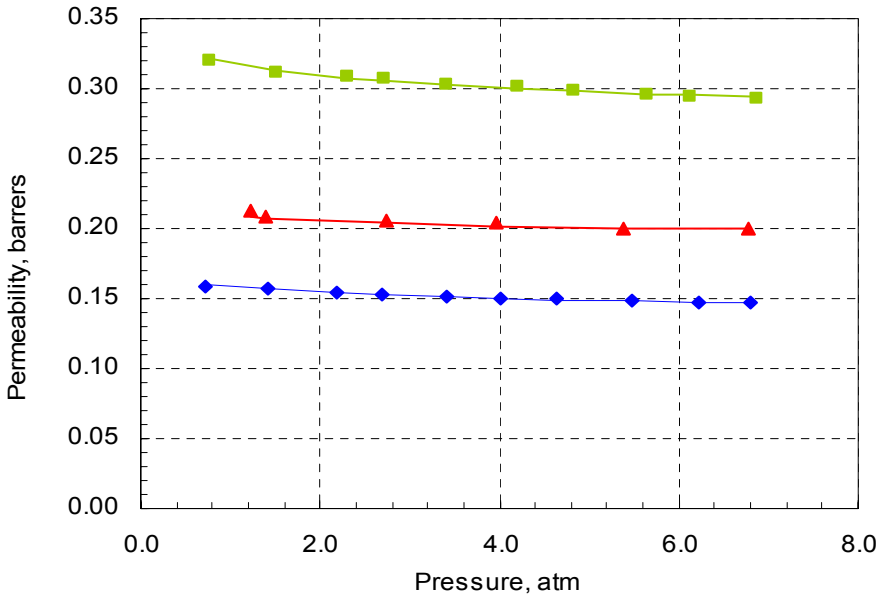

Figure 6.3: Carbon dioxide permeability in PET

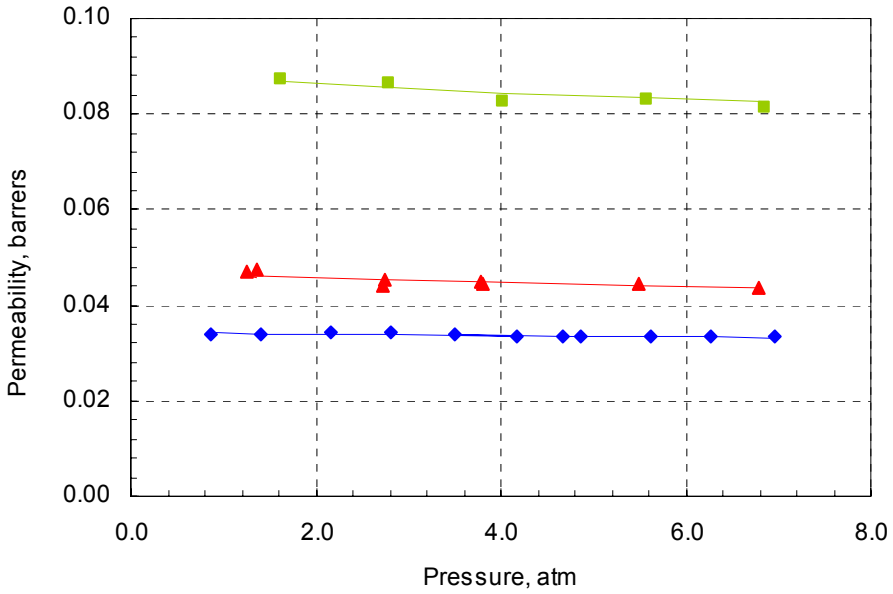

Figure 6.4: Oxygen permeability in PET

Table 6.1: Dual Mode Parameters for Methanol, O_2 and CO_2 in PET

	Amorphous	**Non-annealed**	**Annealed**
Carbon Dioxide			
b, atm^{-1}	0.470±0.16	0.468±0.11	0.455±0.16
C_H' ccSTP/ccPoly	3.582±0.83	2.310±0.42	1.640±0.48
k_d ccSTP/ccpoly/atm	0.633±0.06	0.406±0.04	0.600±0.04
$D_D x10^{-9} cm^2/s$	3.38±0.01	1.94±0.01	2.460±0.02
F	0.093±0.005	0.070±0.004	0.090±0.005
Oxygen			
b, atm^{-1}	0.068±0.005	0.053±0.02	0.075±0.02
C_H' ccSTP/ccPoly	0.855±0.15	0.470±0.10	0.550±0.13
k_d ccSTP/ccpoly/atm	0.035±0.007	0.028±0.004	0.030±0.005
$D_D x10^{-9} cm^2/s$	10.81±0.05	8.17±0.03	9.50±0.08
F	0.213±0.012	0.160±0.015	0.180±0.010
Methanol			
b, atm^{-1}	133.5 ± 35.5	124.1 ± 28.3	144.4 ± 15.2
C_H' ccSTP/ccPoly	1.37 ± 0.07	1.22 ± 0.06	0.71 ± 0.11
k_d ccSTP/ccpoly/atm	74.3 ± 5.3	47.9 ± 7.2	63.1 ± 2.1
$D_D x10^{-10} cm^2/s$	4.21± 0.50	2.68 ± 0.38	1.83 ± 0.19
F	~0	~0	~0

6.2 TRANSPORT OF CARBON DIOXIDE AND OXYGEN MIXTURES

Transport properties of two feed mixtures were studied to verify that the dual mode model for mixture transport is applicable. These are: a) CO_2/O_2 mixture with 90% CO_2 and b) CO_2/O_2 mixture with 10% CO_2 (Air Gas, Radnor, PA). All measurements were performed at 35°C. As mentioned in chapter 2, the dual mode model predicts that in mixture, the permeabilities of the penetrants are depressed relative to the pure gas permeability due to competition effects between penetrants for the available transport sites and transport pathways. Based on the parameters evaluated for the pure gases above, CO_2 has a greater affinity for the non-equilibrium sites than O_2. This is expected due to the greater critical temperature of CO_2 vs. O_2. In mixture, this leads to the prediction that O_2 permeability will decrease more than CO_2. Table 6.2 shows the dual mode model predictions, based on reduction in permeability calculated using equation 6.1 below. The results obtained match the predictions of the dual mode model for mixture permeation within the experimental error. It also further confirms that CO_2 sorption levels at 100 psia are not high enough to lead to conditioning or plasticization effects.

$$1-\frac{P_{Amix}}{P_{Ao}} = 1-\frac{1+\dfrac{F_A K_A}{(1+b_A p_A + b_B p_B)}}{1+\dfrac{F_A K_A}{(1+b_A p_A)}} \qquad 6.1$$

Table 6.2: CO_2/O_2 90/10 mixture permeation and comparison with predictions of the dual mode model for mixture transport

Gases →	Carbon Dioxide		Oxygen	
Sample ↓	Predicted permeability reduction (%)	Experimental permeability reduction (%)	Predicted permeability reduction (%)	Experimental permeability reduction (%)
Amorphous	0.53	2.54±0.14	16.20	15.11±5.30
Annealed	0.45	0.63±0.08	12.70	12.22±3.60
Non-annealed	0.25	0.60±0.07	11.48	7.08±2.34

Table 6.3: CO_2/O_2 10/90 mixture permeation and comparison with predictions of the dual mode model for mixture transport

Gases →	Carbon Dioxide		Oxygen	
Sample ↓	Predicted permeability reduction (%)	Experimental permeability reduction (%)	Predicted permeability reduction (%)	Experimental permeability reduction (%)
Amorphous	2.02	2.34±0.86	1.73	1.23±0.61
Annealed	1.54	2.83±0.50	1.31	1.81±0.30
Non-annealed	0.79	3.09±0.41	1.05	1.84±0.20

6.3 TRANSPORT OF OXYGEN/METHANOL BINARY MIXTURES

Mixtures of oxygen/methanol were studied to evaluate their transport properties. Gas pressures have been maintained at nearly 100 psia to maximize the flux. Pure gas permeability was measured after complete evacuation. Thereafter methanol was

introduced into the feed stream in increasing steps of activity. The data discussed below is consists of points that were measured on different films. At a given activity level, feed and permeate characterization was done at least 5 times, and usually more. The error bars are based on the standard deviation of the permeability that was then calculated.

All the three films- amorphous, annealed and non-annealed PET were tested for oxygen permeability in the presence of methanol. Since the dual mode model had provided an excellent fit for the CO_2/O_2 system, the initial hypothesis was that the model predictions will hold for O_2/MeOH system at low activities. Significant reduction, up to 20% of the pure gas permeability was predicted by the model using equation 6.1. The results obtained for the different films are shown in Figure 6.5 along with the dual mode prediction. For clear comparison across the samples, and different films of the same sample, the change in permeability is plotted *as a percentage of the pure gas permeability* i.e.$(P_{mix}-P_{pure})/P_{pure}$. A negative change implies reduction in the permeability (as would be predicted by dual mode).

The observations that stand out in the figure below are:

1. The annealed film permeabilities lie very close to the dual mode model prediction except at the high activity of MeOH of 85%.
2. Oxygen permeability in the amorphous and non-annealed films lies above the dual mode prediction even at the low activity level of p/p_o~0.2.
3. At the high activity end, there is a clear upswing in O_2 permeability for both the non-annealed and amorphous films. However, surprisingly, the non-annealed film shows the upturn earlier at p/p_o~0.7 whereas amorphous PET increases at p/p_o~0.9.

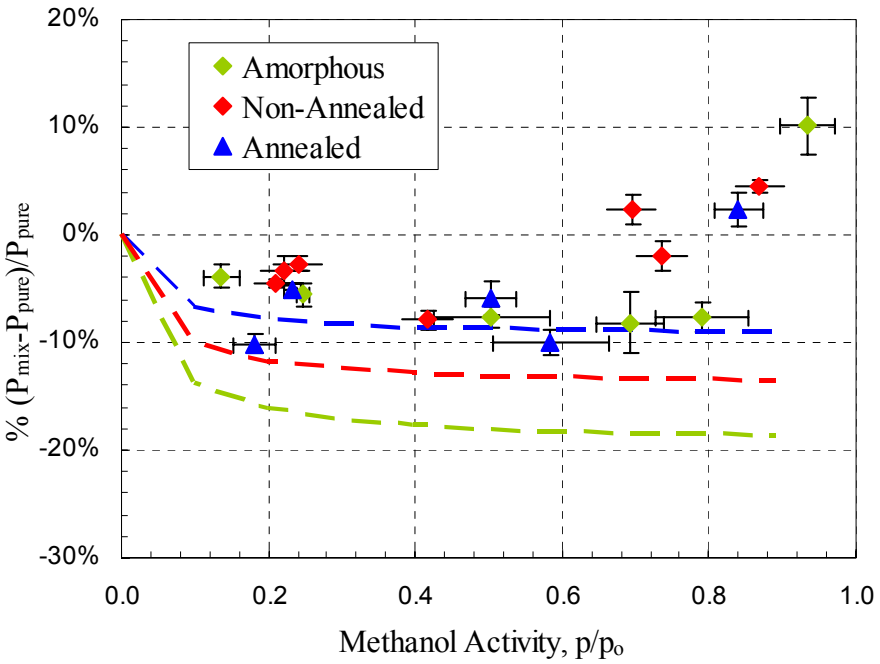

Figure 6.5: Permeability of oxygen in the O_2/MeOH system at 35°C at different activities of methanol. The dashed lines are the reduction predicted by the dual mode model.

In the present case of O_2/MeOH transport in the annealed film, data points from 3 films have been shown in the figure above, and it is believed that the fluctuations in the data are due to sample to sample differences. Overall, up till 60% activity of methanol, dual mode model predictions hold well. The increase in the permeability of O_2 at the 85% activity level will be discussed subsequently. Annealing a biaxially oriented glassy polymer above its glass transition temperature leads to increased chain mobility which helps to relieve the stresses in the material that are created during the orientation process. In thermodynamic terms, some of the entropy that is lost due to ordering in the orientation process is regained. In a crystallizable polymer, annealing above T_g leads to crystallization, with rearrangements in the amorphous phase to a more stress free morphology. Studies which maintain that a third phase- rigid amorphous phase is present

at the interface of the crystals and the regular phase, do not necessarily relate to stresses in the sample [24]. In the annealed, biaxially oriented, semicrystalline sample being studied here, lower susceptibility to conditioning, and reduced overall free volume with respect to the non-annealed, semicrystalline sample has been demonstrated through methanol sorption and desorption experiments discussed in section 4.1.1. The annealed film sorbs less methanol, and its k_d value is also smaller than the other two samples. This suggests that the polymer chains are better packed. Similar trends in the permeability and solubility of O_2 and CO_2 are also observed. The annealed film is also least susceptible to conditioning and plasticization effects of methanol as seen using pure methanol sorption and desorption of pure methanol. This fact is apparent since the annealed sample is the least conditioned of the three types considered. The improved swelling resistance of this film explains why multi-component transport in the presence of methanol follows the dual mode model very closely at the low and intermediate activity levels. These results also lead to the inference that the stresses in the non-annealed sample, which has a crystalline fraction very similar to that of the annealed film, have a significant influence on the transport properties as well as plasticization of the polymer.

The morphology of the amorphous regions of the non-annealed, biaxially oriented, semi-crystalline sample and the amorphous film is clearly influenced by the presence of methanol even at low activities. Since rubbery as well as glassy polymers experience plasticization, it appears reasonable to focus attention on the permeability enhancement as a plasticization of these normally densified regions in the glass. As a first assumption, consistent with such a simplified picture, the reduction in the permeability of the gas due to competition for these sorption sites may still occur, but this may be offset by an

increase in the transport of the gas through the equilibrium regions of the polymer. This is a highly idealized picture, but it provides a framework for understanding some of the observed trends. In such a framework, the extent of plasticization of the normally densified regions should be compared to the permeability predicted by the dual mode model. The value for $P_{dual\text{-}mode}$ is easily evaluated using the dual mode model parameters and the measured pure gas permeability. In the figure below, $(P_{mix}\text{-}P_{dual\text{-}mode})/ P_{dual\text{-}mode}$ is plotted as a function of methanol activity, and 0% corresponds to the case where the measured permeability matches the dual mode prediction.

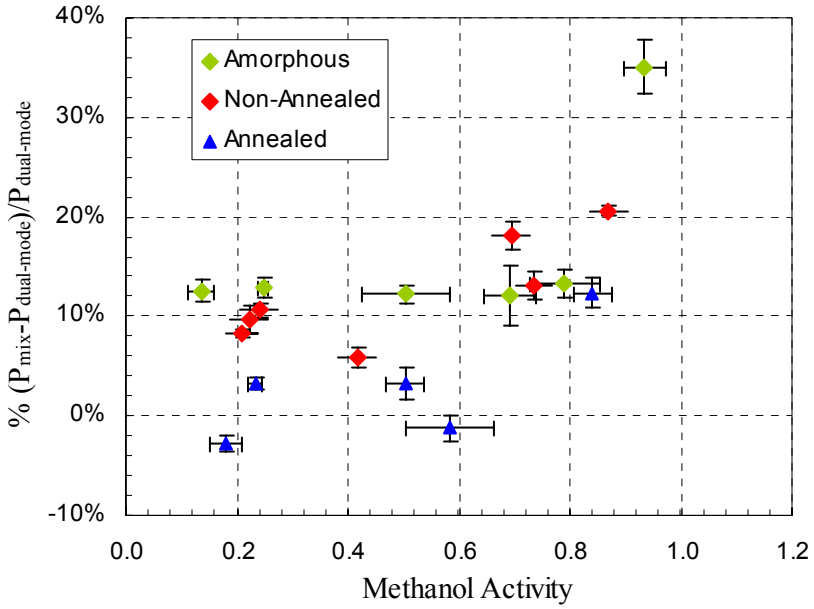

Figure 6.6: Permeability of O_2 is O_2/MeOH mixture compared with the dual mode model prediction.

Figure 6.6 shows that the amorphous sample is plasticized more than the non-annealed sample as the gas permeabilities are closer to the dual mode prediction than the

non-annealed sample. The amorphous sample is presumably more susceptible to plasticization than the semi-crystalline films due to the absence of the restricting effect of the crystals and the orientation. It is possible that even at p/p_o=0.20, where the dual mode isotherm is followed, methanol is able to induce some morphological changes. Characterized by an increase in permeability, plasticization induced by CO_2 has been seen in many cases even though the sorption isotherm at corresponding pressures follows dual mode [25]. However, it is very surprising that the gas permeability in the amorphous film stays at the same level of ~12% enhancement up till almost 80% methanol activity, and then increases dramatically at 90% activity of methanol. The non-annealed sample shows smaller deviation above the dual mode model but an upturn in the permeability is observed at only 70% activity of methanol. This is counter-intuitive in the first glance, as one would expect the crystallinity and orientation of the non-annealed to help suppress the plasticization effect till a higher activity level as is actually observed for the annealed sample. The major difference between the annealed and the non-annealed sample is the extent of the stress in the amorphous regions. It is hypothesized that this upturn may have to do with how the stress relaxation process in the oriented amorphous regions occurs due to sorption of methanol. This may lead to a relative increase in the free volume accessible to the gas as well as the distribution of free volume in the material. Clearly, the situation is quite complex and characterization methods such as positron annihilation lifetime spectroscopy may be useful to probe the fraction of free volume and the size of the free volume holes [26, 27]. In addition to such arguments related ti the generalized changes in the free volume distribution in the bulk amorphous phase, effects related to the complex morphology due to the presence of crystalline domains may be present. Annealing a film

may allow the stresses in the interphase region between the bulk amorphous phase and the crystalline domains to be relieved with possible re-organization of polymer segments. The non-annealed film may have residual stresses that, upon methanol sorption, gain mobility leading to significant permeability increases. Characterization methods such as small angle x-ray scattering may be used to estimate the size of the dimension of the interphase and gain some insight into possible differences [28, 29].

Irrespective of the morphology, at nearly 80% activity of methanol, all the samples show enhanced oxygen permeability. A single test that was made for CO_2 transport in the annealed sample at 80% activity also showed an enhancement in the CO_2 permeability of 9% with respect to the dual mode prediction. The amorphous regions of all the samples have sorbed sufficient methanol to cause significant enhancement in the free volume and the chain mobility. This corresponds to nearly 36 ccSTP/ccpoly of methanol in the amorphous regions. Compared with the extent of CO_2 and O_2 sorption in PET under these conditions, this is quite high. Based on the dual mode model, similar concentrations of CO_2 will not be achieved in the amorphous sample until 50 atm of CO_2 pressure. At these pressures and 35^{o}C, Kamiya et al. have reported that PET undergoes CO_2 induced crystallization which means the polymer has already undergone glass transition [30]. It is not being suggested that methanol induces glass transition of the polymer-penetrant system at 80% activity, but these numbers do give a perspective of what these concentration levels of highly sorbing species in PET are capable of doing and why the gas permeability increases so much.

6.4 MULTI-COMPONENT TRANSPORT

Transport properties of the ternary mixture of CO_2/O_2/MeOH were also investigated in the three PET samples at 35°C. The partial pressure of the gases was maintained at 100 psia, and methanol activity was increased in a step wise manner. Figures 6.7 and 6.8 show the change in O_2 and CO_2 permeability with respect to the pure gas permeability respectively. Figures 6.9 and 6.10 show the change in O_2 and CO_2 permeabilities with respect to the dual mode model prediction respectively.

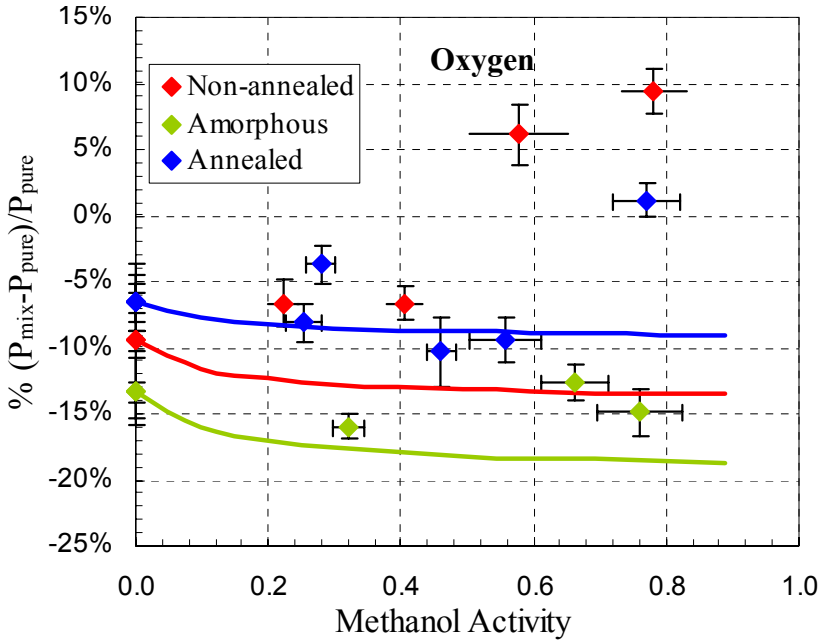

Figure 6.7: Oxygen permeability with respect to pure gas permeability in O_2/CO_2/MeOH mixture. Solid lines are the dual mode model predictions with respect to the pure gas permeability

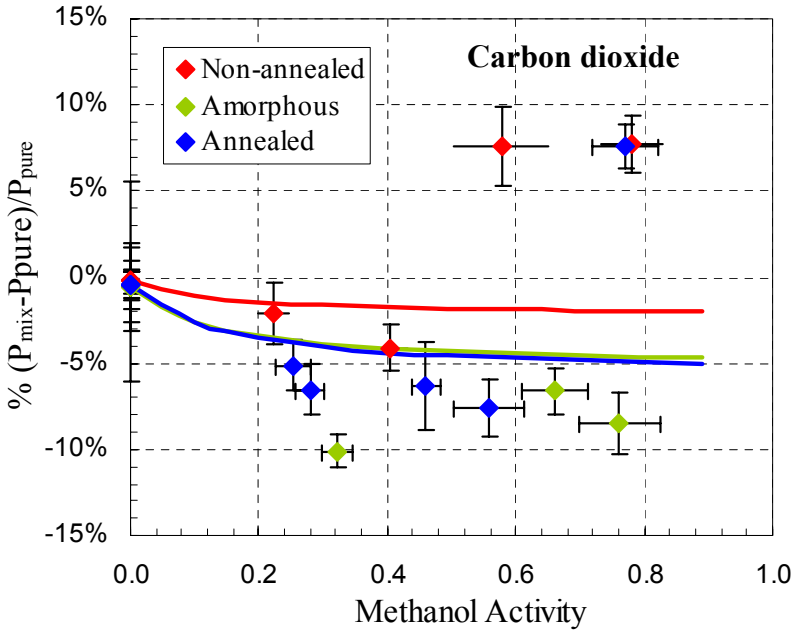

Figure 6.8: CO_2 permeability with respect to pure gas permeability in O_2/CO_2/MeOH mixture. Solid lines are the dual mode model predictions with respect to the pure gas permeability

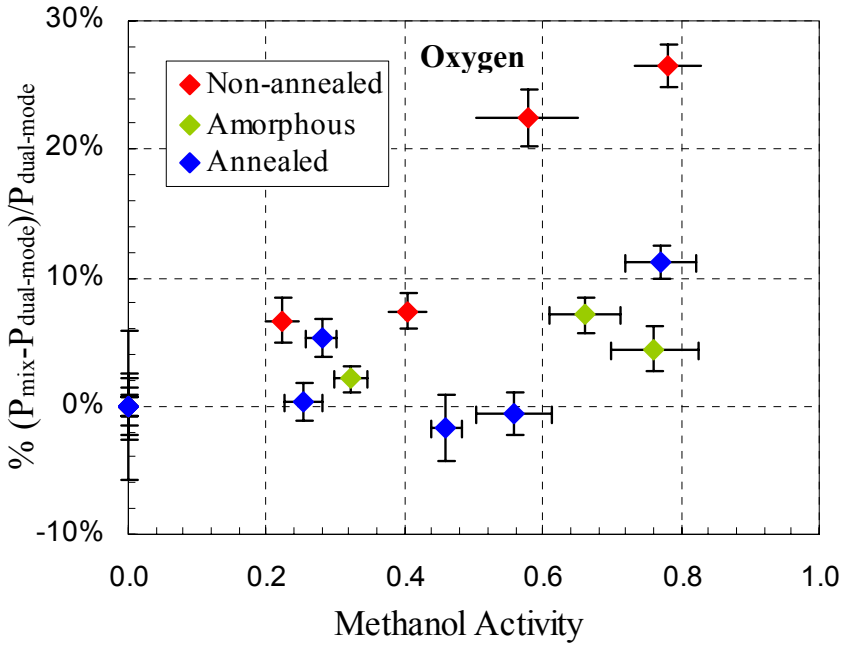

Figure 6.9: O_2 permeability with respect to the dual mode prediction in O_2/CO_2/MeOH mixture

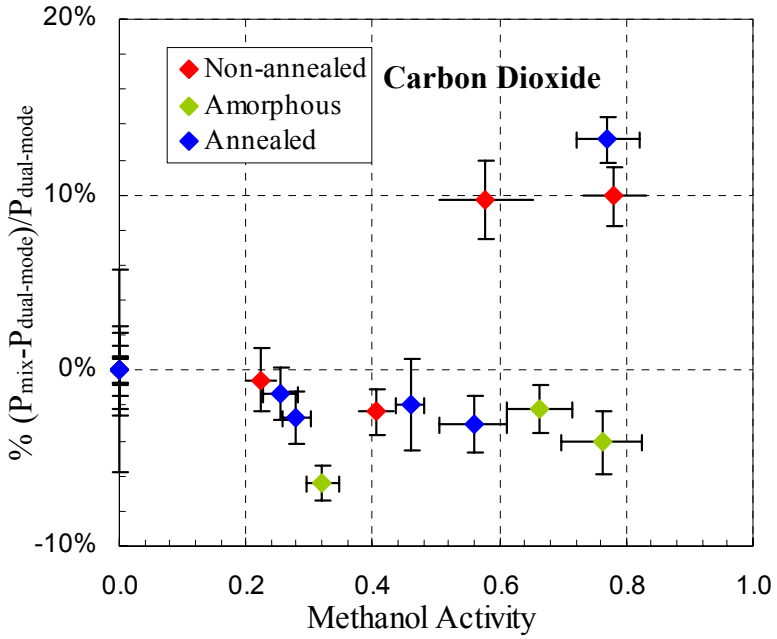

Figure 6.10: CO_2 permeability with respect to the dual mode prediction in O_2/CO_2/MeOH mixture

The key observations are:

1. In the high activity limit of methanol, the semicrystalline samples show an increase in the permeability of oxygen and carbon dioxide. For the amorphous film, with O_2/CO_2 50/50 feed, $p/p_o>0.80$ could not be achieved at the time of writing and the experiment will be conducted soon. However, it is strongly believed that the permeability upswing will be observed.
2. In the low and medium activity range in the amorphous sample, the reduction in the oxygen permeability with respect to pure gas is more for the ternary system than it was for the binary system. Carbon dioxide, on the other hand, is depressed below the prediction of the dual mode model.

3. The semi-crystalline films show CO_2 permeabilities consistent with the dual mode predictions at low activities. The permeability goes below dual mode at intermediate activities, and then swings up just like oxygen does in the case of O_2/MeOH system.
4. At the low and intermediate activity levels, O_2 permeability in the annealed sample shows dual mode characteristics. In the non-annealed sample, O_2 permeability is reduced, but not as much as the dual mode prediction, and it indicates increases at high activities.

The increases observed for CO_2 and O_2 permeabilities at high activities of methanol are very consistent with the results of the O_2/MeOH binary system. This is very encouraging and confirms the hypothesis proposed in the binary system that the high amounts of sorbed methanol induce large increases in the mobility of the polymer chain segments. Similarly, oxygen permeability at low and medium acitivities of methanol in the annealed film show dual mode type responses, as was observed in the binary mixture. The results of oxygen transport in the non-annealed sample at low methanol activities are also consistently above the dual mode predictions. The non-annealed sample plasticizes earlier at p/p_o=0.60 and the annealed sample shows the same effect at a higher activity. This confirms that the stresses in the non-annealed sample play an important role.

Upon comparison with the O_2/MeOH/Amorphous PET system, it seems that the most unusual effect is that the O_2 permeability is more depressed. This is a surprising result and is well beyond the experiemental uncertainty. Depression below dual mode implies that a reverse type of effect is occuring- i.e. there are some anti-plasticization effects as opposed to plasticization of the polymer. Antiplasticization is basically related to a

reduction in the free volume of the mixture with respect to the neat polymer which leads to a reduction in the gas permeabilities due to free volume hole filling. Several researchers have looked at polymer-diluent systems which show anti-plasticization effects, especially when additives are added to the material. Ruiz-Trevino addded fluorene and napthalene based structures to polysulfone and observed a reduction in the free volume of the polymer due to the anti-plasticization effect [31]. Similarly, al-Juaied [3] and Madden [4] observed significant loss in the permeability of CO_2 and CH_4 in the presence of small amounts of heavy hydrocarbons such as toulene and n-heptane. Chern observed combined competition and anti-plasticization effects due to water in Kapton polyimide [32]. Ruiz-Trevino proposed a free volume model to estimate the specific volume of the mixture at various concentrations of the additive. This model predicts a minima in the specific volume of the mixture. At low concentrations, the free volume of the polymer-diluent system decreases (anti-plasticization) and eventually starts increasing due to plasticization. Madden also showed the same effect for the toulene-CO_2-CH_4 system and n-heptane-CO_2-CH_4 system [4]. In the present case of CO_2/O_2/MeOH feed in amorphous feed, similar effects are seen. It must be clarified that it is not being suggested that methanol sorption is leading to a reduced free volume because O_2 permeability in O_2/MeOH mixture actually increases above the dual mode. It is only being hypothesized that the overall free volume of the PET-mixed feed system may be reduced when CO_2 is introduced in the feed as compared to the case of O_2 and MeOH only. This is a surprising result.

The basic question that needs to be addressed is why the system switches from showing plasticization effects in O_2/MeOH to antiplasticization in the ternary system at

low and intermediate activities. One explanation could be that methanol induces a change not only in the total free volume of the system, but also in the size of the free volume holes that are present in the polymer. Free volume holes in this context refer to the size of the unoccupied volume elements in the polymer, and should not be confused with the Langmuir types sites described by the dual mode model. As Hong et al showed, sorption of CO_2 in polycarbonate at high pressure changed the distribution of free volume in the polymer [26, 33]. Park et al have suggested that the size and shape of a molecule may affect the way the molecule accesses free volume in the polymer [34]. It is possible that in the case of PET, methanol induced change in the free volume system is probed differently by O_2 and CO_2. This leads to a depression in the gas permeability below what would be predicted by the dual mode model. One way to confirm this will be to perform CO_2/MeOH mixture transport measurements. If this hypothesis is correct, CO_2 permeability in the amorphous film will be depressed below the dual mode prediction. The antiplasticization effect is suppressed in the case of the semi-crystalline samples which show only slight reductions below the dual mode predictions. This is presumably due to the presence of the crystals which have a restraining effect on amorphous regions. Apparently the crystals do not allow sufficient rearrangement of the free volume elements to induce a significant deviation below the dual mode.

From a packaging perspective, this reduction in permeability is encouraging. The O_2/CO_2/MeOH system is one step closer to the actual package conditions. Both the gases have a lower flux than the respective pure components in all the samples as long as the activity is not too high. The only key component missing here is humidity and future

work may focus on the addition of humidity to these feed streams to analyze its inflence on the polymer.

6.5 MODELING OF PLASTICIZATION EFFECTS

So far, the mixture transport results have been analyzed within the framework of the dual mode model. Results with mixtures containing methanol showed some very interesting results which do not fit the dual mode model in its present form, i.e. the parameters C_H', b and k_d are the same for a gas, irrespective of the composition of the mixture. As was mentioned in section 2.4, when the polymer is conditioned or plasticized, the penetrants probe a different morphology which may not be described by the same dual mode model parameters as measured for the pure gas. Several attempts have been made to extend the dual mode model to incorporate these effects [35, 36]. The problem has also been approached using the free volume theory [37, 38]. Before going into results of the multi-component CO_2/O_2/MeOH/PET system, it is useful to establish a framework for analyzing the present data.

6.5.1 Free volume Theory

The elements of the free volume theory introduced briefly in section 2.2.6 where the initial description of diffusivity in terms of the fractional free volume (FFV) by Fujita was described [39]. Considerable work has been done to understand transport properties of polymers using free volume concepts. Similar to the dependence of diffusivity on FFV, an expression for permeability may be written as [40]:

$$P_{Ao} = A_A \exp(-\frac{B_A}{FFV_o}) \qquad 6.2$$

A_A and B_A are constants for a given gas-polymer pair. Within a class of polymers such as polyesters, polysulfones, polyimides etc. it has been proposed that the values of A_A and B_A will apply. Similar to equation 2.33, permeability of a semicrystalline polymer with impermeable crystals may be written as:

$$P_{Ao} = A_A \exp(-\frac{B_A}{\phi_a FFV_o}) \qquad 6.3$$

ϕ_a is the amorphous volume fraction of the polymer and FFV_o is the fractional free volume of the neat, amorphous polymer. Fractional free volume is calculated using equation 2.31 shown below:

$$FFV_o = \frac{\hat{V}_g - \hat{V}_o}{\hat{V}_o} \qquad 2.31$$

The specific volume of the glass, $\hat{V}_g$, at the desired temperature and pressure may be calculated using its density in g/cc. The specific occupied volume, $\hat{V}_o$, is calculated from van der Waal's volume using Bondi's group contribution method by summing the individual contributions [41].

$$\hat{V}o = 1.3\sum_k \hat{V}_{w,k} \qquad 6.4$$

$\hat{V}_{w,k}$ is the van der Waal's volume of the different groups in the polymer. Park and Paul suggest that to correlate the permeability across a spectrum of polymers and penetrants, a

factor γ_{nk} must be incorporated into equation 6.4 which accounts for the fact that different gases may be sensitive to different parts of the free volume distribution. This empirical factor has been evaluated for many different polymer-penetrant systems [34]. Since the Bondi's group contribution method is commonly used, this is being used here and the γ_{nk} is a constant at 1.3. To illustrate clearly the physical meaning of the quantities being considered here, a schematic of specific volume vs. temperature us shown in Figure 6.11 below. There could be some debate about the description of the occupied volume, which has been taken independent of temperature in this case. Vrentas and Duda have suggested that the occupied volume at temperature T be considered as the sum of the volume at 0K and the interstitial volume associated with the vibrational and rotational motions of the molecules [38]. While this approach is as reasonable as the summation of the van der Waal's volume, the former suffers from the disadvantage of being less easily accessible and measurable for polymeric systems. The use of group contribution methods is consequently very common for polymer transport analysis [4, 42].

Plasticizing penetrants are known to increase the chain mobility and enhance the free volume of the polymer-penetrant system. In such a case, the permeability of a gas in mixture may be compared with the pure gas permeability using:

$$\frac{P_A}{P_{Ao}} = \exp\left(\frac{B_A}{\varphi_a}\left(\frac{1}{FFV_o} - \frac{1}{FFV,mix}\right)\right) \qquad 6.5$$

$$FFV_{mix} = \frac{\hat{V}_{g,mix} - \hat{V}_{o,mix}}{\hat{V}_{o,mix}} \qquad 6.6$$

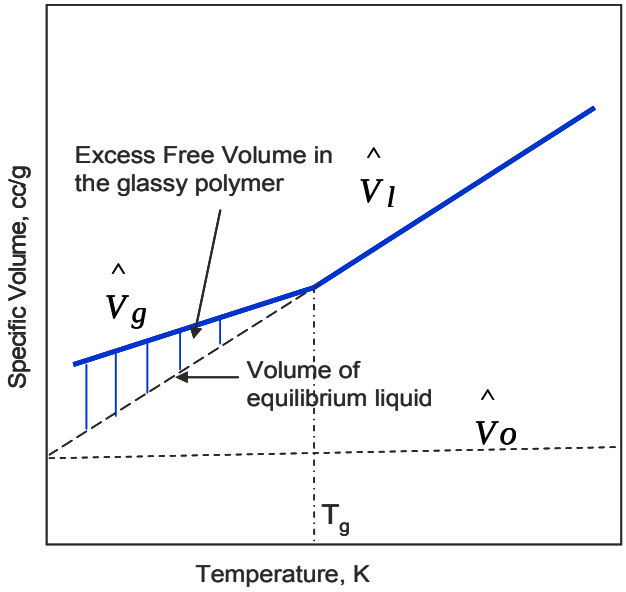

Figure 6.11: Schematic of specific volume vs. temperature

Researchers have adopted both, experimental and theoretical methods of estimating the fractional free volume of the mixture. In situ PALS, direct estimation of specific volume of the mixture using density measurement where possible and volume dilation are experimental approaches that have been used to estimate specific volume of the fractional free volume of the mixture [31, 33, 43, 44]. In situ PALS is not accessible to us at present, and density measurements will be difficult to perform as the methanol will desorb by the time the sample density may be measured. The fractional free volume of the PET-methanol system has been estimated as described below. The occupied volume of a mixture can be calculated using equation 6.7 [45]

$$\hat{V}_{o,mix} = w_p \hat{V}_{o,p} + w_s \hat{V}_{o,A} \qquad 6.7$$

w_p and w_A are the weight fractions of the polymer and the solvent respectively. The polymer and solvent occupied volumes may be calculated using equation 6.4 and the weight fractions are known from the sorption isotherm of the pure solvent in the polymer. For given temperature and pressure conditions, where the pressure of the penetrant on the upstream of the polymer film is small, and the effect of the penetrant on the polymer free volume is additive and equation 2.34 may be modified to [46]:

$$FFV_{mix} = FFV_o(T,P,0) + \gamma' C_A \qquad 6.8$$

γ' is a constant for a given polymer-penetrant system and V_{fs} is the polymer fractional free volume. Since, FFV_o is already known, only the parameter γ' needs be estimated. Along similar lines, an expression for the specific volume may also be written as:

$$\hat{V}_{g,mix} = \hat{V}_g(T,P,0) + \gamma C_A \qquad 6.9$$

For most free volume modeling of glassy polymers, FFV_{mix} is used which incorporates the excess free volume of the glass or the specific volume of the glassy sample [31, 47, 48]. However, in the case of plasticization and/or dilation, as noted earlier, the simplest approach is to assume that the segments in the normally densified (Henry's Law regions) of the glassy polymer are affected most by the sorption of the species such as CO_2 or other plasticizing penetrants [35, 49]. Indeed, in most polymers, increased mobility and diffusivity are well known to occur as the local concentration of the penetrant increases. Since both the rubbery and glassy polymers experience plasticization, this first order approximation seems reasonable. Fleming et al showed that for the CO_2-polycarbonate system, the dilation of the polymer was well predicted if the concentration of CO_2 in the Henry's Law regions of the polymer was assumed to contribute to the swelling of the

polymer [43]. Jordan also suggests that increase in diffusion coefficient of a polymer conditioned at high CO_2 pressures may be attributed to the 'disruption or loosening' of the equilibrium packing [22]. It seems that instead of using $\hat{V}_{g,o}$, the specific volume of the equilibrium liquid $\hat{V}_{l,o}$ should be used. Additional free volume will be contributed by the penetrant sorbed in the equilibrium region of the polymer. This concept is shown schematically in Figure 6.12.

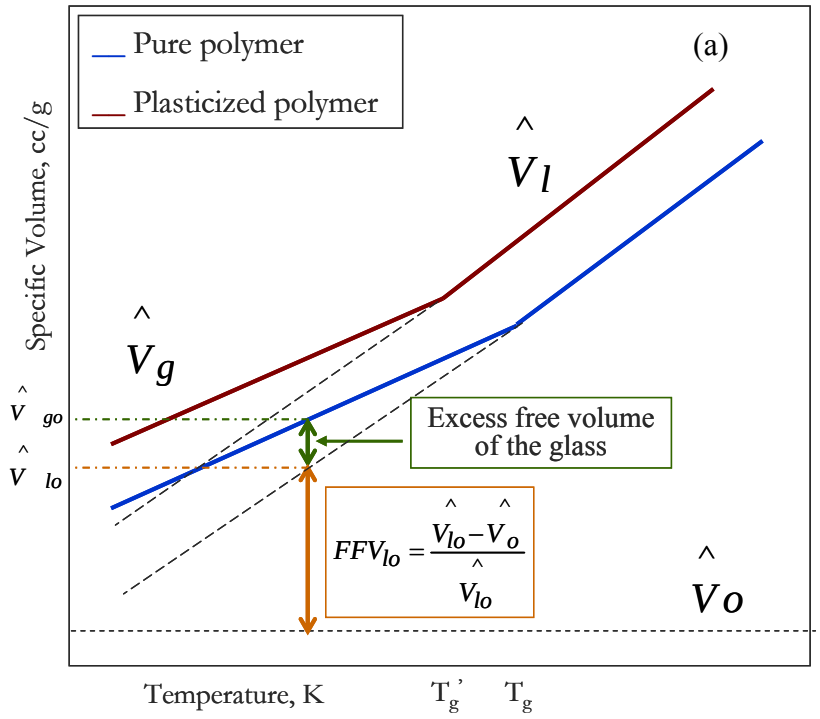

Figure 6.12: (a) Free volume associated with the glassy and densified regions of the neat polymer. (b) Free volume associated with the glassy and densified regions of the plasticized polymer.

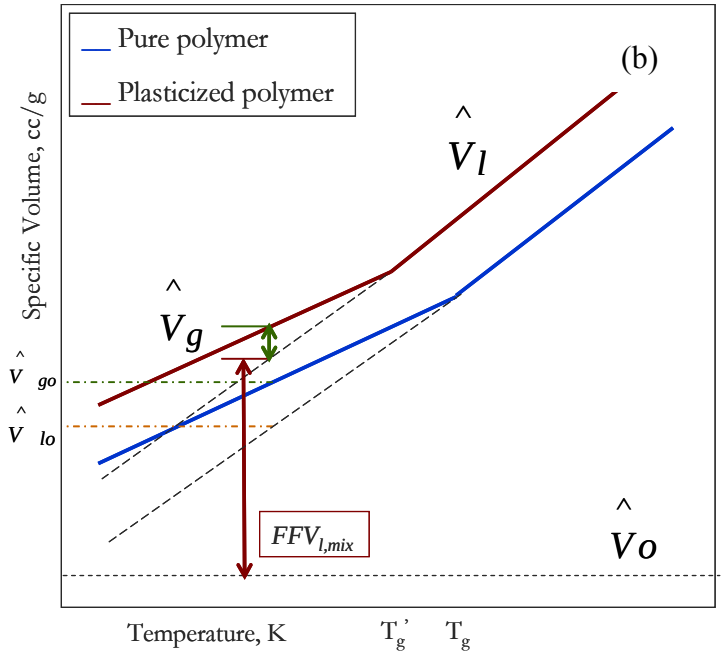

The categorization of free volume associated with different regions of the glassy polymer is akin to the dual mode model where two different sorption/transport sites are described. The equilibrium sites follow Henry's Law sorption and the Langmuir type isotherm is observed for sorption into the excess free volume regions. Thus, this approach serves to bring together the dual mode model theory and the free volume theory for analysis of transport phenomena in glassy polymers. Mathematically, the two theories come together in the following equation [50]:

$$C_H' = \frac{\hat{V}_g - \hat{V}_l}{\hat{V}_g}\rho^* \qquad 6.10$$

C_H' is the hole saturation capacity of the polymer and ρ^* is the partial molar volume of the penetrant in the polymer in cc/mol. ρ^* for CO_2 is known to be 46 cc/mol, and is a very well established value based on the solubilization of CO_2 in various organic liquids, and this value has also been shown to fit polymeric systems also [43, 50]. Therefore, based on the dual mode sorption isotherm of CO_2 in the polymer, $\hat{V}_{l,o}$ may be estimated. Once $\hat{V}_{l,o}$ is known, $\hat{V}_{l,mix}$ may be estimated using the modified form of equation 6.9

$$\hat{V}_{l,mix} = \hat{V}_l(T,P,0) + \gamma'' C_{A,D} \qquad 6.11$$

$C_{A,D}$ is the concentration of the penetrant in the dissolved mode. Since the dual mode model parameters and the total concentration are known for a given pressure, $C_{D,A}$ may be estimated is units of ccSTP/ccpoly using

$$C_{A,D} = C_A - \left(\frac{C'_{HA} b_A p_A}{(1 + b_A p_A)} \right) \qquad 6.12$$

A penetrant in its sorbed state in a polymer is considered to be in a condensed state. Thus, properties such as liquid density may be used to estimate its molar volume in the polymer. The assumption of an ideal mixture such that the partial molar volume is equal to the pure component molar volume is inherent here. Moreover, in the absence of more thermodynamic information about the polymer-penetrant system, the volumes may be assumed to be additive in the Henry's Law region. Thus, the specific volume of mixture per gram of the polymer may also be written as

$$\hat{V}_{l,mix} = \hat{V}_l + \frac{\hat{V}_A . C_{A,D} . MW}{22414 . \rho_{poly}} \qquad 6.13$$

$\hat{V}_A$ is the specific volume of the penetrant, MW is its molecular weight, and ρ_{poly} is the polymer density. Thus, γ'' may be estimated by combining equations 6.11 and 6.13. The value of $\hat{V}_{o,mix}$ may be estimated using equation 6.7 and thus, the $FFV_{l,mix}$ may be estimated from

$$FFV_{l,mix} = \frac{\hat{V}_{l,mix} - \hat{V}_{o,mix}}{\hat{V}_{l,mix}} \qquad 6.14$$

It must be kept in mind that all the above analysis is performed using the properties of the amorphous polymer because sorption occurs only in the amorphous regions and the crystals are impermeable. Thus, the $FFV_{l,mix}$ is the fractional free volume of the amorphous regions of the polymer. The presence of crystals is accounted for in equations 6.3 and 6.5.

So far, no mention has been made of the reduction in the glass transition temperature of the polymer-penetrant system due to sorption of the plasticization. Closer examination of Figure 6.12 shows that the reduction in T_g is accompanied with a reduction in the excess free volume associated with the glassy polymer. This makes perfect physical sense because greater proximity to the T_g, measured through $(T-T_{g,m})$ implies greater chain mobility and some of the packing defects will gain motion enough to become well packed. The loss of such a packing defect leads to a loss in Langmuir type sites and a reduction in C_H'. It is well known that for a given polymer-penetrant mixture, C_H' reduces with increasing temperature and goes to zero at T_g. For a polymer-diluent system, Kamiya et al proposed the following relation [44]:

$$C_H^{'} = C_{Ho}^{'} \frac{(T_{gm} - T)}{(T_{go} - T)} \qquad 6.15$$

T_{gm} is the mixture glass transition temperature, T_{go} is the pure polymer glass transition temperature and $C_{Ho}^{'}$ is its saturation capacity. Couchman and Karasz [51], Ruiz-Trevino and Paul [45] and Chow [52] propose relations that may be used to predict the glass transition temperature of the mixture. The relation proposed by Couchman has no adjustable parameters and may be used to predict $T_{g,m}$. However, in the present instance, the glass transition temperature and heat capacity changes could not be measured using DSC for the semi-crystalline samples. This has been discussed in section 3.4.2. Thus, in the absence of such information, $C_H^{'}$ for the sorbing components has been assumed to be constant with methanol concentration. The change in the specific volume associated with this reduction is also expected to be small and is not expected to add significant error to the analysis.

A major drawback of this free volume model is that it does not account for competition effects that are frequently observed in glassy polymers. In a system such as PET-methanol, reduction in permeability owing to competition effects is observed at low activities of methanol and significant increases are seen only at p/p_o= 0.70 or above. Since the free volume of the mixture is estimated by assuming additivity of the component specific volumes, the FFV_{mix} is found to increase with methanol fraction. This increase would suggest that plasticization occurs, when actually dual mode competition effects dominate and permeability depressions are observed. Thus, the free volume theory does not account for the combined effects of dual mode competition and plasticization.

6.5.2 Extended Dual Mode Model

Attempts have also been made to extend the dual mode model to account for plasticization. Since plasticization mainly effects the diffusivity of a penetrant, Stern et al proposed that an exponential dependence of D_D on the concentration of the plasticizing penetrant [35, 53]. When penetrant induced swelling accompanies such behavior, a similar exponential dependence of k_D on concentration has been assumed [54]. In fact, such a dependence of k_D has been shown to describe Flory-Huggins type isotherms very well [55]. Chern et al quantified the reduction in the permeability of CO_2 below the dual mode prediction in the Kapton^{TM} polyimide/H_2O/CO_2 system by simply calculating the D_D of CO_2 at different relative humidities. In the present system, at the low and intermediate activity levels in the ternary and the binary system, D_D values may be evaluated for the gases. Usually D_D is evaluated from the plot of diffusivity or permeability vs. pressure of the penetrant. However, in this case, only one pressure – 100 psia has been considered and D_D values will be evaluated at each activity.

6.6 MODELING MULTI-COMPONENT TRANSPORT IN PET

The fractional free volume of the mixture is evaluated using the equations described in section 6.5.1 above. Parameters used have been shown in the table below. The occupied volume has been calculated from the group contribution methods [41]. The specific volume of the liquid like regions is calculated using equation 6.10 where C_H' for CO_2 shown in Table 6.1. The mixture specific volume is calculated using equation 6.13, where $C_{A,D}$ is estimated by subtracting the Langmuir contribution from the total concentration at that activity. The total concentration is estimated using the Flory-

Huggins equation or the dual mode model as the case may be depending on the activity of methanol. Since all calculations are for the amorphous phase of the polymers, the density used is 1.331 g/cc. The occupied volume of the mixture is also additive and $C_{A,D}$ is used to estimate the free volume associated with the sorbed methanol.

Table 6.4: Values of some of the parameters for free volume calculations

Parameter	Value
$\hat{V}_o$, cc/g	0.637
$\hat{V}_{o,A}$, cc/g	0.880
$\hat{V}_g$, cc/g	0.751
$\hat{V}_{l,A}$, cc/g	1.286
ρ^*_{CO2}, cc/mol	46
ρ_{poly}, g/cc	1.331

Figure 6.12 shows the relative increase in permeability with respect to the fractional free volume of the mixture. The last, 80% activity point which corresponds to an FFV_{mix} of 0.156 for CO_2/O_2/MeOH feed in the amorphous PET sample was being measured at the time of writing. However, the O_2/MeOH data in Figure 6.11(a) shows that despite an increase in the fractional free volume, the permeability does not increase after the initial enhancement. The annealed sample does not lie above the dual mode prediction in the low activity regions despite prediction of an increase in the FFV_{mix}. These combined

effects of plasticization and competition are, therefore, not captured by the free volume model with additive specific volumes. To date, there is no study which attempts to predict the dual mode competition effects in glassy polymers using the free volume theory. These results therefore suggest the applicability of the modified dual mode model. A modified D_D may be calculated for O_2 transport in O_2/MeOH/Amorphous PET system up till FFV_{mix}= 0.154 which corresponds to 69% activity. With the other parameters remaining constant, this value is evaluated to be 1.21×10^{-8} cm^2/s. Similar trends are seen for the non-annealed sample but to a lower activity or FFV_{mix}. In this region, the new, enhanced D_D for the O_2/MeOH system is evaluated to be 1.03×10^{-8} cm^2/s. The major limitation of this analysis at this stage is its inability to predict the transport properties observed for the ternary feed mixture.

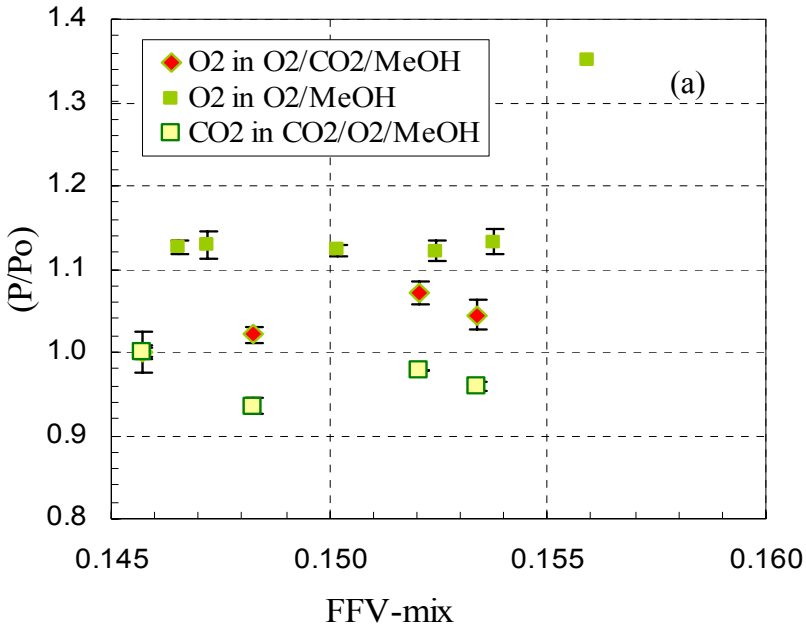

Figure 6.13: Permeability increase as a function of the fractional free volume of the PET-MeOH mixture (a) O_2 and CO_2 in amorphous PET; (b) O_2 in the semicrystalline samples; (c) CO_2 in the semicrystalline samples

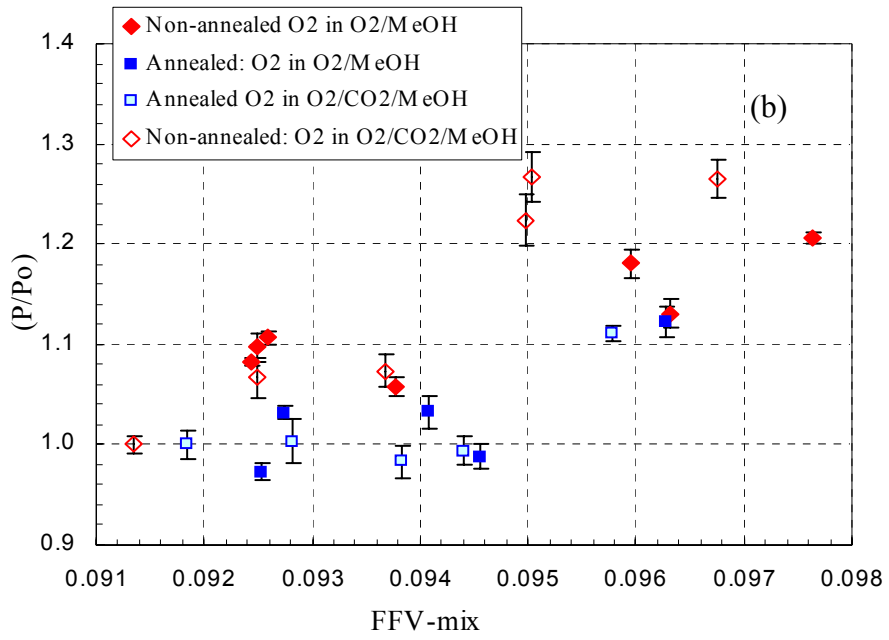
Non-annealed O2 in O2/MeOH
Annealed: O2 in O2/MeOH
Annealed O2 in O2/CO2/MeOH
Non-annealed: O2 in O2/CO2/MeOH
(b)
(P/Po)
FFV-mix
1.4
1.3
1.2
1.1
1.0
0.9
0.091
0.092
0.093
0.094
0.095
0.096
0.097
0.098

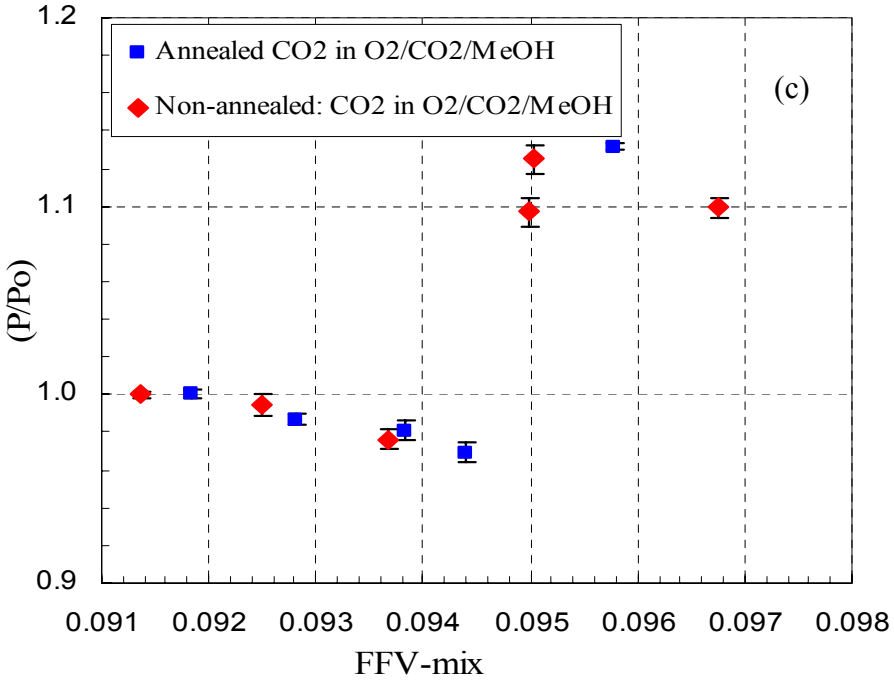
Annealed CO2 in O2/CO2/MeOH
Non-annealed: CO2 in O2/CO2/MeOH
(c)
(P/Po)
FFV-mix
1.2
1.1
1.0
0.9
0.091
0.092
0.093
0.094
0.095
0.096
0.097
0.098

At the high activity points, significant swelling occurs. These points have therefore, been used to evaluate the value of B_A using equation 6.5. This approach makes sense because the upswing in gas permeability occurs only after a certain concentration of methanol in the amorphous phase of the polymer has been achieved. The idea is akin to a critical amount of sorption of CO_2 at the plasticization pressure beyond which permeability increases and may be modeled using the free volume theory [49]. Parallels may also be drawn with the work of Jordan et al who propose that a critical concentration of a gas is needed in the polymer (polycarbonate in this case) before conditioning effects may be observed by exchanging the CO_2 feed with a probe gas such as oxygen or methane [21]. Since the permeability measurement was not made at activities between 70 and 80%, it is difficult to say what this critical concentration may be. However, the concentration at 80% activity is definitely above this critical concentration.

Based on equation 6.5, the slope of a plot of $\ln(P/P_o)$ vs. $1/FFV_o$-$1/FFV_{mix}$, where P_o is the dual mode prediction, may be used to evaluate B_A. Since B_A is usually said to be a constant for transport of a gas in a class of polymers, it seems reasonable to assume that the value will be the same for PET with different morphologies. The simplification here is that the effect of crystallinity will be negligible on the value of B_A, which may not be the true in the strict sense because crystals, like chemical crosslinking, may reduce the mobility of the amorphous polymer chain segments. However, in the absence of many data points in the high activity region for the annealed and the amorphous films, it seems best to correlate all the points to a single value. Figure 6.14 shows the plot for evaluation of B from the slope. B_{O2} = 0.25 and B_{CO2}=0.23 are evaluated from the slopes. The values of B_{O2}, calculated individually for the semicrystalline sample are very similar to the

average B_{O2} obtained using all the data points. Only for the amorphous PET film, in the case of O_2/MeOH, B_{O2} is calculated to be high at 0.668. This may be due to the fact that the amorphous film swells more than the semicrystalline films and the B_A value has no influence of crystallinity whereas most of the points in the plot below are for semi-crystalline samples.

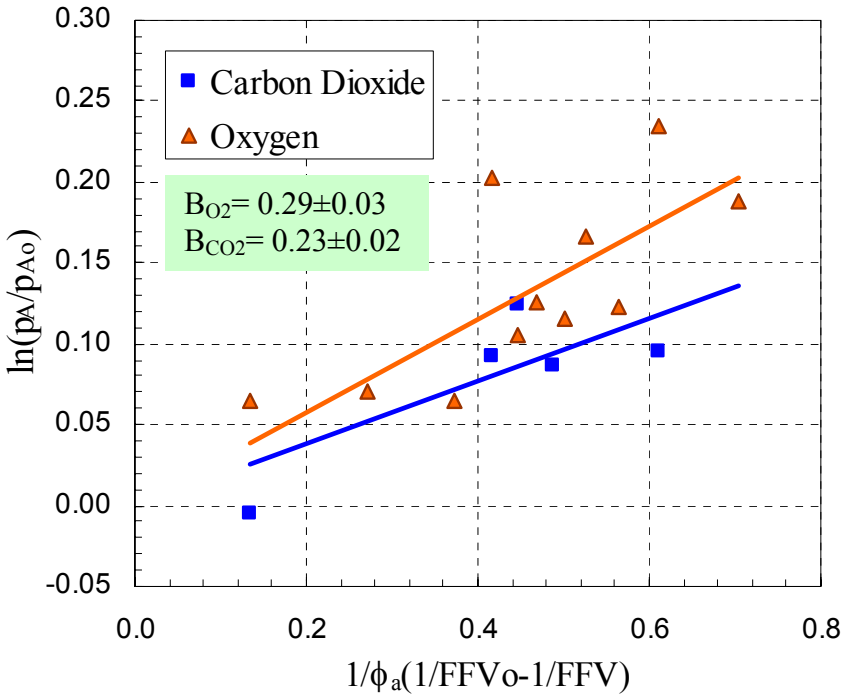

Figure 6.14: Plot of permeability change vs. fractional free volume change

Upon comparison with the values reported by Park and Paul for various polymers, it is found that the while these values are of the same order of magnitude, they are lower than values of 0.860 and 0.839 for CO_2 and O_2 respectively [34]. This may be because these authors use high permeability polymers which are commonly investigated for membrane based applications. No barrier polymer has been included in their plot. These

authors suggest a correction factor of $\gamma_{n,k}$ for different gas polymer pairs to evaluate the occupied volume more accurately. If this method is used to calculate $\hat{V}_o$, the occupied volume is much higher and consequently, the FFV is much lower. This method may lead to a larger value of B_A. However, the applicability of such an approach needs to be justified. Park and Paul have included only high permeability polymers in their database. In fact, polymers such 3,4'-PSF:3,4'polysulfone and bisphenol-A polyetherimide, which have low oxygen permeability of nearly 0.4 barrers and FFV of 0.149 and 0.150 respectively have been ignored from their data base. This is largely because the objective of their paper was to provide a predictive methodology for high permeability polymers. Barrier polymers are by their very definition, low permeability polymers and generalizations for high permeability materials may not fit them. Therefore, it appears reasonable that the value of B_A does not fit the within the class of high permeability polymers. It is evident that a closer examination of the free volume theory to obtain the parameters from literature is needed for glassy barrier polymers.

6.7 SUMMARY

The major observations and conclusions from the multi-component transport work are summarized below.

1. Methanol is a swelling agent at high activities and causes large increases in the permeability of O_2 and CO_2. This has been modeled using the free volume theory. A modified form of the theory is proposed for analysis of plasticization effects to account for the fact that these non-ideal effects induce changes only in the free

volume of the equilibrium liquid like regions of the polymer and not the non-equilibrium, excess free volume regions. Concentration dependent free volume increase has been modeled to obtain the value of the parameter B_A for O_2 and CO_2. It also seems that there is a critical concentration of methanol in the amorphous phase at which permeability shows an upturn. However, at present, there is no understanding of why this concentration is penetrant dependent and how its value may be predicted for larger flavor molecules

2. At low and intermediate activities, the influence of both, plasticization and competition is evident in the O_2/MeOH system and large enhancements in the permeability are not observed. Despite being below the critical concentration level, methanol is able to induce some conditioning of the polymer which leads to enhancement in the permeability of the amorphous and non-annealed films. These effects do not fit the free volume theory and hence, a simple extended form of the dual mode model has been used to estimate changes in the diffusivity of the gas at these activities.
3. The ternary system of CO_2/O_2/MeOH system highlights the need to investigate the possibility changes not just in the fractional free volume of the polymer induced by methanol, but also the need to understand the change in distribution of free volume and how it may be accessed by different gases. CO_2 is found to depress below the dual mode level in the amorphous film and oxygen permeability is also lower than was found in the case of O_2/MeOH
4. Crystallization and annealing of the polymer sample suppresses the swelling and plasticization effects at the low and high activities. However, residual stress are

found to be detrimental to the overall performance of the polymer as sorption induced stress relaxation occurs at lower activities only and leads to an enhancement of gas permeability. Crystallinity offsets the above effect by preventing the ultimate increase in the permeability at the high activities beyond that of the amorphous sample. However, from a packaging standpoint, since the bottle is blow molded and may have residual stresses, a swelling penetrant at intermediate activities may also lead to loss in the barrier properties.

6.8 REFERENCES

1. Ponangi, R.P. and P.N. Pintauro, *Separation of Volatile Organic Compounds from Dry and Humidified Nitrogen Using Polyurethane Membranes.* Industrial & Engineering Chemistry Research, 1996. **35**(8): p. 2756-2765.

2. Jian, K. and P.N. Pintauro, *Asymmetric PVDF hollow-fiber membranes for organic/water pervaporation separations.* Journal of Membrane Science, 1997. **135**(1): p. 41-53.

3. Al-Juaied, M. and W.J. Koros, *Performance of natural gas membranes in the presence of heavy hydrocarbons.* Journal of Membrane Science, 2006. **274**(1-2): p. 227-243.

4. Madden, W.C., *Hollow Fibre Membranes for Gas Separation Applications*, in *School of Chemical and Biomolecular Engineering*. 2005, Georgia Institute of Technology: Atlanta.

5. Miltz, J., C.H. Mannheim, and B.R. Harte. *Packaging of juices using polymeric barrier containers*. in *Barrier Polymer and Structures*. 1990. Washington D.C.: American Chemical Society.

6. Hansen, A.P. and D.K. Arora, *Loss of Flavor Comounds from Aseptically Processed Food Products Packaged in Aseptic Containers*, in *Barrier Polymers and Structures*, W.J. Koros, Editor. 1990, American Chemical Society: Washington DC.

7. Dhoot, S.N., B.D. Freeman, and M.E. Stewart, *Sorption and transport of linear and branched ketones in biaxially oriented polyethylene terephthalate.* Polymer, 2004. **45**(16): p. 5619-5628.

8. Sarria-Vidal, M., B. Nijssen, and J. Simal-Gandara, *Sorption of toluene and methanol by reusable poly (ethylene terephthalate) bottles.* Recent Research Developments in Agricultural & Food Chemistry, 1998. **2**(Pt. 2): p. 781-786.

9. van Willige, R.W.G., et al., *Influence of flavour absorption on oxygen permeation through LDPE, PP, PC and PET plastics food packaging.* Food additives and contaminants, 2002. **19**(3): p. 303-13.

10. Koros, W.J., ed. *Barrier polymers and structures:Overview*. Barrier Polymers and Structures, ed. W.J. Koros. 1990, American Chemical Society: Washington D.C.

11. Linssen, J.P.H., R.W.G. van Willige, and M. Dekker, *Packaging -Flavor Interaction*, in *Novel Food Packaging Techniques*, R. Ahvenainen, Editor. 2003, CRC Press: Cambridge, England. p. 590 pp.

12. Hirose, K., et al., *Sorption of d-limonene by sealant films and effect on mechanical properties.* ACS Symposium Series, 1988. **365**(Food Packag. Interact.): p. 28-41.

13. Sadler, G.D. and R.J. Braddock, *Oxygen permeability of low density polyethylene as a function of limonene absorption: an approach to modeling flavor \"scalping\".* Journal of Food Science, 1990. **55**(2): p. 587-8.

14. Gerlowski, L.E., *Water Transport through Polymers: Requirements and designs in Food Packaging*, in *Barrier Polymers and Structures*, W.J. Koros, Editor. 1990, American Chemical Society: Washington DC.

15. Koros, W.J., *Sorption and transport of gases in glassy polymers*, in *Chemical Engineering*. 1977, University of Texas: Austin. p. 274 pp.

16. Vieth, W.R., H.H. Alcalay, and A.J. Frabetti, *Solution of gases in oriented poly(ethylene terephthalate).* Journal of Applied Polymer Science, 1964. **8**(5): p. 2125-38.

17. Hirose, T., et al., *Sorption and transport of carbon dioxide in poly(ethylene terephthalate) crystallized by sorption of high-pressure CO2.* Journal of Applied Polymer Science, 1989. **37**(6): p. 1513-25.

18. Koros, W.J. and D.R. Paul, *Sorption and transport of carbon dioxide in poly(ethylene terephthalate) above and below the glass transition temperature.* Organic Coatings and Plastics Chemistry, 1978. **39**: p. 172-7.

19. Michaels, A.S., *Solution of gases in Polyethylene Terephthalate.* Journal of Applied Polymer Science, 1963. **34**(1): p. 1-12.

20. Patton, C.J., R.M. Felder, and W.J. Koros, *Sorption and transport of benzene in poly(ethylene terephthalate).* Journal of Applied Polymer Science, 1984. **29**(4): p. 1095-110.

21. Jordan, S.M. and W.J. Koros, *Characterization of carbon dioxide-induced conditioning of substituted polycarbonates using various \"exchange\" penetrants.* Journal of Membrane Science, 1990. **51**(3): p. 233-47.

22. Jordan, S.M., W.J. Koros, and G.K. Fleming, *The effects of carbon dioxide exposure on pure and mixed gas permeation behavior: comparison of glassy polycarbonate and silicone rubber.* Journal of Membrane Science, 1987. **30**(2): p. 191-212.

23. Pope, D.S. and W.J. Koros, *Gas sorption-induced dilation of poly(4-methyl-1-pentene).* Journal of Polymer Science, Part B: Polymer Physics, 1996. **34**(11): p. 1861-1868.

24. Olson, B.G., et al., *Positron Annihilation Lifetime Spectroscopy of Poly(ethylene terephthalate): Contributions from Rigid and Mobile Amorphous Fractions.* Macromolecules, 2003. **36**(20): p. 7618-7623.

25. Wind, J.D., et al., *Carbon dioxide-induced plasticization of polyimide membranes: pseudo-equilibrium relationships of diffusion, sorption, and swelling.* Macromolecules, 2003. **36**(17): p. 6433-6441.

26. McGonigle, E.A., et al., *Permeability of N2, Ar, He, O2 and CO2 through biaxially oriented polyester films - dependence on free volume.* Polymer, 2000. **42**(6): p. 2413-2426.

27. Olson, B.G., S. Nazarenko, and A.M. Jamieson, *Probing the amorphous structure of semicrystalline PET by positron annihilation life time spectroscopy.* Annual Technical Conference - Society of Plastics Engineers, 2005. **63rd**: p. 2075-2079.

28. Mahendrasingam, A., et al., *Observations of structure development during crystallisation of oriented poly(ethylene terephthalate).* Polymer, 2003. **44**(19): p. 5915-5925.

29. Peterlin, A. and R. Corneliussen, *Small-angle x-ray diffraction studies of plastically deformed polyethylene. II. Influence of draw temperature, draw ratio, annealing temperature, and time.* Journal of Polymer Science, Polymer Physics Edition, 1968. **6**(7): p. 1273-82.

30. Mizoguchi, K., et al., *Crystallization of poly(ethylene terephthalate) under high-pressure gases.* Polymer Communications, 1990. **31**(4): p. 146-8.

31. Ruiz-Trevino, F.A. and D.R. Paul, *Modification of polysulfone gas separation membranes by additives.* Journal of Applied Polymer Science, 1997. **66**: p. 1925-1941.

32. Chern, R.T., et al., *\"Second component\" effects in sorption and permeation of gases in glassy polymers.* Journal of Membrane Science, 1983. **15**(2): p. 157-69.

33. Hong, X., et al., *Free-Volume Hole Properties of Gas-Exposed Polycarbonate Studied by Positron Annihilation Lifetime Spectroscopy.* Macromolecules, 1996. **29**(24): p. 7859-7864.

34. Park, J.Y. and D.R. Paul, *Correlation and prediction of gas permeability in glassy polymer membrane materials via modified free volume based group contribution method.* Journal of Membrane Science, 1997. **125**(1): p. 23-39.

35. Zhou, S. and S.A. Stern, *The effect of plasticization on the transport of gases in and through glassy polymers.* Journal of Polymer Science, Part B: Polymer Physics, 1989. **27**(2): p. 205-22.

36. Kamiya, Y., et al., *Sorption and dilation in poly(ethyl methacrylate)-carbon dioxide system.* Journal of Polymer Science, Part B: Polymer Physics, 1989. **27**(4): p. 879-92.

37. Vrentas, J.S., J.L. Duda, and H.C. Ling, *Antiplasticization and volumetric behavior in glassy polymers.* Macromolecules, 1988. **21**(5): p. 1470-5.

38. Vrentas, J.S. and J.L. Duda, *Diffusion in polymer-solvent systems. I. Reexamination of the free-volume theory.* Journal of Polymer Science, Polymer Physics Edition, 1977. **15**(3): p. 403-16.

39. Fujita, H., *Diffusion in Polymer-Diluent Systems.* Fortschr. Hochpolym.-Forsch.,, 1961. **3**: p. 1-47.

40. Paul, D.R. and Y. Maeda, *Response to comments on \"Effect of antiplasticization on gas sorption and transport. III. Free volume interpretation\".* Journal of Membrane Science, 1989. **40**(1): p. 109-12.

41. van Krevelen, D.W., *Properties of Polymers*. 3rd ed. 1990, New York: Elsevier.

42. Maeda, Y. and D.R. Paul, *Effect of antiplasticization on gas sorption and transport. III. Free volume interpretation.* Journal of Polymer Science, Part B: Polymer Physics, 1987. **25**(5): p. 1005-16.

43. Fleming, G.K. and W.J. Koros, *Dilation of polymers by sorption of carbon dioxide at elevated pressures. 1. Silicone rubber and unconditioned polycarbonate.* Macromolecules, 1986. **19**(8): p. 2285-91.

44. Kamiya, Y., et al., *CO2 sorption and dilation of poly(methyl methacrylate).* Macromolecules, 1998. **31**(2): p. 472-478.

45. Ruiz-Trevino, F.A. and D.R. Paul, *A quantitative model for the specific volume of polymer-diluent mixtures in the glassy state.* Journal of Polymer Science, Part B: Polymer Physics, 1998. **36**(6): p. 1037-1050.

46. Fang, S.M., S.A. Stern, and H.L. Frisch, *A "Free Volume" model of permeation of gas and liquid mixtures through polymeric membranes.* Chemical Engineering Science, 1974. **30**: p. 773-780.

47. Pixton, M.R. and D.R. Paul, *Relationships between structure and transport properties for polymers with aromatic backbones*, in *Polymeric Gas Separation Membranes*, Y. Yampolskii, Editor. 1994, CRC Press: Boca Raton.

48. Maeda, Y. and D.R. Paul, *Effect of antiplasticization on gas sorption and transport. II. Poly(phenylene oxide).* Journal of Polymer Science, Part B: Polymer Physics, 1987. **25**(5): p. 981-1003.

49. Bos, A., et al., *CO2-induced plasticization phenomena in glassy polymers.* Journal of Membrane Science, 1999. **155**(1): p. 67-78.

50. Koros, W.J., *Sorption and transport of CO_2 above and below glass transition of poly(ethylene terephthalate).* Polymer Engineering and Science, 1980. **20**(1): p. 14-19.

51. Couchman, P.R. and F.E. Karasz, *A classical thermodynamic discussion of the effect of composition on glass-transition temperatures.* Macromolecules, 1978. **11**(1): p. 117-19.

52. Chow, T.S., *Glass transition temperature of polymer-diluent systems.* Ferroelectrics, 1980. **30**(1-4): p. 139-45.

53. Stern, S.A. and V. Saxena, *Concentration-dependent transport of gases and vapors in glassy polymers.* Journal of Membrane Science, 1980. **7**(1): p. 47-59.

54. Nadakatti, S.M., J.H. Kim, and S.A. Stern, *Solubility of light gases in poly(n-butyl methacrylate) at elevated pressures.* Journal of Membrane Science, 1995. **108**(3): p. 279-91.

55. Houde, A.Y., et al., *Permeability of dense (homogeneous) cellulose acetate membranes to methane, carbon dioxide, and their mixtures at elevated pressures.* Journal of Applied Polymer Science, 1996. **62**(13): p. 2181-2192.

CHAPTER 7 : SUMMARY AND RECOMMENDATIONS FOR FUTURE WORK

7.1 SUMMARY OF CONTRIBUTIONS

The aim of this work was to enhance the understanding of the effect of the flavor molecules on the transport properties of PET and establish a framework for analyzing real, more complicated systems and newer barrier polymers. Towards this end, this work has provided the first study that investigates multi-component transport of gases and vapors in barrier polymers in a systematic manner to understand the influence of highly sorbing vapor components on transport properties. There are many literature reports which investigate the package performance under specific conditions, but none compare the effects of crystallinity and annealing on the package performance [1-3].

In pursuit of the overall objective, a system has been designed to perform multi-component permeation studies, prepare custom feeds and analyze the permeate. Several process related issues were ironed out, and the only capability missing in this equipment is the ability to handle water vapor permeation with vacuum on the downstream. Methanol has been identified as suitable system to model the effect of flavor components on transport properties. The equilibrium sorption isotherm and sorption kinetics of methanol have been measured in PET for the first time. Different morphologies have also been used to investigate the effect of crystallinity and annealing. Methanol isotherm shows dual mode sorption effects at low activities and swelling at high activities. It has been shown that methanol is a good model compound to study because O_2 and CO_2

permeation in the presence of methanol show significant differences at low activities and high activities of methanol. This system therefore retains all the complexity that a real package might encounter.

It has been shown that at high activity, methanol swells the amorphous regions of PET considerably, and the permeability of oxygen and carbon dioxide in presence of methanol are higher than the respective pure gas permeabilities. This effect has been analyzed within the framework of Fujita's free volume theory. However, to model the changes, it has been proposed, for the first time, that plasticization induced changes in the free volume should really be considered only in the equilibrium packed regions of the glassy polymer. This hypothesis is very reasonable given that plasticization occurs in both rubbery and glassy polymers.

Upon application of the free volume theory to the mixture transport, the parameter B_A (refer to equation 6.2), has been evaluated for O_2 and CO_2. This has brought to light an important and interesting aspect that addresses the fundamentals of transport as described by free volume theory. The value of B_A, calculated using V_o from Bondi's group contribution method is lower than that predicted by Park et al for a large number of polymers [4, 5]. While it is a simplification to assume that the free volume parameters for a given gas are the same for a large number of polymers, the results fit the permeabilities of the high free volume polymers considered in their study. Park et al also propose an alternate method of calculating the occupied free volume of polymers. Based V_o value, estimated using the expression proposed by them the $FFV_{amor\text{-}PET}$ is evaluated to be very low; while this $FFV_{amor\text{-}PET}$ may predict a value for B_A that is higher than the present estimation, Park et al did not use such low free volume polymers when developing the

parameters for evaluation of specific occupied volume. This work therefore reveals the need for developing an appropriate method for evaluation of the occupied volume of a polymer and consequently, a value for the parameters A_A and B_A, which may accurately predict the permeabilities of barrier polymers.

Comparison of samples with different processing history has shown that annealing helps to suppress the non-ideal effects such as plasticization in the polymer. On the other hand, despite the presence of crystals, unrelaxed stresses in an oriented polymer may be detrimental as methanol sorption induced relaxation of these stresses appears to be responsible for an increase in gas permeability at lower activities when compared with the annealed and amorphous materials. Overall, the restraining effect of the crystals seems to be responsible for the lower enhancements in the permeability.

Another significant contribution of this work has been towards prediction of the solubility of gases and vapors. Sorption and diffusion properties of a series of lower alcohols were measured for the first time in PET. The experimental results were analyzed in conjunction with the literature values to identify a better correlation between the solubility parameters of the penetrant with its solubility in PET. The difference between the solubility of species with similar critical temperature was explained based on the difference between their dispersive and hydrogen bonding parameters with respect to PET.

7.2 FUTURE RECOMMENDATIONS

Two observations in the present multi-component study are not very well understood at present. Certain experiments are proposed below to understand the phenomena and confirm proposed explanations:

1. The non-annealed sample shows swelling at a lower activity of methanol unlike the annealed and the amorphous sample. This observation may be attributed to the presence of stresses in an oriented, non-annealed film. One way of confirming that stress related effects may be the cause of permeability enhancement at relatively low activities, could be the measurement of the plasticization pressures of other plasticizing penetrants such as CO_2. High pressure CO_2 is a plasticizer for PET and the plasticization pressure is the pressure at which a minimum in the permeability vs. pressure plot is observed [6, 7]. Based on the increases in permeability of the gases among the annealed, non-annealed and amorphous samples, it is expected that the pure CO_2 permeability will show an upturn at a lower pressure in the non-annealed films than in the annealed or amorphous films. Alternately, the free volume distribution may also be probed with positron annihilation studies in the presence and absence of methanol vapor as was done by Hong et al for the polycarbonate/CO_2 system [8]. Since concentration of methanol at equilibrium with 60% activity of methanol is the level at which permeability starts increasing, this activity should be maintained in the PALS system and the free volume distribution and the total free volume of the annealed, non-annealed and amorphous samples maybe compared.

2. Depression of CO_2 below the dual mode sorption level was observed in the amorphous sample in the ternary system of O_2/CO_2/MeOH. Smaller depressions below the dual mode prediction are observed for the semi-crystalline films. This result needs to be confirmed using CO_2/MeOH system. If, as is proposed, the change in free volume distribution is being probed differently by CO_2 and O_2, then CO_2/MeOH system should show similar trends, with O_2 being eliminated from the picture. In addition, the free volume distribution obtained from the PALS study proposed above may be used to understand the difference between the behavior of CO_2 and O_2.
3. A natural extension of this work with O_2/CO_2/MeOH will be the inclusion of water vapor in the feed which is a key component in all packaged foods and beverages. The interaction of two condensable penetrants in the matrix, along with the gases, will simulate the actual package conditions more closely.

From an overall perspective of the field of transport of gases and vapors, specifically in barrier polymers and in glassy polymers in general, the present study poses a few questions. Research that provides answers to these questions will augment the understanding of transport not only in PET, but also for polymers in general. Possible studies have been discussed below.

1. To understand the equilibrium sorption of various polymers, it has been proposed in this work that the Hansen solubility parameters, δ_d (dispersive solubility parameter), δ_h (hydrogen bonding parameter), and δ_p(dipole-dipole interaction parameter) must be considered individually with respect to the PET solubility parameters. Empirical relations may be developed to enable prediction of the solubility of a larger

penetrant such as flavor molecules which may not always be experimentally accessible due to the time scales of diffusion involved. For the development of such a correlation, organic moieties with functionalities that have not been investigate till now such as –COOH, -C=C- , $-NH_2$ and even cyclic compounds need to be studied. Based on the δ_d and δ_h, this data may be used to understand the behavior of multi-functional organic compounds. Systematic variation of the size of the molecules will allow correlation of the size with functionality of the flavor molecule and its solubility in PET. This will be a valuable study to the food packaging community as it directly addresses the issue of flavor scalping and prevents the need of long experiments.

2. To ensure that the above correlation will be applicable to other glassy polymers also, data available in literature for the sorption of gases and vapors in widely studied polymers such as poly(methyl methacrylate) and polystyrene may be correlated with the solubility parameters of the respective polymers [9-12].

3. An important issue highlighted by this work has been the need to know the critical concentration of a sorbed penetrant in the polymer that may lead to significant swelling and loss of barrier properties. At present, conditioning effects of methanol observed below this critical concentration level are modeled within the dual mode model framework; whereas observed permeability enhancements above this critical level are successfully explained by the free volume theory. Since the same sorbed concentration of different penetrants may affect the polymer morphology differently, it is important to understand which properties of the species determine the increase in free volume, and how that may affect gas permeability in vapor

laden streams. These properties may include: size of the penetrant, its interaction with the polymer, and its physical constants such as glass transition temperature. Berens proposed that the inflection point in the sorption isotherm corresponds to the concentration level at which the polymer-penetrant system may undergo glass transition [13]. While this may not necessarily be the case, as is suggested by this study, and also by Wind et al, T_g of the system may be indicative of the polymer chain mobility and the free volume [14]. Since the glass transition temperature of the system will be a function of the penetrant T_g also, studies of sorption complimented by measurement of glass transition temperature of the system and volumetric dilation may be interesting. In-situ spectroscopic ellipsometry on thin films may be used to simultaneously measure sorption and dilation of the polymer [14]. Dilation may be used to obtain changes in the free volume of the polymer [15]. This data may be used to estimate the concentration level for a penetrant which leads to large enhancement in the free volume. To compare the effect of different penetrants, this concentration level may be correlated with the T_g of the penetrant for a given polymer or with $T_{g,mix}$ to compare different polymers. Such studies have applications not only in barrier materials with regard to flavor scalping, but also for membrane based separations where contaminants are detrimental to the membrane performance [16].

4. To resolve the issue of the difference in the value of B_A evaluated in this work for barrier polymers which have low permeabilities, it is important to establish an unambiguous method of evaluating the fractional free volume using the occupied volume of the polymer. PALS is a technique that can be used to evaluate FFV from

the lifetime of the o-positron and the intensity. Since occupied volume is not an input, these independent measurements of FFV may be compared with predictions from different estimation methods across various barrier polymers [17]. This will be a significant addition to the understanding and prediction of gas transport properties in glassy polymers.

7.3 REFERENCES

1. van Willige, R.W.G., et al., *Influence of flavour absorption on oxygen permeation through LDPE, PP, PC and PET plastics food packaging.* Food additives and contaminants, 2002. **19**(3): p. 303-13.

2. Hansen, A.P. and D.K. Arora, *Loss of Flavor Comounds from Aseptically Processed Food Products Packaged in Aseptic Containers*, in *Barrier Polymers and Structures*, W.J. Koros, Editor. 1990, American Chemical Society: Washington DC.

3. Mohney, S.M., et al., *Permeability and solubility of d-limonene vapor in cereal package liners.* Journal of Food Science, 1988. **53**(1): p. 253-7.

4. van Krevelen, D.W., *Properties of Polymers*. 3rd ed. 1990, New York: Elsevier.

5. Park, J.Y. and D.R. Paul, *Correlation and prediction of gas permeability in glassy polymer membrane materials via modified free volume based group contribution method.* Journal of Membrane Science, 1997. **125**(1): p. 23-39.

6. Bos, A., et al., *CO2-induced plasticization phenomena in glassy polymers.* Journal of Membrane Science, 1999. **155**(1): p. 67-78.

7. Kamiya, Y., et al., *Sorptive dilation of polysulfone and poly(ethylene terephthalate) films by high-pressure carbon dioxide.* Journal of Polymer Science, Part B: Polymer Physics, 1988. **26**(1): p. 159-77.

8. Hong, X., et al., *Free-Volume Hole Properties of Gas-Exposed Polycarbonate Studied by Positron Annihilation Lifetime Spectroscopy.* Macromolecules, 1996. **29**(24): p. 7859-7864.

9. Sarti, G.C., C. Gostoli, and S. Masoni, *Diffusion of alcohols and relaxation in poly(methyl methacrylate): effect of thermal history.* Journal of Membrane Science, 1983. **15**(2): p. 181-92.

10. Katime, I.A., F.J. Juanes Garcia, and P.M. Sasia, *Anomalous behavior of PMMA in the methyl isobutyl ketone/methanol system.* European Polymer Journal, 1988. **24**(6): p. 557-60.

11. Hopfenberg, H.B., D.J. Enscore, and V. Stannett, *Sorption and Transport in glassy polymeric microspheres.* Organic Coatings and Plastics Chemistry, 1978. **39**: p. 242-247.

12. Immergut, E.H. and J. Brandrup, eds. *Handbook of Polymers*. 7th Edn. ed. 1989, Wiley and Sons: New York. pp 684.

13. Berens, A.R., *Transport of plasticizing penetrants in glassy polymers.* ACS Symposium Series, 1990. **423**(Barrier Polym. Struct.): p. 92-110.

14. Wind, J.D., et al., *Carbon dioxide-induced plasticization of polyimide membranes: pseudo-equilibrium relationships of diffusion, sorption, and swelling.* Macromolecules, 2003. **36**(17): p. 6433-6441.

15. Jordan, S.S. and W.J. Koros, *A Free Volume Distribution Model of Gas Sorption and Dilation in Glassy Polymers.* Macromolecules, 1995. **28**(7): p. 2228-35.

16. Madden, W.C., *Hollow Fibre Membranes for Gas Separation Applications*, in *School of Chemical and Biomolecular Engineering*. 2005, Georgia Institute of Technology: Atlanta.

17. Jean, Y.C., et al., *Correlations between gas permeation and free-volume hole properties probed by positron annihilation spectroscopy.* Journal of Polymer Science, Part B: Polymer Physics, 1995. **33**(17): p. 2365-71.

APPENDIX A: GAS CHROMATOGRAPHY FOR FEED AND PERMEATE COMPOSITION ANALYSIS

Gas chromatography (GC) has been used to analyze the composition of the permeate in case of mixed gas or mixed gas vapor feeds. The feed composition of custom prepared gas/vapor mixtures has also been analyzed similarly. The instrument is a 6890N from Agilent Technologies (Palo Alto, Ca). The valve diagram of the GC is shown below.

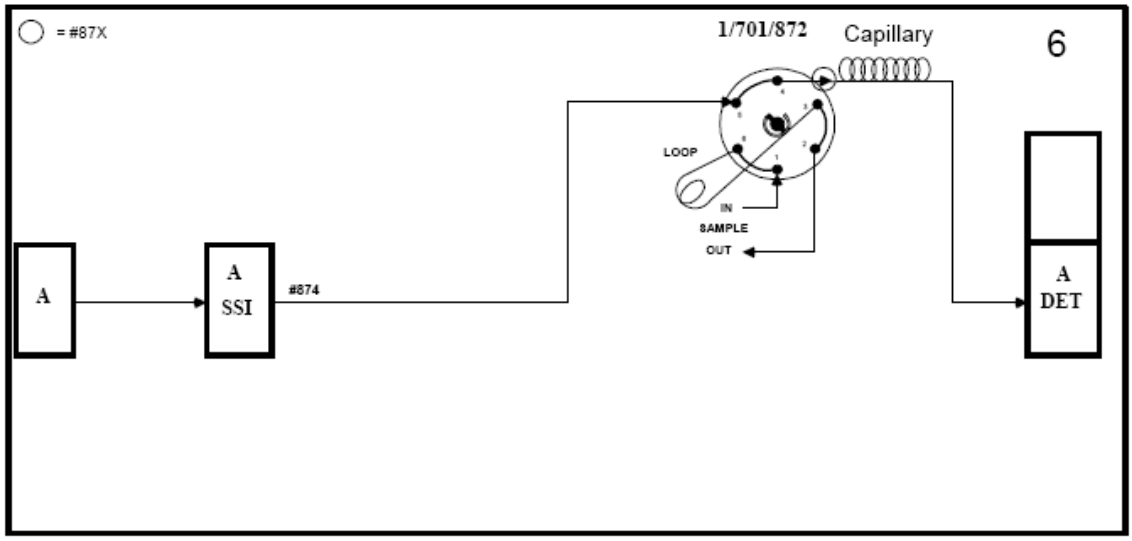

Figure A. 1: Valve configuration for gas sampling

A 2 cc sample loop has been used. The 'sample in' port is connected to the permeate and the feed side, whereas the 'sample out' port is connected to a 100 Torr MKS Baratron^{TM} transducer and vacuum pump in series. The following are the operating conditions at the time of a GC run.

Table A. 1: GC operating conditions

Paramater	Sample with methanol (Method-MeOH.m)	Gas mixture only (Method-Gases.m)
Oven Temperature	120°C	120°C
Total Run Time	4.00 min	4.00 min
Back Inlet	150°C	125°C
Split Ratio	10:1	50:1
Column	HP Plot Q, 30m long, 0.32mm diameter, 0.20μ coating width	
Column flow	3.4 mL/min at 20 psi	3.5mL/min at 18.75 psi
Carrier Gas	Helium	
Detector reference gas flow	20.0 mil/min	
Detector make-up gas flow	7.0 mL/min	
Heated Valve Box	130°C	120°C

The GC was calibrated using pure gases and vapors. Pure CO_2 and O_2 were expanded into the sample loop from the downstream of the permeation box and allowed to equilibrate for 3 minutes. Different pressures in the range of 0-10 Torr for the gases were injected. Methanol vapor was expanded into the GC from a vapor source volume that was

kept outside the permeation box. The vapor was prepared by taking liquid methanol in a vial. Dissolved and headspace air was removed by freeze-pump-thaw cycles. The vapor in the headspace of the liquid vial was then allowed to expand into a 1000 cc volume that was connected to the vial. This volume had been evacuated previously. Vapor from this volume was expanded into the GC sample loop. Methanol vapor in the range of 0-0.5 Torr was used. These pressures were chosen because this was the expected range of partial pressures in the permeate. All the transfer lines were *heated to least 70^oC* to ensure that methanol did not adsorb on the transfer lines which would results in smaller peaks.

Upon expansion into the sample loop, the sample (may be a gas or vapor) was allowed an equilibration time of 3 minutes if the pressure is higher than 5 Torr and 5 minutes of the pressure was less than 5 Torr. Care had been taken to ensure that the leak rate of atmospheric air into the transfer lines was minimal and that no leak peak for air was observed during blank runs. The calibration factors obtained are shown below:

Table A. 2: Calibration factors for CO_2, O_2 and methanol

Paramater	**Sample with methanol (Area/Torr)**	**Gas mixture only (Area/Torr)**
Methanol	46.465	-
Oxygen	46.136	27.27
Carbon Dioxide	67.748	35.23

During a permeation run, the mixed gas/vapor feed was analyzed by expanding the feed mixture into the sample loop. Nearly 20-30 Torr of the mixture was injected. This ensured that methanol partial pressures lay in the calibration range. Mole fraction of methanol in the feed was calculated using equation A.1

$$Y_{MeOH} = \frac{A_{MeOH}}{\beta_{MeOH} . P_{injected}} \qquad \text{A. 1}$$

$P_{injected}$ is the pressure read off by the transducer in the GC transfer line. A_{MeOH} is the measured area, and β_{MeOH} is the calibration factor. The method- MeOH.m was used for these calibrations.

When sufficient permeate was collected, which was at least a total pressure of 2 Torr, it was expanded into the sample loop. Lower pressures than that took much longer to expand because of the large pressure drop across the transfer line and the sample loop (the sample loop is made of 1/16" tubing). Also, areas were small, especially for methanol at low activities. Pressures for CO_2/MeOH mixtures and O_2/CO_2/MeOH mixture were higher; in the range 3-6 Torr as the total flux was higher. Care was also taken to ensure that methanol partial pressures did not exceed 0.5 Torr in the downstream in most cases. This is because control tests of methanol adsorption were carried out only up till 0.5 Torr. The permeate was allowed to expand into the sample loop for 5 mins after which the run was started. Areas of the species were obtained and their mole fraction was calculated using the following expression:

$$Y_A = \frac{A_A / \beta_A}{A_A / \beta_A + A_B / \beta_B + A_C / \beta_C} \qquad \text{A. 2}$$

A_i is the area of the species and β_i is the calibration factor. The permeability of the species was then calculated using the following:

$$\frac{dp_A}{dt} = Y_A * \frac{dp_{Total}}{dt} \qquad \text{A. 3}$$

$$P_A = \frac{\frac{dp_A}{dt} \times 101325 \times V \times 10^{-6} \times 22414 \times l \times 14.696}{60 \times 760 \times 8.314 \times T \times A \times \Delta p \times 76} x10^{10}\ Barrers \qquad \text{A. 4}$$

P_A is the permeability; dp_A/dt is the rate of pressure rise for a given species in Torr/min. *For oxygen, the actual dp/dt is evaluated by subtracting out the measured leak rate.* This was because it is air that leaks in, and contributes only to the oxygen peak, not the other gases. V is the downstream volume in cc. R=8.314 J/mol/K, *l* is the film thickness in cm, Δp, in psia, is the pressure differential across the film which is the upstream pressure in this case. A is the film area in cm^2. When needed, selectivity has been calculated using the ratio of the permeability calculated for O_2 and CO_2 using equations A.2 - A.4.